

Forsmark site investigation

Evaluation of overcoring stress measurements in boreholes KFM01B, DBT-1 and DBT-3 and hydraulic stress measurements in boreholes KFM01A, KFM01B, KFM02A and KFM04A at the Forsmark site

Daniel Ask, Vattenfall Power Consultant AB

December 2007

Svensk Kärnbränslehantering AB

Swedish Nuclear Fuel
and Waste Management Co
Box 250, SE-101 24 Stockholm
Tel +46 8 459 84 00



Forsmark site investigation

Evaluation of overcoring stress measurements in boreholes KFM01B, DBT-1 and DBT-3 and hydraulic stress measurements in boreholes KFM01A, KFM01B, KFM02A and KFM04A at the Forsmark site

Daniel Ask, Vattenfall Power Consultant AB

December 2007

Keywords: In situ stress state, Integrated Stress Determination Method, Reliability of stress data, Geological and geophysical correlation.

This report concerns a study which was conducted for SKB. The conclusions and viewpoints presented in the report are those of the author and do not necessarily coincide with those of the client.

Data in SKB's database can be changed for different reasons. Minor changes in SKB's database will not necessarily result in a revised report. Data revisions may also be presented as supplements, available at www.skb.se.

A pdf version of this document can be downloaded from www.skb.se.

Summary

This report comprises a review of rock stress measurements conducted within the site investigation program at Forsmark up to and including year 2004. The stress data encompassed in the analysis were chosen by SKB and involve overcoring stress data from boreholes KFM01B /Sjöberg 2004/, DBT-1 and DBT-3 /Ingevald and Strindell 1981/, as well as hydraulic stress data from boreholes KFM01A, KFM01B, KFM02A, and KFM04A /Klee and Rummel 2004/. The study presented in the report was completed in April 2006.

The primary objective of the study was to analyze the state of stress indicated by the overcoring and hydraulic measurements and to apply an integrated stress analysis approach including both data sets. A secondary objective was to discuss the homogeneity of the stress field. It is emphasized that the results in the report are based on neglect of potential horizontal stress gradients, i.e. that the stress data in all investigated boreholes at the Forsmark site support the same stress field, and that stresses can be described by linear functions versus depth.

The results of the analysis of overcoring data in borehole KFM01B revealed similar stress magnitudes as reported from earlier overcoring measurements at Forsmark (boreholes DBT-1 and DBT-3; /Sjöberg et al. 2005/). However, only the results at Level 1 (about 240 metres vertical depth, mvd) in KFM01B are judged fair. At Level 2 (406–475 mvd), sample disturbance as a result of core discing and spalling failures in the pilot hole walls, as well as potential influence of nearby located discontinuities, significantly reduce the reliability of the stress estimates. The overcoring data in DBT-1 and DBT-3 provide a fairly uniform picture of the state of stress. However, the strain versus time response during overcoring was not available in this early version used of the *Borre Probe*. Moreover, core discing was abundant and the elastic parameters were determined using a combination of biaxial and uniaxial tests of cores but, due to insufficient documentation, in a partly unknown manner. Because the results in DBT-1 and DBT-3 cannot be verified, the results are regarded with some scepticism.

As concerns hydraulic data, the report presents, besides the analysis of the measurements performed in four boreholes at Forsmark, the general approach for hydraulic rock stress measurements. This approach is to be regarded as the opinion of the author, although it has also been reviewed and complemented by Prof. Francois Cornet, Institut de Physique du Globe de Paris (IPGP).

The results of the hydraulic stress measurements performed during 2004 in boreholes KFM01A, KFM01B, KFM02A and KFM04A at Forsmark are not optimal. The primary reason can be correlated to the lack of reliable fracture orientation data. These problems are manifested in the very large amount of data that were excluded (33–46%) in the stress calculations by /Klee and Rummel 2004/. This study has revealed that only 11 tests involve unambiguous data and another 14 tests partly unambiguous data. These defeats aside, a few important conclusions may be drawn from the hydraulic data: (1) the vertical direction is a principal direction; (2) the vertical stress closely reflects the theoretical weight of the overburden rock mass; and (3) maximum horizontal stress is oriented approximately 134°N.

Heterogeneous data primarily involve the depth section 412 to 518 mvd in borehole KFM02A. These data can be correlated with a major deformation zone denominated ZFMNE00A2, which is dipping about 24° towards SSE. The low normal stress values could possibly be explained by that fractures have propagated and reached across one of the packers inducing some by-pass that closes when the pressure becomes low enough.

A new estimation of the stress field at the Forsmark site was derived, but the results are somewhat inconclusive as the two types of data, hydraulic and overcoring, indicate significantly different states of stress. Successful attempts were however made by a joint solution using

both data sets. The advantage of the joint solution is twofold; the results include the maximum amount of data and the major uncertainty involved in the overcoring data can be handled by solving the elastic parameters *in situ*.

The joint solutions were obtained by employing both known and unknown values of the elastic parameters. For the case when the elastic parameters are known, the values obtained from biaxial tests on overcoring samples are used. This implies that overcoring and hydraulic data are given the same weight in the joint solution. However, when the elastic parameters are unknown, the overcoring data are only represented by measured strains and do not help constraining stress magnitudes. Instead, for this case, the hydraulic stress data completely constrain the joint solution. This calculation thus represents *in situ* values of the elastic parameters. Because the elastic parameters constitute a major uncertainty in the overcoring method, the author favors the latter solution. However, the two data sets are not optimal for a joint solution as the number and distribution of data differ significantly between methods. As a result, the solution must be regarded merely as a guideline and not for design purposes until new and more reliable data have been collected at the Forsmark site.

What can be appreciated with the existing data sets is that one principal stress is vertical and closely resembles the theoretical weight of the overburden. Moreover, maximum horizontal stress is oriented about 134°N, although this needs to be confirmed as the amount of data is sparse. An overwhelming majority of the overcoring strain data support these conclusions as described with the constrained overcoring calculations.

After completion of the study presented in this report, errors and uncertainties in the borehole deviation measurements made in the Forsmark investigation boreholes were observed and quantified (except for boreholes DBT-1 and DBT-3 which were not analysed in this respect). Furthermore, errors and uncertainties have been identified for the rotational orientation of the BIPS-instrument used for producing video images of the borehole wall. Because data from the deviation measurements and BIPS-images are part of the SKB system for borehole mapping, the so called Boremap system, also the orientation of geological structures, like fractures and rock contacts, may be affected. These lately discovered errors and uncertainties are not considered in the present report, because at the time of performance of this study they were not known and their significance hence not quantified. The extent of the problem, which for most borehole sections preliminarily has been estimated at a few degrees (but is known to be larger in some sections), is for the time being considered to be in the same order of magnitude as for the other parameters discussed in this report, or even significantly less. Besides, it is mainly SKB's borehole deviation measurements that have been used in the measurements referred to in this report. As a consequence, this additional source of error and uncertainty is not judged to overthrow the results in this study. A more firm analysis of consequences of the problem for stress calculations is however not possible until the orientations of the addressed geological structures have been revised.

Sammanfattning

Denna rapport presenterar resultaten från en granskning och utvärdering av bergspänningsdata utförd inom ramen för platsundersökning Forsmark. Dataunderlaget för analysen valdes av SKB och omfattar överborrningsdata från borrhålen KFM01B /Sjöberg 2004/, DBT-1 och DBT-3 /Ingevald och Strindell 1981/ samt hydrauliska data från borrhål KFM01A, KFM01B, KFM02A och KFM04A /Klee och Rummel 2004a/. Studien slutfördes i april 2006.

Det primära målet med studien var att analysera spänningstillståndet som de två metoderna indikerat samt att utföra en integrerad spänningsanalys avseende data från båda metoderna. Ett sekundärt mål var att diskutera spänningsfältets homogenitet. Det bör understrykas att resultaten i denna rapport är baserade på antagandena att horisontella spänningsgradienter kan försummas, dvs att data från samtliga undersökta borrhål representerar en och samma spänningsdomän, samt att spänningsförändringarna mot djupet kan beskrivas med linjära funktioner.

Analysen av överborrningsdata från borrhål KFM01B uppvisade liknande resultat som tidigare erhållits vid överborrningsmätningar i Forsmark i borrhålen DBT-1 and DBT-3 /Sjöberg m fl 2005/. Dock bedöms endast de erhållna resultaten från Nivå 1 (ca 240 m vertikaldjup, mvd) i KFM01B som tillförlitliga. Resultaten från Nivå 2 (406–475 mvd) har en avsevärt lägre tillförlitlighet på grund av ”core discing”, spjälkbrott i pilothållsväggarna samt av sannolik influens av närliggande strukturer. Överborrningsdata i hålen DBT-1 och DBT-3 uppvisar en relativt tydlig trend mot djupet, men på grund av att töjningsresponsen under överborrnning inte registrerades med den tidigare versionen av *Borre-cellen*, som användes vid dessa mätningar, kan inte resultaten analyseras i detalj. Detta i kombination med förekomsten av core discing, samt att de elastiska parametrarna har bestämts med ett ovanligt och, på grund av bristfällig dokumentation, delvis okänt förfarande (okänd kombination av enaxiell- och biaxiell testning) gör att resultaten inte kan ges full trovärdighet.

I denna rapport presenteras också, förutom en analys av de hydrauliska bergspänningsmätningar som utförts i borrhålen KFM01A, KFM01B, KFM02A och KFM04A, generella riktlinjer för sådana mätningar. Beskrivningen skall ses som författarens åsikter, även om de har granskats och kompletterats med kommentarer från Prof. Francois Cornet, Institut de Physique du Globe de Paris (IPGP).

Resultaten från de hydrauliska mätningarna, som utfördes under 2004 i de fyra ovan nämnda borrhålen, är inte optimalt, främst beroende på bristen av tillförlitliga sprickorienteringsdata. Detta återspeglas också i det stora antal data (33–46 %) som förkastades i analysarbetet /Klee and Rummel 2004/. Den nu genomförda granskningen av data indikerade att endast 11 av 85 tester är av fullgod kvalitet samt att ytterligare 14 tester är användbara, om än med lägre kvalitet. Med hjälp av de hydrauliska mätningarna kan dock tre viktiga generella slutsatser dras: (1) en huvudspänning är vertikal; (2) den vertikala huvudspänningen motsvarar den teoretiska vikten av överliggande bergmassa; samt (3) orienteringen av största huvudspänning är ca 134°N.

Heterogena data återfanns framför allt mellan 412 och 518 mvd i borrhål KFM02A. Dessa data kan korreleras till zon ZFMNE00A2, som stupar ca 24° mot SSO. De låga normalspänningsvärdena som uppmättes i området kring denna zon kan tolkas på två sätt, att zonen påverkar spänningarna eller att sprickor propagerat runt packrarna.

Analysen av spänningssituationen i Forsmark visade sig problematisk och resultaten från överborrnings- och hydrauliska data uppvisar väsentliga skillnader i både spänningsmagnituder och orienteringar. I syfte att försöka lösa detta problem utfördes en kombinerad analys baserad på båda datamängderna. Eftersom i detta fall de två datamängderna har inbyggda, i vissa fall

stora osäkerheter, liksom att antalet data i vissa djupintervall är litet, förordas lösningar erhållna med båda datamängderna inkluderade. Fördelarna med denna strategi är dels att antalet data som ingår i lösningen blir betydligt större, och dels att den största osäkerheten i överborrningsmetoden, de elastiska parametrarna, kan undvikas genom att dessa löses *in situ*.

De kombinerade lösningarna utnyttjar såväl kända som okända värden på de elastiska parametrarna. I lösningen med kända elastiska parametrar används resultaten från biaxialtester på överborrningskärnor. Detta medför att överborrningsdata och hydrauliska data får samma vikt i den integrerade lösningen. När däremot de elastiska parametrarna är okända, representeras överborrningsdata enbart av uppmätta töjningar och bidrar därför inte vid beräkningen av spänningsmagnituderna. I det fallet styrs lösningen i stället till största delen av det hydrauliska dataunderlaget. Eftersom de elastiska parametrarna bestämda med biaxialtestning utgör en betydande osäkerhetsfaktor i överborrningsmetoden, förordar författaren alternativet där dessa parametrar i stället löses *in situ*.

Det bör betonas att de två datamängderna trots allt inte är optimala för den kombinerade lösningen, eftersom antalet data och fördelningen av mätpunkter i bergmassan för de två mätmetoderna skiljer sig markant. Av den anledningen skall lösningen enbart ses som en grov indikation på det rådande spänningsfältets karaktär i Forsmark. En mer robust lösning kräver nya och mer tillförlitliga data. De datamängder som ingått i föreliggande analys visar dock tydligt att en huvudspänning är vertikal och motsvarar den teoretiska vikten av överliggande bergmassa. Dessutom tycks största huvudspänningen vara orienterad ca 134°N, men nya data krävs för att verifiera detta.

Efter slutförande av denna studie har vissa fel och osäkerheter i krökningsdata uppdagats för borrhålen inom Forsmarks platsundersökning (de tidigare borrhålen DBT-1 och DBT-3 har inte reviderats i detta avseende). Fel och osäkerheter har också identifierats i vissa borrhålssektioner för den s.k. BIPS-sondens orientering. BIPS-sonden är en färgvideokamera som används för att producera bilder av borrhålsväggen. Eftersom såväl krökningsdata som BIPS-bilder ingår i SKB:s borrhålskarteringssystem, det s.k. Boremapsystemet, kan även orienteringen av geologiska objekt såsom sprickor och bergartskontakter vara behäftade med vissa fel och osäkerheter. Då denna studie genomfördes var dessa brister okända och deras betydelse följaktligen inte kvantifierade. Felen och osäkerheterna, som preliminärt uppskattats till att i allmänhet vara begränsade till några få grader (men som i vissa sektioner kan vara större), bedöms vara av ungefär samma storleksordning som fel och osäkerheter för övriga parametrar som diskuteras i rapporten, eller mindre än dessa. Dessutom är det främst borrhålsorienteringar som använts vid de mätkampanjer som ingår i analysen. Preliminärt kan effekterna därför bedömas ha begränsad betydelse för resultaten i denna rapport. En mer tillförlitlig analys av inverkan på spänningsberäkningarna är dock inte möjlig förrän orienteringarna av de geologiska strukturer som berörs har reviderats.

Contents

1	Introduction	9
2	Objective and scope	11
3	Rock stress measurements – a review of two methods, overcoring and hydraulic measurements, applied at the Forsmark site investigations	13
3.1	Overcoring (OC)	13
3.1.1	Measurement and analysis	13
3.1.2	Theory	15
3.2	Hydraulic fracturing (HF) and hydraulic tests on pre-existing fractures (HTPF)	16
3.2.1	Measurement and analysis	16
3.2.2	Theory for hydraulic fracturing (HF)	20
3.3	The Integrated Stress Determination Method (ISDM); Theory for hydraulic tests on pre-existing fractures (HTPF)	21
3.3.1	Parameterization	22
3.3.2	Inversion of overcoring and hydraulic data	24
3.3.3	Misfit functions	25
3.3.4	Monte Carlo search for <i>a priori</i> values to the Gradient method	27
3.3.5	General about the inversion method and help functions	27
4	The Forsmark site – analysis of rock stress data	29
4.1	General geological setting	29
4.2	Overcoring measurements in borehole KFM01B	32
4.2.1	Results of re-evaluation	33
4.2.2	Discussion of re-evaluation results	35
4.2.3	Correlation with geological/geophysical data	37
4.3	Overcoring measurements in borehole DBT-1	38
4.3.1	Results of brief re-evaluation	39
4.3.2	Correlation with geological/geophysical data	41
4.4	Overcoring measurements in borehole DBT-3	41
4.4.1	Results of brief re-evaluation	41
4.4.2	Correlation with geological/geophysical data	42
4.5	Hydraulic stress measurements in Forsmark	43
4.5.1	Borehole information	43
4.5.2	Choice of test sections	44
4.5.3	Parameterization of the stress field	45
4.5.4	Inversion procedure	45
4.5.5	Hydraulic fracturing tests	46
4.5.6	Hydraulic tests on pre-existing fractures (HTPF)	50
4.5.7	Determination of fracture orientations	52
4.5.8	Correlation with geological/geophysical data	53
5	New stress estimations	55
5.1	New stress inversions using all available unambiguous or partly unambiguous hydraulic data	55
5.1.1	The profiling approach	57
5.1.2	The cluster approach	57
5.2	Forced overcoring stress calculations	59
5.2.1	Results using Constraint 1	60
5.2.2	Results using Constraints 1 and 2	61
5.2.3	Results using Constraints 1, 2, and 3	63
5.2.4	Results using Constraints 1, 2, 3, and 4	65

5.3	Summary of results using overcoring stress data and comparisons with hydraulic solutions	66
5.4	Integrated approach – Joint overcoring and hydraulic stress calculations	67
5.4.1	Joint inversion	69
5.4.2	Summary of results using joint inversions	69
6	Discussion and conclusions	73
6.1	Overcoring data	73
6.2	Hydraulic data	74
6.3	New stress estimation	74
7	Acknowledgements	75
8	References	77
Appendix A	Single hole interpretation KFM01A, KFM01B, KFM02A, KFM04A including measurement depth for overcoring and hydraulic data	83

1 Introduction

As part of the site investigation programme managed by Swedish Nuclear Fuel and Waste Management Co (SKB), a re-evaluation of the existing overcoring and hydraulic rock stress data available up to and including 2004 from the Forsmark site was conducted. The re-evaluation, which is presented in this report, was based upon an integrated solution, which is directly dependent on the results from the overcoring and hydraulic measurement campaigns, and therefore it is first necessary to review the original results.

Normally, site investigations managed by SKB are performed in compliance with internal SKB controlling documents of two kinds: activity plans and method documents (the latter consisting of method descriptions, method instructions and descriptions of measurement systems). Regarding the present activity, there exist no SKB method documents, and the activity was not aiming at providing data to be stored in SKB's databases. SKB's instructions to the Contractor were presented during a meeting at the SKB Stockholm head office 2004-10-18 (participants: Activity Leader Rolf Christiansson, SKB, professor Derek Martin, University of Alberta, Canada (SKB representative) and Dr Daniel Ask, Vattenfall Power Consultant (Contractor representative)). The meeting was followed by e-mail correspondence with additional instructions and the work started 2004-10-27. The study was completed in April 2006 and refers to data from the Forsmark site investigation available prior to 2005.

In situ stress measuring methods represent point-wise estimates of local stress tensors that usually probe a considerably smaller rock volume than that of the rock mechanical problem in question. The regional stress tensor is obtained from successive rock stress measurements of local stress tensors. However, the regional stress tensor cannot, generally, be obtained simply by averaging local stress tensors because of their large variations /Amadei and Stephansson 1997/. Primarily, the variability in local stress tensors results from discontinuities in the rock volume. The results from the overcoring and hydraulic data sets are therefore reviewed with particular emphasis on the evaluation of uncertainties as well as on the validity of the hypothesis on homogeneity, continuity and linear elasticity.

The collected stress measurement data commonly involve a number of heterogeneous measurement points. Experience has shown that these outliers are a result of either the variability in the rock mass (e.g. discontinuities at different scales, rock boundaries, anisotropy) or a result of that the theoretical assumptions involved in the stress measuring technique are not fulfilled (e.g. linear-elastic, homogeneous, and isotropic rock mass; /Cornet et al. 2007/). Developing some understanding of these local stress variations helps reconcile results from other stress measuring techniques.

Throughout this report, stresses are denoted using a geomechanical sign convention with compressive stresses taken as positive. Stress orientations are given with respect to geographic North according to coordinate system RT90, 2.5 gon W 0:-15, using a right-hand rule notation.

2 Objective and scope

The primary objective of this report is to improve the knowledge of the *in situ* stress field at the Forsmark site through a uniform data analysis of overcoring and hydraulic stress measurements. A secondary objective is to identify heterogeneous measurement points and attempt to explain the causes for such deviations. The re-evaluated data set will be used for new stress determinations using the Integrated Stress Determination Method (ISDM; /Cornet 1993a, Ask 2004ab/).

The report includes compilation and analysis of overcoring and hydraulic stress measurements from the Forsmark site and assessment of the state of stress for the site considering geological/geophysical conditions.

The stress data chosen for the present analysis involve six boreholes, firstly KFM01A, KFM01B, KFM02A, and KFM04A (Figure 2-1), in which hydraulic stress measurements have been carried out within the currently performed site investigation. In borehole KFM01B overcoring rock stress measurements have been performed as well. Secondly, boreholes DBT-1 and DBT-3 (Figure 2-1), which are also included in the analysis, were drilled and overcoring rock stress measurements performed in the 1970's during projecting of the Forsmark nuclear power plants, whereas the overcoring measurements in KFM01B were performed in 2003 as part of the Forsmark site investigations.

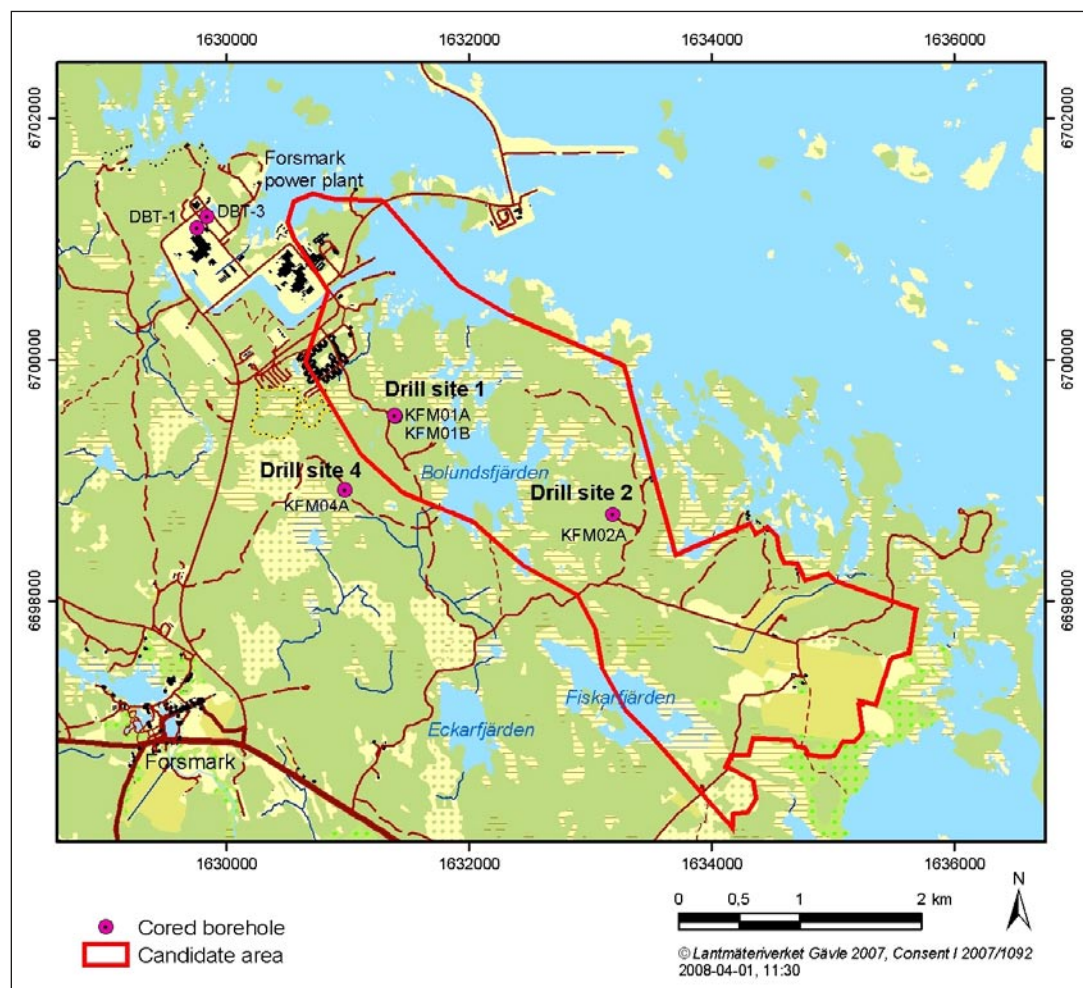


Figure 2-1. Map of the Forsmark site investigation area with the candidate area selected for the most abundant investigations. The cored boreholes inside and outside the candidate area included in the analysis of rock stress measurements presented in this report are shown.

3 Rock stress measurements – a review of two methods, overcoring and hydraulic measurements, applied at the Forsmark site investigations

3.1 Overcoring (OC)

3.1.1 Measurement and analysis

The overcoring method is based on coring a larger diameter borehole over a coaxial small-diameter pilot hole in which a strain-measuring instrument is installed. During overcoring, a rock sample containing the measurement device is, partially or entirely, relieved from the stress field in the surrounding rock mass. The state of stress is inferred from measurement of strain (or displacement) associated with the relief /Amadei and Stephansson 1997/.

The overcoring data involved in this report, performed in the cored boreholes KFM01B, DBT-1, and DBT-3, emerge from measurements conducted with the *Borre Probe* /Sjöberg and Klasson 2003/ and the *SSPB cell* /Ingevald and Strindell 1981/, respectively, which are both CSIR-type cells including 9 strain gauges in the axial and tangential directions, as well as gauges inclined 45° from the axial direction. The *SSPB cell* is the pre-decessor of the *Borre Probe*, which has undergone several major improvements during three decades.

The strain used for stress calculation was chosen at stable points before and after the overcoring process (Figure 3-1). The standard deviation of the strain measurements should preferably be determined from the distribution of strain gauge readings with the same or similar orientation in the borehole. However, in the present case with limited data in each borehole, such an estimation could not be conducted. Instead, the observed difference between measured and calculated strains using standard least squares technique was assumed to correspond to a 99% confidence interval of the strains. Strictly, this does not correspond to standard deviation as the approach mixes two sorts of errors – those associated with the measurement process and those associated with the interpretative model – which is not a rigorous method.

Following overcoring, the recovered overcore sample is placed in a biaxial test chamber to determine the elastic parameters Young's modulus, E , and Poisson's ratio, ν . During biaxial testing, the overcore sample is first subjected to a step-wise increase in applied pressure to the desired maximum pressure level (10 MPa for the *Borre Probe* to avoid fracturing of the overcore sample; /Ask 2003a/), followed by a step-wise decrease to zero pressure while the resulting strains are measured /e.g. Amadei and Stephansson 1997/. The loading and unloading thus allows examination of possible inelastic and anisotropic behaviour of the overcore sample /Amadei 1983ab/. The results are plotted as strains versus applied pressure (Figure 3-2) and, in theory, the strain gauges within each group (i.e. axial, tangential, and 45° inclined) should respond identically to loading/unloading (see insert in Figure 3-2). To mimic the overcoring phase, the values of E and ν are taken as secant values, calculated from the strain data during the unloading of the overcore sample.

This course of action for biaxial testing was followed for the measurements in KFM01B. As for boreholes DBT-1 and DBT-3 a combination of uniaxial- and biaxial testing was applied (cf. Sections 4.3 and 4.4). However, the documentation of these tests is not accurate enough to permit a firm analysis of quality aspects of the testing procedure, which hence hampers a reliable assessment of data and uncertainties involved.

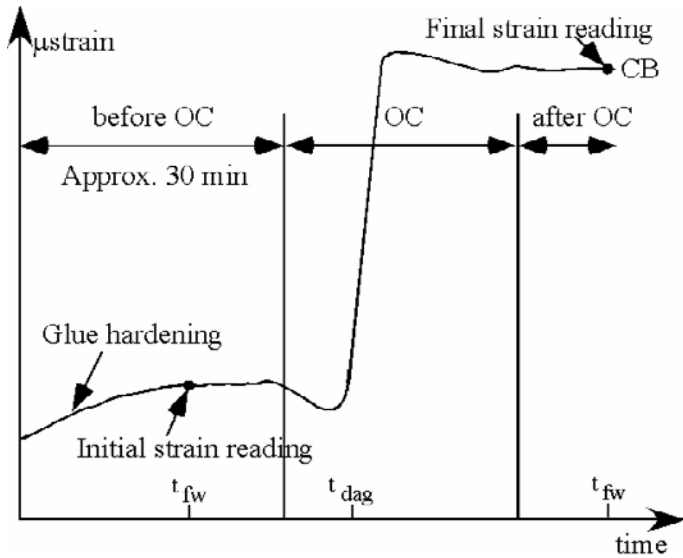


Figure 3-1. Schematic response of a tangential strain gauge versus time during OC. The strongest strain gauge response occurs at t_{dag} , i.e. when the drill bit is at the position of the strain gauge. The time interval before overcoring is occupied by the glue hardening process. t_{fw} and CB denote the time when flush-water is activated/terminated and core breaks, respectively (modified after /Ask 2003a/).

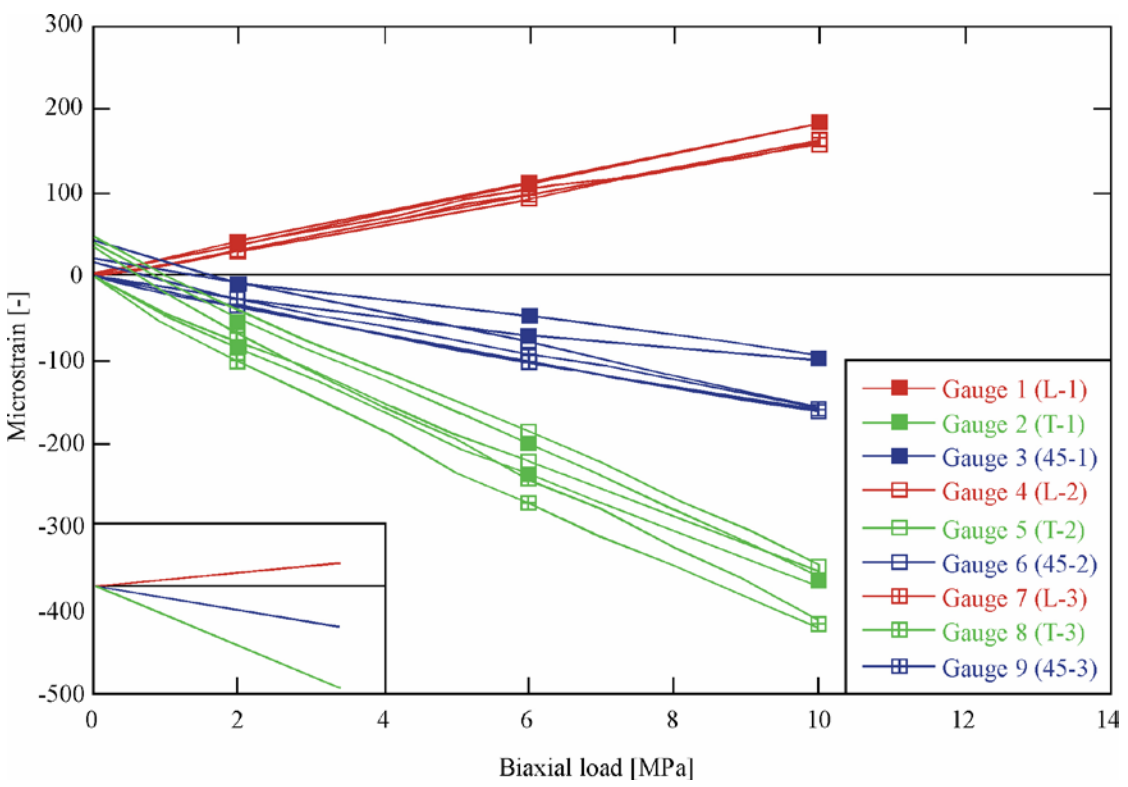


Figure 3-2. Result from biaxial testing in borehole KAV04A, Oskarshamn site, with hypothetical results from biaxial testing of an ideal elastic material in the lower left corner (modified after /Ask 2008/).

3.1.2 Theory

The overcoring theory generally assumes that the rock is linearly elastic and isotropic, although anisotropic solutions exist /e.g. Amadei and Stephansson 1997/. The deformation of the overcore sample during stress relief is assumed to be identical in magnitude to that produced by the *in situ* stress field, but of opposite sign. Application of elastic theory also requires knowledge of the elastic parameters of the overcore sample, Young's modulus, E , and Poisson's ratio, ν . Furthermore, it is assumed that the rock mass is both continuous and homogeneous and that the measuring probe is mounted far enough from the end of the borehole, to ensure that no stress/strain variations exist along the axis of the probe /e.g. Merrill 1964, Amadei and Stephansson 1997/. With these assumptions, displacements from stress concentrations around a borehole are given by /Hirashima and Koga 1977/:

$$u_r = \frac{1+\nu}{2E} r \left[\frac{R^2}{r^2} (\sigma_x + \sigma_y) + \left\{ 1 + 4(1-\nu) \frac{R^2}{r^2} - \frac{R^4}{r^4} \right\} \{ (\sigma_x - \sigma_y) \cos 2\theta + 2\tau_{xy} \sin 2\theta \} \right. \\ \left. + \left\{ \frac{1-\nu}{1+\nu} (\sigma_x + \sigma_y) - 2 \frac{\nu}{1+\nu} \sigma_z \right\} \right] \quad (1)$$

$$u_\theta = -\frac{1+\nu}{2E} r \left[\left\{ 1 + 2(1-2\nu) \frac{R^2}{r^2} + \frac{R^4}{r^4} \right\} \{ (\sigma_x - \sigma_y) \sin 2\theta - 2\tau_{xy} \cos 2\theta \} \right] \quad (2)$$

$$u_z = \frac{1+\nu}{E} \left[2r \left(1 + \frac{R^2}{r^2} \right) (\tau_{yz} \sin \theta + \tau_{zx} \cos \theta) + \frac{z}{1+\nu} \{ \sigma_z - \nu(\sigma_x + \sigma_y) \} \right] \quad (3)$$

where R is the borehole radius, r the radial distance to the measurement point, and θ is the location of a strain gauge in the borehole according to the chosen coordinate system. The *Borre Probe* device includes strain gauges in the axial and tangential directions as well as gauges inclined 45° from the axial direction. For these orientations, the following relationships are valid:

$$\epsilon_\theta = \frac{1}{R} \left\{ (u_r)_{r=R} + \left(\frac{\partial u_\theta}{\partial \theta} \right)_{r=R} \right\} \quad (4)$$

$$\epsilon_z = \left(\frac{\partial u_z}{\partial z} \right)_{r=R} \quad (5)$$

$$\gamma_{\theta z} = \frac{1}{R} \left(\frac{\partial u_z}{\partial \theta} \right)_{r=R} \quad (6)$$

$$\epsilon_{45^\circ} = \frac{1}{2} (\epsilon_\theta + \epsilon_z + \gamma_{\theta z}) \quad (7)$$

where

$$\frac{\partial u_\theta}{\partial \theta} \Big|_{r=R} = -\frac{4(1-\nu^2)}{E} R [(\sigma_x - \sigma_y) \cos 2\theta + 2\tau_{xy} \sin 2\theta] \quad (8)$$

$$\frac{\partial u_z}{\partial z} \Big|_{r=R} = \frac{1}{E} [\sigma_z - \nu(\sigma_x + \sigma_y)] \quad (9)$$

$$\frac{\partial u_z}{\partial \theta} \Big|_{r=R} = \frac{R}{E} [4(1+\nu)(\tau_{yz} \cos \theta - \tau_{zx} \sin \theta)] \quad (10)$$

Combining Equations 4 to 10 and using $r = R$, gives the final solution:

$$\varepsilon_{\theta} = \left[(\sigma_x + \sigma_y) - 2(1 - \nu^2) \{ (\sigma_x - \sigma_y) \cos 2\theta + 2\tau_{xy} \sin 2\theta \} - \nu\sigma_z \right] / E \quad (11)$$

$$\varepsilon_z = \left[\sigma_z - \nu(\sigma_x + \sigma_y) \right] / E \quad (12)$$

$$\varepsilon_{\pm 45^\circ} = 0.5(\varepsilon_{\theta} + \varepsilon_z \pm 4(1 + \nu)(\tau_{yz} \cos\theta - \tau_{zx} \sin\theta) / E) \quad (13)$$

The elastic properties are derived using the theory for an infinitely long, thick-walled circular cylinder subject to uniform external pressure, and the assumption that plane stress applies /e.g. Worotnicki 1993, Amadei and Stephansson 1997/:

$$E = \frac{p}{\varepsilon_{\theta}} \frac{2}{1 - \left(\frac{D_i}{D_o} \right)^2} \quad (14)$$

$$\nu = -\frac{\varepsilon_z}{\varepsilon_{\theta}} \quad (15)$$

where p is the applied load, ε_{θ} and ε_z are the tangential and axial strains, respectively, and D_i and D_o are the inner and outer diameters of the cylinder, respectively.

3.2 Hydraulic fracturing (HF) and hydraulic tests on pre-existing fractures (HTPF)

3.2.1 Measurement and analysis

A hydraulic fracturing (HF) measurement involves subsequent pressurization of a sealed-off section in a borehole until the borehole wall fractures. During these measurements, the pressure in the sealed-off test section versus time is recorded (Figure 3-3). The pressure required to induce fractures is called the breakdown pressure, P_b . Succeeding re-pressurizations, resulting in re-opening pressures, P_r , are usually defined as the points, for each pressurization cycle, where the pressure-time curve begins to deviate from linearity (Figure 3-3). A more objective method for defining P_r using the statistical reference threshold method is given in /Lee and Haimson 1989/.

When the hydraulic system is sealed, or shut-in, two mechanisms are controlling the observed pressure drop in the test section: (1) the movement of the fluid in the system is stopped, giving zero frictional losses (difference between propagation pressure and instantaneous shut-in pressure, P_s); and (2) the excess fluid in the system, which is a function of the system compressibility, further propagates the fracture and depletes into the rock mass (difference between P_s and fracture closure pressure). This yields the instantaneous shut-in pressure, P_s , on the pressure time curve. At that instant, the pressure in the test section is equal to the magnitude of the minimum horizontal stress.

The shut-in pressure, P_s , was originally determined using graphical methods, e.g. the inflection point method /Gronseth and Kry 1983/, the maximum curvature method /Hardy 1973, Hayashi and Sakurai 1989/, or the tangent intersection method /Enever and Chopra 1986/, Figure 3-4.

Later, when data sampling became digital, more advanced methods were applied, which are summarized in /Guo et al. 1993/. /Klee and Rummel 2004/ used the inflection point method to determine P_s in hydraulic fracturing measurements at the Forsmark site. However, they also specified maximum (at zero flow) and minimum (Muskat method; /Aamodt and Kuriyagawa 1981/ shut-in pressures, P_{smax} and P_{smin} . In this report, the maximum and minimum shut-in pressures determined by /Klee and Rummel 2004/ were used to describe the confidence intervals

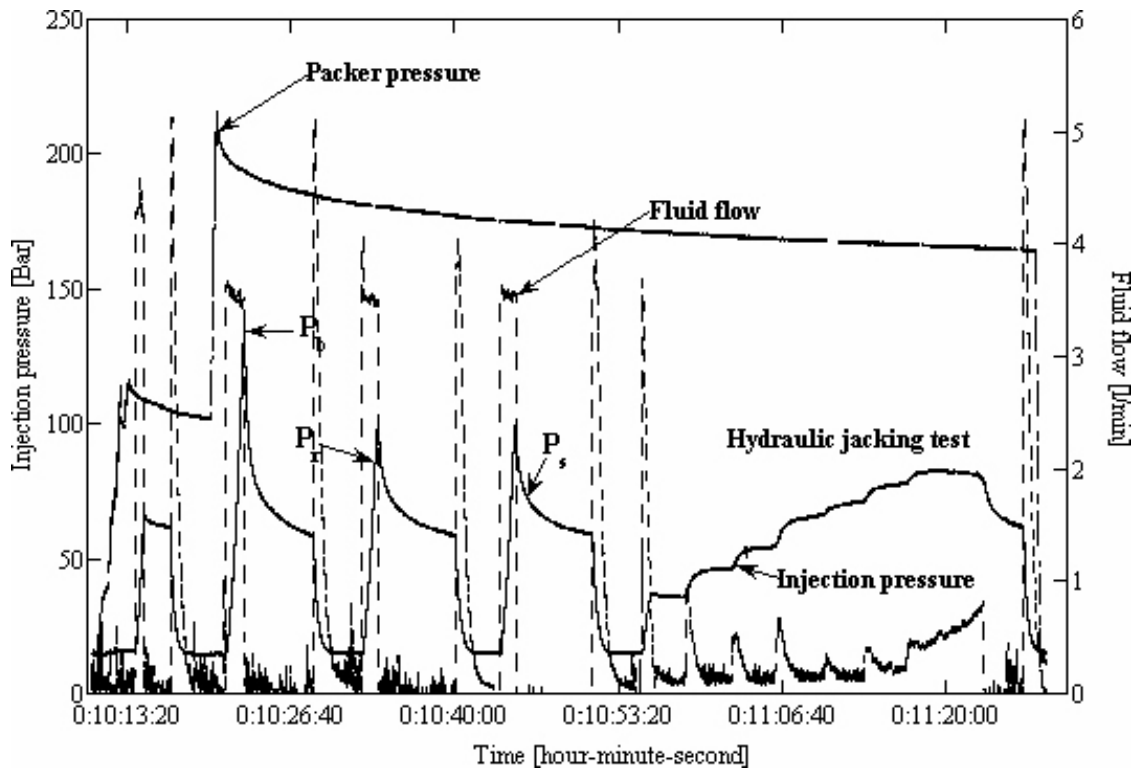


Figure 3-3. Pressure versus time record from a hydraulic fracturing measurement with permeability test, fracturing and two re-opening cycles and finally a hydraulic jacking test or step-pressure test /after Ask 2003b/.

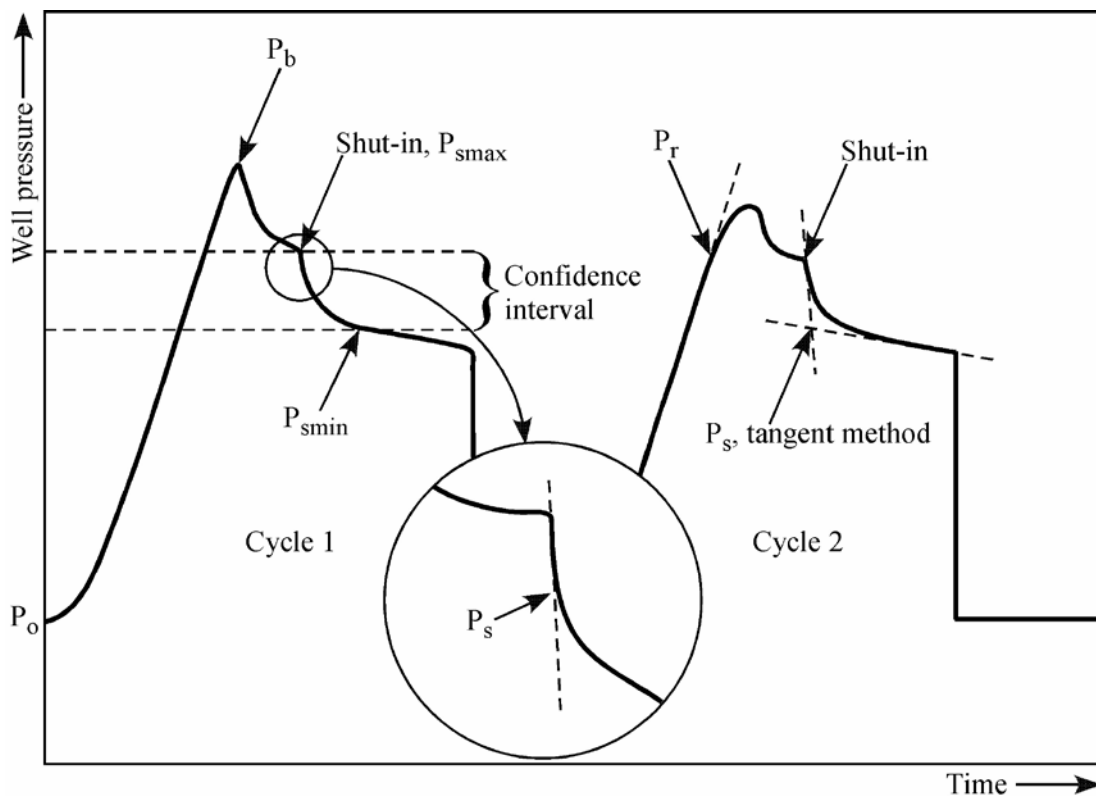


Figure 3-4. Idealized pressure versus time record from a hydraulic fracturing measurement and determination of P_s using the inflection point method (first cycle) and tangent method (second cycle). P_o denotes the formation pore pressure /after Ask 2004b/.

(99%) for the shut-in pressures, Figure 3-4. It is outside the scope of this report to use other interpretation methods to determine P_s , but the methods of /Klee and Rummel 2004/ will be briefly discussed in Section 4.5.

The HTPF method (Hydraulic Testing of Pre-existing Fractures) is normally associated with a hydraulic jacking or step-pressure test (Figure 3-3 and Figure 3-5), which is made to determine the borehole pressure that exactly balances the fracture normal stress. A steady injection flow should be attained at each pressure level, before proceeding to the next level. The distinctive features of the pressure curve in Figure 3-5 are two slightly non-linear slopes connected with a plateau part. This plateau is used to determine the fracture normal stress. Generally, it is assumed that the fracture remains closed for pressures less than the fracture normal stress. For pressures above the fracture normal stress, the fracture opens, and a considerably higher flow rate is required to keep the fracture open. The fracture re-opening is gradual, and depends on the fracture normal stiffness and effective stress inside the fracture near the borehole /Rutqvist 1995/. In tests on granite, /Cornet et al. 2003/ showed that the fracture normal stress from hydraulic jacking may be overestimated for a mean fracture opening of less than 15–20 μm , and for a channeling-controlled fluid flow. They concluded that hydraulic jacking tests should discard results from the opening phase.

A cyclic hydraulic jacking test consists of a step-wise increase in borehole pressure to a maximum flow rate. This is followed by a step-wise decrease in borehole pressure until back-flow is obtained /e.g. Rutqvist 1995/. Back-flow occurs when the injection flow is too small to keep the fracture open. As the fracture closes, the flow is reversed, causing a temporary flow increase on the flow chart /Rutqvist and Stephansson 1996/. The results are plotted on graphs for borehole pressure versus fluid flow at the end of each pressure level (Figure 3-6).

The orientations of the fractures are usually determined with oriented impression packers, geophysical logging, or electrical imaging methods /Haimson and Cornet 2003/. Each of these tools have drawbacks: (1) impression packers yield unsatisfactory results in strongly inclined boreholes and for test sections with multiple fractures; (2) the resolution of geophysical logs may not allow detection of very small fractures; and (3) electrical images may yield unsatisfactory results in certain rock types such as claystone and salt (although recently improved; /Haimson and Cornet 2003/). For an axially induced fracture in a vertical borehole, the orientation of maximum horizontal stress, σ_H , is equal to the strike of the fracture, Figure 3-7. The minimum horizontal stress, σ_h , is perpendicular to σ_H .

Because the HTPF solution is obtained by an inversion scheme, it is crucial that the fracture orientations are accurately known to reduce uncertainties in the solution (fracture azimuth is generally most important). If there are multiple fractures within the HTPF test section, it is also very important to determine which of these fractures that has been opened. Therefore, electrical imaging tools are preferable. The method for determining the fracture orientation and its standard deviation of an inclined fracture is given in Figure 3-8. Two sinusoidal curves are drawn which

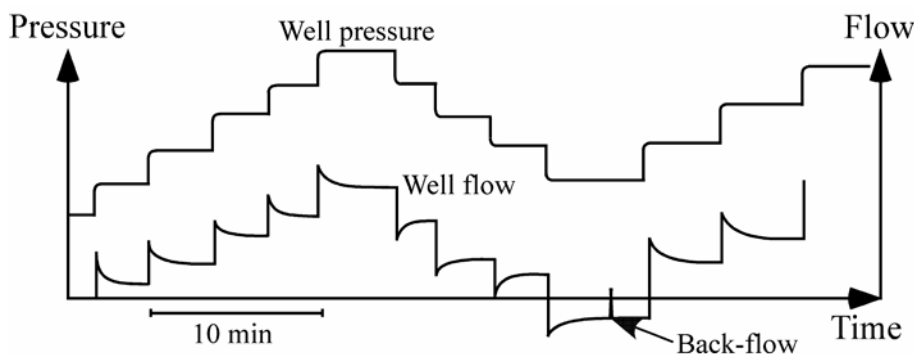


Figure 3-5. Pressure and flow rate versus time record from hydraulic jacking test /after Rutqvist 1995/.

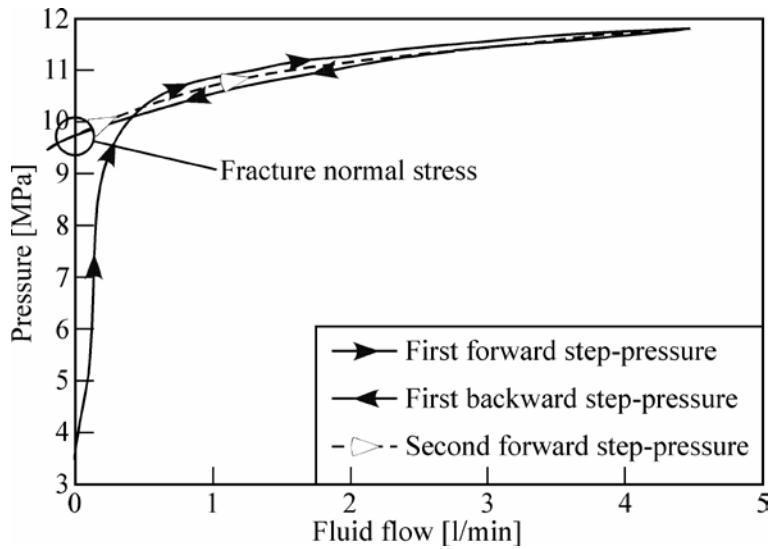


Figure 3-6. Pressure versus flow rate and determination of fracture normal stress at zero-flow pressure of a cyclic hydraulic jacking test /modified after Rutqvist and Stephansson 1996/.

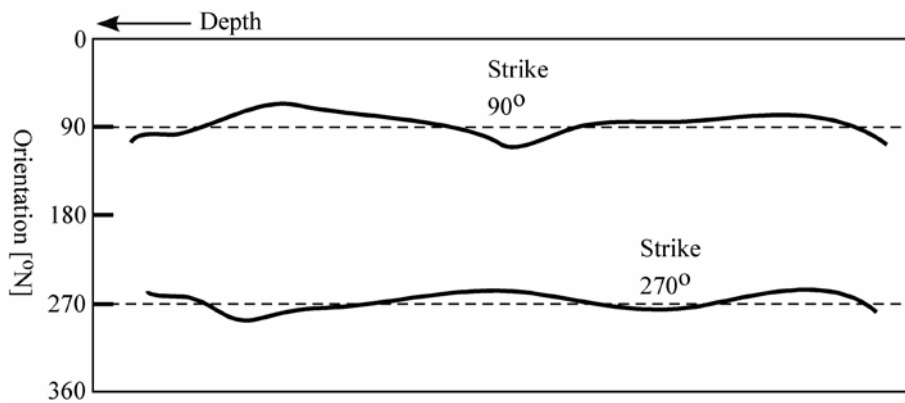


Figure 3-7. Imprint of an induced axial fracture (solid lines) and mean vertical plane occupied by the fracture (dashed lines; after /Ask 2004a/).

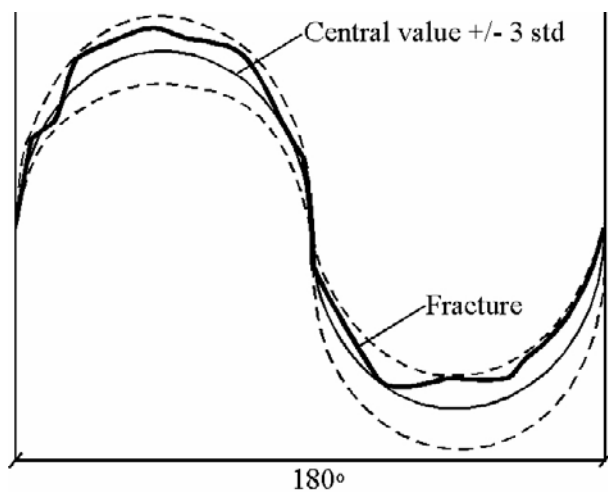


Figure 3-8. Schematic view of how fracture orientation and standard deviation is determined for an inclined fracture. Two sinusoidal curves (dotted lines) that completely cover the extent of the fracture (thick solid line) describe the standard deviation of the fracture orientation, whereas its orientation is given by the central value (thin solid line; modified after /Ask 2001/).

completely cover the extent of the fracture (dotted lines in Figure 3-8) and the fracture orientation is then given by the central value, whereas its standard deviation is determined from the scatter described by the two sinusoidal curves /Ask 2001/.

3.2.2 Theory for hydraulic fracturing (HF)

Consider a vertical borehole in a horizontal plate composed of an ideally elastic and isotropic material with one of the principal stresses in the direction of the borehole, and subjected to a homogeneous stress field. The resulting stress concentration around the borehole includes radial (σ_{rr}), circumferential ($\sigma_{\theta\theta}$), and shear stresses ($\sigma_{r\theta}$; Figure 3-9). Their theoretical relationship for applied far-field stresses has been described by /Kirsch 1898/ and /Jaeger and Cook 1969/:

$$\sigma_{rr} = \frac{(\sigma_H + \sigma_h)}{2} \left(1 - \frac{R^2}{r^2}\right) + \frac{(\sigma_H - \sigma_h)}{2} \left(1 - 4\frac{R^2}{r^2} + 3\frac{R^4}{r^4}\right) \cos 2\theta + \Delta P \frac{R^2}{r^2} \quad (16)$$

$$\sigma_{\theta\theta} = \frac{(\sigma_H + \sigma_h)}{2} \left(1 + \frac{R^2}{r^2}\right) - \frac{(\sigma_H - \sigma_h)}{2} \left(1 + 3\frac{R^4}{r^4}\right) \cos 2\theta - \Delta P \frac{R^2}{r^2} \quad (17)$$

$$\sigma_{r\theta} = -\frac{(\sigma_H - \sigma_h)}{2} \left(1 + 2\frac{R^2}{r^2} - 3\frac{R^4}{r^4}\right) \sin 2\theta \quad (18)$$

where σ_H and σ_h are the maximum and minimum horizontal stresses, R is the borehole radius, r the radial distance to the measurement point, ΔP is difference between the borehole fluid pressure, P_b , and the formation pore pressure, P_o . Note that these equations are subject to the hypothesis of fluid percolation (in case fluid percolation is absent, the term $\Delta P \cdot R^2/r^2$ is reduced to ΔP in Equations 16 and 17). At the borehole wall, where $r = R$, the formulas reduce to:

$$\sigma_{rr} = P_b - P_o \quad (19)$$

$$\sigma_{\theta\theta} = (\sigma_H + \sigma_h) - 2(\sigma_H - \sigma_h) \cos 2\theta - P_b - P_o \quad (20)$$

$$\sigma_{r\theta} = 0 \quad (21)$$

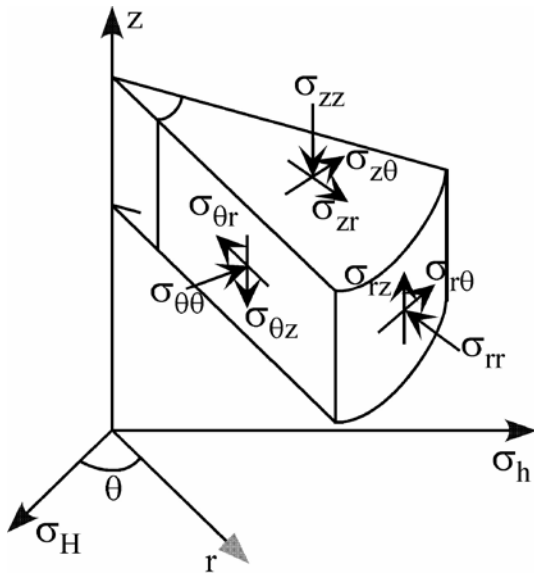


Figure 3-9. Coordinate system and the orientation of stress components in cylindrical coordinates (modified after /Lund 2001/ and /Brudy 1995/).

Maximum and minimum stress concentrations occur at $\theta = 90^\circ$ and $\theta = 0^\circ$. These two angles represent the borehole breakout and hydraulic fracturing conditions, respectively. For the hydraulic fracturing case, Equation (20) reduces to:

$$\sigma_{\theta=0^\circ} = 3\sigma_h - \sigma_H - P_b - P_o \quad (22)$$

At the time of fracture initiation, $\sigma_{\theta=0^\circ} = -T$, where T is the tensile strength of the material. Rearranging Equation (22) then gives the classical hydraulic fracturing formula /Hubbert and Willis 1957/:

$$\sigma_H = T + 3\sigma_h - P_b - P_o \quad (23)$$

A few different solutions for σ_H exist depending on if the rock is porous or non-porous and if the fluid is penetrating or non-penetrating /e.g. Schmitt and Zoback 1989, Amadei and Stephansson 1997, Ito et al. 1999/. Equation (23) is dependent on the tensile strength of the rock, which normally is determined using Brazilian tests and, less commonly, using hydraulic fracturing measurements on cores /Haimson and Cornet 2003/. One drawback with the Brazilian test is that it does not mimic the conditions of the hydraulic fracturing test, and it has not been established that the obtained tensile strength is representative for hydraulic fracturing measurements /Haimson and Cornet 2003/. Both methods include a scale-effect between field and laboratory dimensions. For cases where the tensile strength is not known, /Bredehoeft et al. 1976/ introduced a modified hydraulic fracturing equation:

$$\sigma_H = T + 3\sigma_h - P_r - P_o \quad (24)$$

The modified hydraulic fracturing equation has several known uncertainties: (1) there is a non-zero residual aperture after each pressurization cycle and the re-opening pressure, P_r , is therefore dependent on the pressurization rate /e.g. Ratigan 1992, Cornet 1993a, Rutqvist 1995, Rutqvist et al. 2000/; (2) P_r may not be identified objectively on the pressure time record because the fluid volume that is pumped into the test section far exceeds the volume that enters the fracture /Ito et al. 1999/. /Ito et al. 1999/ concluded that the system compliance must be very low (less than $5 \cdot 10^{-7} \text{ m}^3/\text{MPa}$) for correct identification of P_r , and for measurements at great depth a down-hole flow meter is essential; and (3) the induced fracture disturbs the assumption of linear-elastic, homogeneous, and isotropic rock conditions, entailing that P_r is always close to σ_h and independent of the value of σ_H /Rutqvist et al. 2000/. For these reasons, the magnitude of σ_H determined using Equation (24) is very uncertain.

HTPF measurements involve hydraulic tests on pre-existing planes of weakness with, preferably, a large range of fracture directions and inclinations /Cornet 1993a/. In case of multiple fractures within a test section, it is necessary to verify that only one single fracture has been opened. The HTPF method assumes planar fractures with persisting orientation away from the borehole but, unlike the hydraulic fracturing theory, it is independent of pore pressure and tensile strength.

The choice of parameterization for stress calculation depends on the number of measurement points and the range of orientations of the tested fractures. The theory of HTPF measurements is given in the next section describing the Integrated Stress Determination Method.

3.3 The Integrated Stress Determination Method (ISDM); Theory for hydraulic tests on pre-existing fractures (HTPF)

The Integrated Stress Determination Method (ISDM) was suggested as a tool for analysis of hydraulic tests on pre-existing fractures (HTPF) in the 1980s by /Cornet and Valette 1984/, and a full description of the method was presented by /Cornet 1993a/. However, as the name indicates, it was also intended as a means to integrate different types of stress measurement methods and stress indicators. The goal of this approach was to determine the stress field based

on a larger amount of data than normally conducted. Up to date, the ISDM has been used to determine the stress field using HTPF, conventional hydraulic fracturing (HF), flat jack, induced seismicity, focal mechanisms, and various combinations of these. Recently, the theory has been extended also to involve overcoring (OC; four different overcoring devices; /Ask 2004ab/. This latest development includes a possibility to integrate HTPF, HF and OC.

The ISDM involves several steps that for each case study must be considered (Figure 3-10; /Ask 2004a/): (1) the number and type of available data define the parameterization of the stress field within the rock volume of interest. An increasing number of data can solve an increasing number of unknown parameters, provided that the stress data sample more than one stress vector. For example, because the induced fracture during HF generally is parallel with the bore-hole axis, such data can only be used to determine the magnitude and orientation of minimum horizontal stress; (2) the rock volume, which is defined by the distribution of the available stress data, should be considered with respect to the homogenization criterion. Existing discontinuities may lead to sub-divisions of the rock volume and thereby sub-divisions of the data set; (3) selection of a proper mathematical algorithm. The early applications of the ISDM were based on a non-linear least squares method (applied in this report and referred to as the Gradient method) but recent work has been based on Genetic Algorithms /e.g. Yin 1994/; (4) *a priori* values for the Gradient method are determined from available stress data or by using Monte Carlo search for model parameters; and finally (5) the solution is verified (fit with data, resolution of the unknown parameters, strict minimum, comparison with Monte Carlo solutions; Figure 3-10).

In the ISDM, all measurements are assumed to follow normal distribution, i.e. they may be described by their expected value, variance and covariances with other measurements. The analyses of the hydraulic fracturing and overcoring data thus require estimation of the standard deviation of the measured parameters, which is visualized in the following section.

3.3.1 Parameterization

The measured rock volume is discretized into sub-volumes in which the stress field is approximated by its first order linear expansion /Cornet 1993a/. The stress at a point X^m of the m^{th} measurement is given by

$$\sigma(X^m) = \sigma(X) + (x^m - x)\alpha^{[x]} + (y^m - y)\alpha^{[y]} + (z^m - z)\alpha^{[z]} \quad (25)$$

where $\sigma(X^m)$ and $\sigma(X)$ represent the stress tensor in points X^m and X , respectively, and $\alpha^{[x]}$, $\alpha^{[y]}$, and $\alpha^{[z]}$ are second-order symmetrical tensors characterizing the stress gradient in the x -, y - and z -directions.

Equation (25) satisfies the following equilibrium constraints:

$$\text{div}(\sigma(X^m)) - \rho(X)b_i = 0 \quad (26)$$

where $\rho(X)$ is the density of the rock mass in the point X , and b_i is the gravitational acceleration ($b_i = g\delta_{i3}$; $\delta_{i3} = 0$ for $i \neq 3$; $\delta_{i3} = 1$ for $i = 3$). The first order approximation of the stress field requires determination of 22 parameters. If the data set is too small to determine all 22 parameters, the number of unknowns can be reduced using the following assumptions: (1) the lateral stress variations are zero; (2) one principal stress is vertical throughout the volume; (3) if 2 applies, the rock mass density is obtained from direct measurements on cores; (4) there is no rotation of principal stresses (in small rock volumes); (5) the stress field is continuous up to ground surface.

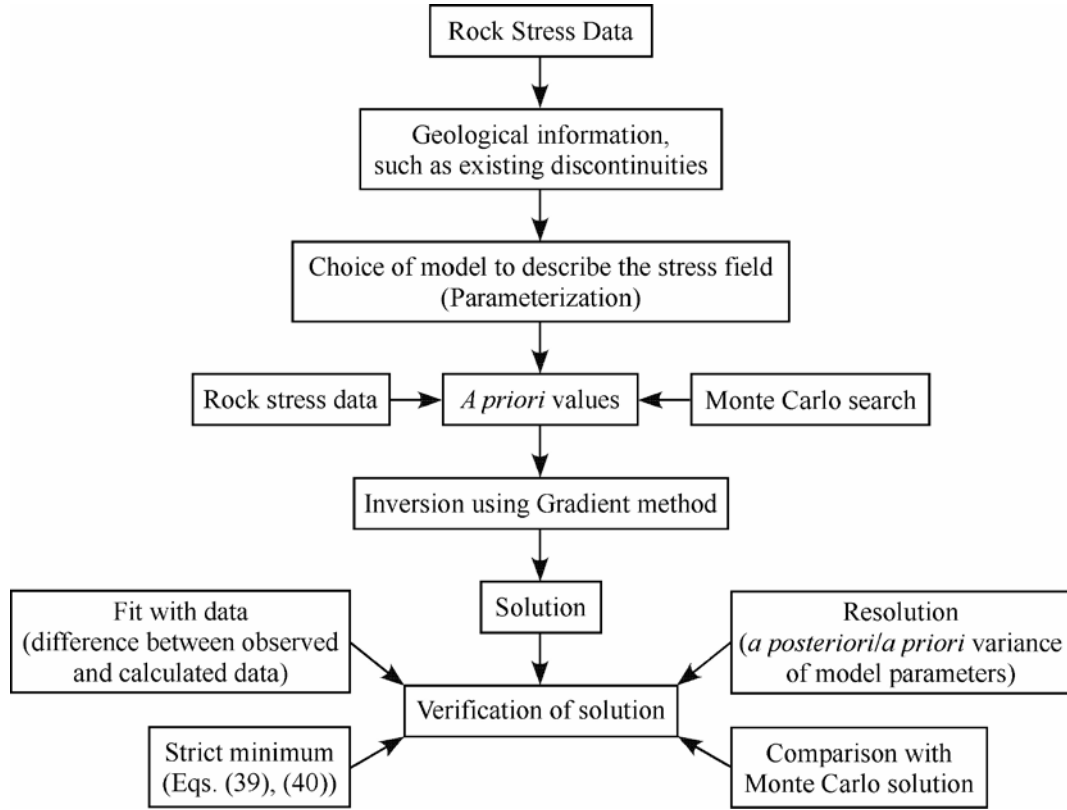


Figure 3-10. Approach for stress determination using the ISDM based on the Gradient method. The rock stress data and the geological/geophysical information control the parameterization of the stress field in the rock mass. A priori values for the Gradient method are derived from available data or from Monte Carlo simulations. When a solution has been found, it is verified using four methods /after Ask 2004a/.

/Klee and Rummel 2004/ applied an ISDM based on Monte Carlo simulation /e.g. Baumgärtner and Rummel 1989/ at the Forsmark site. They assumed that lateral stress variations can be neglected, that the boreholes are vertical and aligned with a principal stress direction, and that the stresses vary linearly with depth. With these assumptions, the stress field is given by seven unknown parameters and the normal stress can be expressed as:

$$\sigma_n(z_i) = (\sigma_{vo} + \alpha_v \cdot z_i) \cdot \cos^2 \varphi_i + \frac{1}{2} \sin^2 \varphi_i \cdot \left\{ \begin{array}{l} \sigma_{Ho} + \sigma_{ho} + (\alpha_H + \alpha_h) \cdot z_i - (\sigma_{Ho} - \sigma_{ho}) \cos 2(\theta_i' - \theta'') \\ -(\alpha_H - \alpha_h) \cdot z_i \cdot \cos 2(\theta_i' - (\theta'' + \eta)) \end{array} \right\} \quad (27)$$

where θ_i' and φ_i are the strike and dip angle of the fracture plane, σ_{vo} , σ_{Ho} , and σ_{ho} are the principal horizontal stresses at the upper limit of the investigated borehole section, α_v , α_H , and α_h are the vertical and horizontal stress gradients, θ'' is the orientation of σ_{Ho} with respect to North, and the angle η takes into account a possible stress field rotation with depth /Klee and Rummel 2004/.

In this report, lateral stress gradients were neglected, i.e. Equation (25) is reduced to

$$\sigma(X^m) = \sigma(X) + (z^m - z)\alpha^{[z]} \quad (28)$$

In the chosen parameterization, $\sigma(X)$ and $\alpha^{[z]}$ are expressed with three Euler angles and three principal values. For $\sigma(X)$, the eigenvalues are S_1 to S_3 and the three Euler angles are E_1 to E_3 , which are expressed in the geographical frame of reference. Corresponding eigenvalues for

$\alpha^{[i]}$ are α_1 to α_3 and the three Euler angles E_4 to E_6 , which are expressed in the $\sigma(X)$ frame of reference. Thus, the gradients α_1 - α_3 correspond to the vertical gradient of S_1 - S_3 only if E_1 - E_3 are equal to E_4 - E_6 /Ask 2004ab/.

3.3.2 Inversion of overcoring and hydraulic data

The ISDM assumes that an *a priori* knowledge of the unknown model parameters exist, which can be formulated in terms of expected value, variance and covariances. In practice, large error bars are placed on assumed central values for the unknown parameters. The HF and HTPF data involve 4 components: the depth, z^m , of the m^{th} fracture plane, the dip direction, ϕ^m , and the dip, φ^m , of the normal to the m^{th} fracture plane with respect to the vertical direction, and the fracture normal stress, σ_n^m . The OC data set includes 12 components: four device dependent correction factors, K_1^n - K_4^n (equal to 1 for the *Borre Probe*), the depth, z^n , of the n^{th} measurement, the dip direction, ϕ^n , and the dip, φ^n , of the n^{th} borehole, the rosette angle, the rotation angle (for the *Borre Probe*), the strain, and the elastic parameters. Thus, for a 12-parameters problem, HF and HTPF data involve $4m+12 = M$ components for m measurements and the OC data $12n+12 = N$ components for n measurements /Ask 2004ab/.

The general expression for the fracture normal stress, σ_n , from HF and HTPF is:

$$\left[\sigma(X^m) \vec{n}^m \right] \vec{n}^m = \sigma_{normal}^m \quad (29)$$

where n^m is the normal of the m^{th} fracture plane and includes the dip direction ϕ^m and the dip φ^m of the normal to the m^{th} fracture plane with respect to the vertical direction.

Corresponding relationships between stress and measured strains in a borehole are:

$$\varepsilon_\theta = \left[(\sigma_x + \sigma_y) K_1 - 2(1-\nu) \left\{ (\sigma_x - \sigma_y) \cos 2\theta + 2\tau_{xy} \sin 2\theta \right\} K_2 - \nu \sigma_z K_4 \right] / E \quad (30)$$

$$\varepsilon_z = \left[\sigma_z - \nu(\sigma_x + \sigma_y) \right] / E \quad (31)$$

$$\varepsilon_{\pm 45^\circ} = 0.5 \left[\varepsilon_\theta + \varepsilon_z \pm 4(1+\nu) (\tau_{yz} \cos \theta - \tau_{zx} \sin \theta) K_3 \right] / E \quad (32)$$

Using HF data to exemplify the methodology, Equation (27) can be formulated in matrix form according to:

$$\sigma_n^m = \left(\left[SB \left[S^\circ + (z^m - z) \cdot AB \cdot A^\circ \cdot AB^T \right] SB^T \right] \vec{n}^m \right) \vec{n}^m \quad (33)$$

where matrices S° and A° represent the stress and gradient tensors, AB includes Euler angles E_4 to E_6 , which describe A° in the S° frame of reference, SB includes the Euler angles E_1 to E_3 , which describe $S^\circ + (z^m - z) \cdot AB \cdot A^\circ \cdot AB^T$ in the geographical frame of reference, z^m is the depth of the m^{th} fracture, and z is the chosen calculation depth (normally the average depth of the data set; /Ask 2004ab/).

A vector π_0 can be created which includes *a priori* values according to:

$$\pi_0 = \text{col} \left[\begin{array}{l} (z_o, \phi_o, \varphi_o, \sigma_{no})^1, \dots, (z_o, \phi_o, \varphi_o, \sigma_{no})^M, \\ E_1, E_2, E_3, E_4, E_5, E_6, S_1, S_2, S_3, \alpha_1, \alpha_2, \alpha_3 \end{array} \right] \quad (34)$$

The corresponding covariance matrix is denominated C_o and is diagonal because measurements and unknowns are supposed to be independent /Cornet 1993b/. Corresponding computed or *a posteriori* vector π is of the form:

$$\pi = \text{col} \left[\begin{array}{l} (z, \phi, \varphi, \sigma_n)^1, \dots, (z, \phi, \varphi, \sigma_n)^M, \\ E_1, E_2, E_3, E_4, E_5, E_6, S_1, S_2, S_3, \alpha_1, \alpha_2, \alpha_3 \end{array} \right] \quad (35)$$

A vector function $f(\pi)$ may be introduced in which the m^{th} component is defined by:

$$f^m(\pi) = \sigma_n^m - \left((SB[S^o + (z^m - z) \cdot AB \cdot A^o \cdot AB^T]SB^T)n^m \right) \quad (36)$$

Note that for the overcoring case, there are three different expressions for $f^m(\pi)$; for axial, tangential and 45°-inclined gauges. Continuing with the hydraulic fracturing data case, the solution of the inverse problem is defined by the minimum of:

$$(\pi - \pi_o)^T C_o^{-1} (\pi - \pi_o) \quad (37)$$

The problem is a conditional least square, i.e. the minimum of the least squares criterion (Equation 37) is sought that satisfies the condition $f(\pi) = 0$. /Tarantola and Valette 1982/ showed that this could be solved using the iterative algorithm based on the fixed-point method:

$$\pi_{n+1} = \pi_o + C_o F_n^T (F_n C_o F_n^T)^{-1} [F_n (\pi_n - \pi_o) - f(\pi_n)] \quad (38)$$

where F is a matrix of partial derivatives of $f(\pi)$ valued at point π .

Accordingly, the components of F are

$$(F_n)_{mj} = \left(\frac{\partial f^m}{\partial \pi_j} \right)_{\pi=\pi_n} \quad (39)$$

where f^m is the m^{th} component of $f(\pi)$ and π_j is the j^{th} component of π . The iterative procedure is stopped when $f(\pi_n)$ is sufficiently close to zero. The procedure is repeated with different *a priori* values for the unknown parameters to verify that the final solution does not depend on the start value. This procedure can be time consuming and possibly inconclusive, but may be overcome by a global search using Monte Carlo simulation for model parameters that yields a minimum misfit with the observed data. The obtained parameters can be used as *a priori* values of the unknowns.

/Tarantola and Valette 1982/ have demonstrated that the stationary point π obtained from the iterative process (Equation 37) corresponds to a strict local minimum of f if, and only if, $C_o^{-1} L_\pi Q_\pi$ is not negative, where Q_π is the linear projector defined by

$$Q_\pi = 1 - C_o F_\pi^T (F_\pi C_o F_\pi^T)^{-1} F_\pi \quad (40)$$

and L_π is the operator defined by

$$L_\pi(V) \equiv V - Q_\pi C_o [K_\pi(V)]^T (F_\pi C_o F_\pi^T)^{-1} F_\pi (\pi - \pi_o) \quad (41)$$

where K_π is the second order partial derivative operator of $f(\pi)$ taken at point π .

3.3.3 Misfit functions

The misfit function may be either formulated with a l_1 -norm (sum of absolute values of differences between expected value by the model and observed value, normalized by some function representing uncertainties on measured data) or with a l_2 -norm (least squares). Once the norm has been adopted, the objective is to identify the model that minimizes the misfit function. This leads to an inverse problem that may be solved, either by the Monte Carlo method or the gradient method. For the gradient method, the algorithm that is being used corresponds to the l_2 -norm, whereas the Monte Carlo method corresponds to the l_1 -norm. For hydraulic fracturing and HTPF data, the misfit is defined by /e.g. Yin and Cornet 1994/:

$$\Psi^h = \sum_{m=1}^M \left| \sigma_n^m - \sigma_{n,calc}^m \right| / (\delta_n^m + \delta_f^m) \quad (42)$$

where δ_n^m is the uncertainty of the normal stress determination and δ_f^m is associated with the maximum rotation of the fracture plane within the domain of uncertainty of its orientation (i.e.

including both dip and dip direction of the fracture). The uncertainty with respect to depth is very small and hence neglected. For overcoring data, the misfit is defined by:

$$\Psi^{oc} = \sum_{n=1}^N |\varepsilon_i^n - \varepsilon_{i,calc}^n| / (\delta_i^n + \delta_{bh}^n) \quad (43)$$

where ε_i is the strain (i denotes axial, tangential, 45°, and 135°-inclined gauges), δ_i^n is the uncertainty of the strain measurement, and δ_{bh}^n is the uncertainty associated with the borehole direction. The overcoring misfit function is simplified, and neglects the uncertainty in strain associated with depth, corrections factors, rosette angle, and elastic parameters. As for the hydraulic fracturing and HTPF data, the uncertainty of the strain associated with depth is small. The correction factors, K_1 to K_4 , are complex functions of, for example, the elastic parameters of the rock and overcoring cell, but regardless, they are always fairly close to one /Worotnicki 1993/. The inclusion of the rosette angle was found costly with respect to time, and was therefore excluded. Finally, because the results from individual data sets are used in the combined inversion (Equation 47), which uses the elastic parameters as unknowns, the elastic parameters cannot be included in the misfit function for overcoring data.

The hydraulic fracturing and HTPF methods are of different nature compared with the overcoring method. Therefore, the global misfit function for a combined data set should include weighting factors, which are quite complex. The general global misfit function can be expressed as /Yin and Cornet 1994/:

$$\Psi^{hoc} = \omega^h \Psi^h + \omega^{oc} \Psi^{oc} \quad (44)$$

An approximate global misfit was used that considers: (1) the volume or area involved by a given measurement in each method, (2) the individual misfit related to the misfit obtained in the combined solution. The weighting factors are expressed as /Ask 2004a/:

$$\omega^h = \frac{A^h}{A^{REV}} \cdot \frac{\Psi^h}{\Psi_{min}^h} \quad (45)$$

$$\omega^{oc} = \frac{V^{oc}}{V^{REV}} \cdot \frac{\Psi^{oc}}{\Psi_{min}^{oc}} \quad (46)$$

where ω^h , A^h , and A^{REV} denote the weighting factor, the measurement area, and the area involved in the Representative Elementary Volume (REV), respectively. Corresponding notations for the overcoring data set are ω^{oc} , V^{oc} (measurement volume) and V^{REV} (REV volume).

It is the ratio $\omega^h \Psi^h / \omega^{oc} \Psi^{oc}$ that determines the weighting of the two data sets in the combined inversion, which, in this simplified global misfit function, is independent of the size of the REV (assumed equal to 1 m³ or 1 m²). The area involved during hydraulic fracturing measurements depends on the injected volume but is of the order 1 m². This corresponds to e.g. 1 litre of injected water and a mean fracture width of 1 mm (assuming no loss of water due to permeability). The volume involved in overcoring measurements equals the volume of the resulting hollow rock cylinder. The global misfit for the combined inversion thus becomes /Ask 2004a/:

$$\Psi^{hoc} = \frac{A^h}{A^{REV}} \cdot \frac{\Psi^h}{\Psi_{min}^h} + \frac{V^{oc}}{V^{REV}} \cdot \frac{\Psi^{oc}}{\Psi_{min}^{oc}} \quad (47)$$

The suggested global misfit function thus gives the hydraulic fracturing data more weight than the overcoring data. Once the global minimum has been found (minimum of Ψ^{hoc}), the confidence interval can be estimated using for example /Parker and McNutt 1980/:

$$\Psi_{90\%}^{hoc} = \frac{1.645(\pi / 2 - 1)(M + N)^{1/2} + M + M}{(M + N) - W} \cdot \Psi_{min}^{hoc} \quad (48)$$

where W is the number of unknown parameters.

Note that the applied approach is different from that of /Klee and Rummel 2004/, which was based on Monte Carlo simulations and minimize the difference between calculated and measured normal stress. The computations are accompanied by plots of the average deviation (AVE) between theoretical and measured stress values as a function of the orientation of σ_H computed for the respective stress field model according to:

$$AVE = \sqrt{\frac{\sum_{i=1}^n (\sigma_{n,theory} - \sigma_{n,measured})^2}{n-1}} \quad (49)$$

where n is the number of measurements. The results are presented as the average stress-depth profile of the 10 best models.

3.3.4 Monte Carlo search for *a priori* values to the Gradient method

Because the solution of the Gradient method may be dependent on the *a priori* choice of model parameters, which may be difficult to define, a global search for model parameters was attempted using Monte Carlo technique. The first global search was conducted with large steps to avoid too time consuming simulations. Successive simulations with smaller steps were then made until a minimum misfit was obtained. The model parameters corresponding to the minimum misfit was then used as *a priori* values in the Gradient method.

3.3.5 General about the inversion method and help functions

The *a posteriori* variance and covariance associated with the unknown model parameters provide a measure of the quality with which the unknown model parameters have been resolved. If *a posteriori* variance is small, the value has been well resolved; if it is nearly equal to the *a priori* variance, the corresponding unknown model parameter has not been resolved. An estimate of the resolution of a model parameter can be obtained by the ratio:

$$I = [a \text{ posteriori variances of model parameter}] / [a \text{ priori variance of model parameter}]$$

This ratio, named the indetermination estimator, verifies $0 \leq I \leq 1$. For a well-resolved model parameter, $I \approx 0$; for a poorly resolved model parameter, $I \approx 1$.

The applied inversion technique is based on the assumption that the data follow Gaussian distribution. Thus for hydraulic stress data, it is assumed that the uncertainties in fracture depth, dip direction, dip and fracture normal stress can be determined. The influence of these uncertainties in these measured data can be evaluated using the theory developed by /Cornet and Valette 1984/. They showed that the influence of a datum, x_d , with respect to an unknown parameter, x_p , can be evaluated using:

$$\frac{P_{p,d} \cdot \varepsilon_d}{\varepsilon_p} \quad (50)$$

where P is an orthogonal projector with respect to C_0^{-1} , and ε_d and ε_p are the standard deviations of the data and model parameter, respectively. /Cornet and Valette 1984/ showed that the influence of a datum on an unknown model parameter is at maximum when $P_{ii}(I-P_{ii})$ is equal to 0.25.

4 The Forsmark site – analysis of rock stress data

The stress data reviewed in this study were chosen by SKB and involved the cored boreholes KFM01B, DBT-1, and DBT-3 (OC) and the cored boreholes KFM01A, KFM01B, KFM02A, and KFM04A (HF and HTPF).

4.1 General geological setting

The geological information given in this report is that presented by /SKB 2004/ and /SKB 2005/ and is determined through an extensive program containing both surface and borehole investigations. The geological information was gathered through various methods such as bedrock mapping, airborne geophysical measurements, rock core mapping, etc. The latter publication /SKB 2005/ refers to the site descriptive model version 1.2.

In general, the Forsmark region is dominated by meta-igneous, quartz-rich rock types that have been affected by ductile deformation. Some few young granites and pegmatite rock types only display a weak foliation /SKB 2004, 2005/. In the descriptive geological model of the Forsmark site, forty-two rock domains (RFM001–RFM042) are presented and they are separated by their basic composition of rock types, grain size, degree of inhomogeneity, and ductile deformation. Two representative domains are labelled as: (i) RFM029, consisting of granite to granodiorite, being metamorphic and of medium grain size, and (ii) RFM032, consisting of granite, being metamorphic and aplitic, see Figure 4-1. RFM029 is dominating the candidate area at the site and is characterized as homogeneous, lineated and weakly foliated, with an inferred lower degree of ductile deformation. RFM032, on the other hand, is a key domain to define a major folded structure in the central part of the region, and is characterized as inhomogeneous, banded foliated and lineated, with an inferred higher degree of ductile deformation. The tectonic foliation and banding in the rock mass strikes mostly in a NW-SE direction, with a steep dip angle. The mineral stretching lineation has a trend towards SE and is moderately steep, with a plunge of 35–50°. A complete description of all rock domains and their presences at the Forsmark region is presented in /SKB 2004, 2005/.

For the boreholes drilled during the three years 2002–2004 and considered in this study (KFM01A, KFM01B, KFM02A, KFM04A), the dominant rock domain encountered is RMF029, with the following exceptions (Appendix A). In borehole KFM04A, RFM018 occurs between 12 and 177 m length, and RFM012 is intersected between 177 and 500 m hole length. RFM017 and RMF018 comprise metamorphic tonalite to granodiorite, whereas RMF012 consists of metamorphic granite to granodiorite (cf. Appendix A).

In the regional scale of the Forsmark area, 879 linked lineaments have been identified. The majority (approximately 700) of these are shorter than 1 km in length. Only a few (seven) have a length exceeding 10 km. Lineament analysis showed that four dominant orientations are present among the major lineaments (NS, NE, NW, and EW), of which the NW orientation appears to be the most represented direction among them.

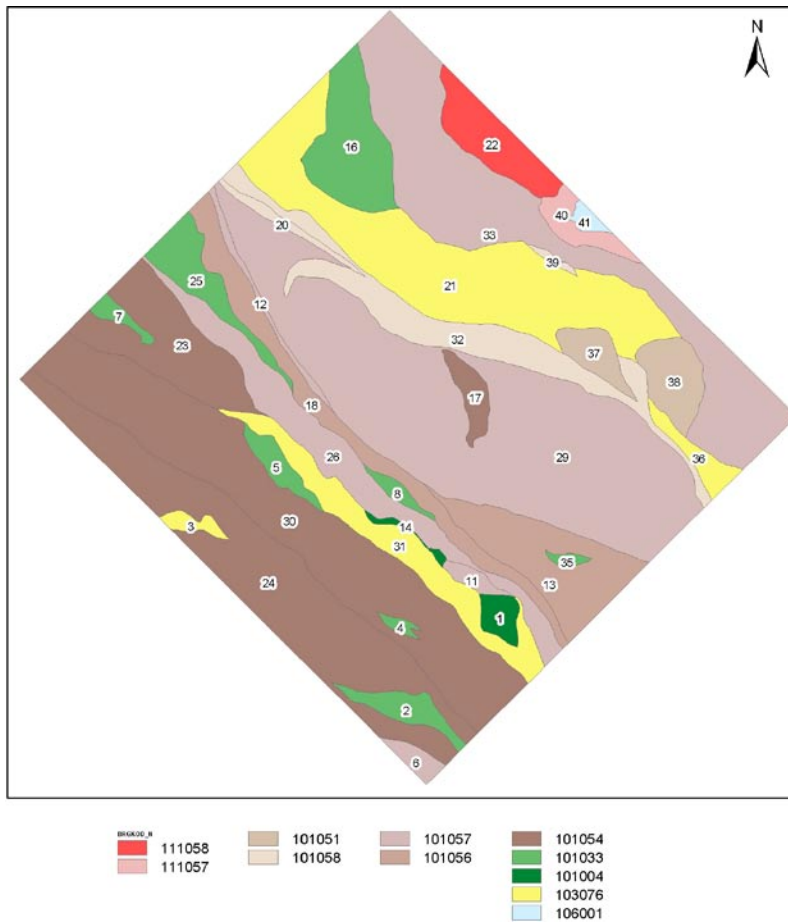


Figure 4-1. Rock domains used in the modelling procedure numbered from 1 to 41 (domain 42 is located outside the map). Surface view of the regional model volume /SKB 2005/. The colours show the rock units that were defined on the basis of dominant rock type, with numbering as follows: 111058 = Granite, fine- to medium-grained, 111057 = Granite to granodiorite, metamorphic, veined to migmatitic, 101051 = Granitoid, metamorphic, fine- to medium-grained, 101058 = Granite, metamorphic, aplitic, 101057 = Granite to granodiorite, metamorphic, 101056 = Granodiorite, 101054 = Tonalite to granodiorite, metamorphic, 101033 = Diorite, quartz diorite and gabbro, metamorphic, 101004 = Ultramafic rock, metamorphic, 103076 = Felsic to intermediate volcanic rock, metamorphic, 106001 = Sedimentary rock, metamorphic, veined to migmatitic.

In general, the deformation zones present at the Forsmark site can be divided into four sets as follows /SKB 2005/:

1. Vertical and steeply SW-dipping zones with NW-WNW strike direction. These zones are both regional in size, such as Singö, Eckarfjärden and the Forsmark deformation zones, and local (length < 10 km) in size, showing both ductile and brittle deformation (Figure 4-2).
2. Steeply dipping zones (brittle deformation) with NE-ENE strike, being locally major to locally minor in size.
3. Steeply dipping zones with NS strike (only one local minor zone).
4. Gently SE-and S-dipping brittle deformation zones, being locally major in size, and occurring mostly in the south-eastern part of the candidate volume (Figure 4-3).

The major deformation zones (Singö, Eckarfjärden and Forsmark) demarcate a tectonic lens, in which the major portion of the candidate area is situated. An important finding from recent drillings at the site is that the dominant rock domain within the candidate volume (RFM029) extends to a depth of c. 1,000 m /SKB 2005/.

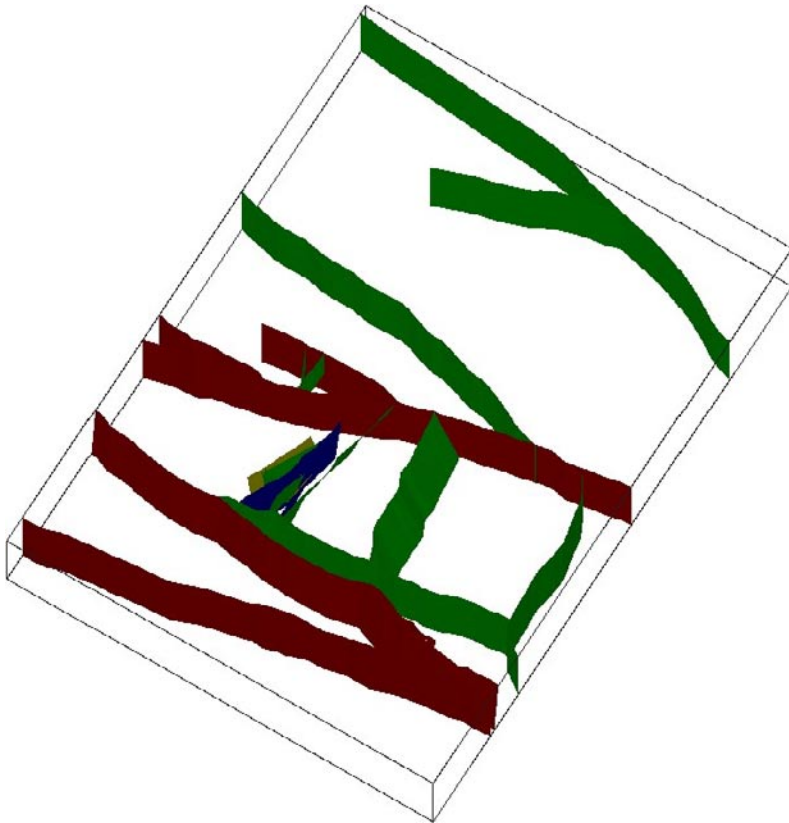


Figure 4-2. Structural model of the candidate site showing steeply dipping zones, the majority with a NW-WNW strike direction, with judged high or medium confidence of occurrence /SKB 2005/.

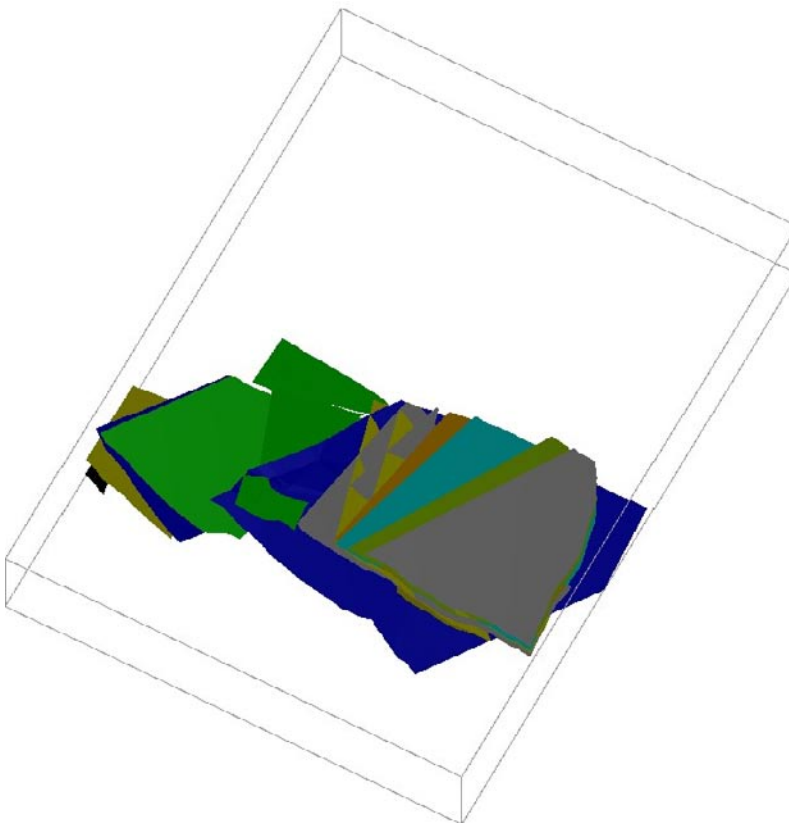


Figure 4-3. Structural model of the candidate site showing gently dipping zones with judged high or medium confidence of occurrence /SKB 2005/.

The superficial bedrock is extensively fractured leading to high transmissivities (recorded in the percussion-drilled boreholes at all four drill sites). However, at depth, the bedrock appears to have a very low hydraulic conductivity /SKB 2004/. Very low fracture intensity and very tight rock was encountered below c. 200–300 mvd, e.g. in borehole KFM01A.

New data and interpretations of possible deformation zones in the area have resulted in a higher degree of confidence of occurrence for some of the more flatly dipping zones. A potential zone of particular interest is termed ZFMNE00A2, with an orientation of 080/24 and outcropping near drill site 1 (boreholes KFM01A and KFM01B), see also Figure 2-1. The uppermost part of this zone intersects boreholes KFM01A and B at c. 16 m borehole length (mbl), KFM02A at c. 415 m and KFM04A at c. 79 mbl, see /SKB 2005/ and Appendix A in the present report.

4.2 Overcoring measurements in borehole KFM01B

Borehole KFM01B at the first drill site, DS1, Figure 2-1, was drilled with 76 mm diameter down to c. 501 m borehole length (mbl). The borehole orientation was 268° with a dip of 79°, measured at the borehole collar. Overcoring measurements were attempted at two measurement levels in the borehole. The first level included overcoring attempts between 235 and 242 mbl. For the second level measurements were initiated at 404 m borehole length but not finalized until at 475 mbl. This large depth interval for Level 2 was required to obtain a complete test series, due to problems with fractured rock, mainly between 415 and 458 mbl, and core discing (at all depths). Consequently, no further attempts were made for a third level in borehole KFM01B. The measurements were conducted according to the activity plan AP PF 400-03-041 (SKB internal controlling document) and all results are stored in the SKB database Sicada, where they are traceable by the activity plan number.

The *in situ* stress state from overcoring was calculated using (i) the measured strain response (difference between strain gauge readings after and prior to overcoring), (ii) recorded orientation of strain gauge rosettes in the borehole, and (iii) values on elastic constants determined from biaxial testing. Since biaxial test data were not available for all samples, data on the elastic constants from the nearest test (in similar geology) was used in the stress calculation.

The overcoring data in borehole KFM01B have already been thoroughly analyzed /Sjöberg 2004, Lindfors et al. 2005/ and the evaluation made in the present report is therefore only a brief summary. One change has though been made; the stresses have been re-calculated minimizing temperature effects observed during overcoring. As in /Lindfors et al. 2005/, the large vertical component in the overcoring data was interpreted as a result of microfractures in the core, and the stress calculation was therefore made where data were adjusted to fit the weight of the overburden rock mass.

Stress calculations using the theories presented in this study require uncertainty estimates of the position and orientation of the cell, strains, elastic parameters, and uncertainties related to the assumption of linear elasticity, homogeneity, and continuity.

The uncertainty related to measured depth is related to the precision of the drilling operation, which in general is high (maximum error $< \pm 0.5$ m) and therefore negligible in this context. The orientation of the strain rosettes is measured using a compass in near-vertical boreholes, which has a precision of about $\pm 1^\circ$. The relative orientations of the three plastic tongues (separated by 120°), on which the strain rosettes are located, are verified after completed overcoring and biaxial tests. The accuracy of this verification is about $\pm 2^\circ$.

After completion of the study presented in this report, it was observed that there are uncertainties in the deviation measurements made in the boreholes involved in this study, except for the “old” boreholes DBT-1 and DBT-3 which have not analysed in this respect. Furthermore, uncertainties have been identified in the rotational orientation of the BIPS-instrument used

for producing video images of the borehole wall (not relevant for DBT-1 and DBT-3). Because deviation measurements and BIPS-images are part of the SKB's system for borehole mapping, the so called Boremap system, which includes orientation of geological structures like fractures and rock contacts, orientation data referred to in this report and stress data based on these orientations are affected. At the time for performance of this study these uncertainties were not known and their significance not assessed. In most borehole sections these errors were preliminarily judged as limited to an order of a few degrees, and are therefore in this study not judged to significantly deteriorate the results of the stress calculations. A more firm analysis of this potential source of error for stress calculations is not possible until the orientations of geological structures in the addressed boreholes have been revised.

The results of the biaxial tests commonly display a scatter in Young's modulus and Poisson's ratio, especially at larger stress magnitudes (depth), which also affects the assumption of linear elasticity, homogeneity, and continuity. As a result, the elastic parameters constitute the main uncertainty in the stress calculation using overcoring data, which is discussed below.

4.2.1 Results of re-evaluation

The overcoring campaign in KFM01B resulted in seven successful tests, four partly successful tests, and seven unsuccessful tests. Of the successful and partly successful tests, three are located at Level 1 (235–242 mbl) and five tests at Level 2 (407–475 mbl). Data analysis indicates that the standard deviations of the strain measurements are fairly low, in average 39 μ strain (range 15–88 μ strain). Excluding the more uncertain data at 406.92 mbl gives an average standard deviation of 29 μ strain in the range 15–42 μ strain. In total, 33 reliable and another 21 less reliable strain measurements, distributed between 235 and 475 mbl are available.

Core discing was abundant for all conducted measurements at Level 1 (Table 4-1). However, the discing was limited to the bottom portion of the samples, thus not significantly affecting the measured strains, nor the ability to conduct biaxial testing. Thus, the measured strains are judged fairly reliable at Level 1.

For Level 2, the core discing was even more extensive (Table 4-1) and with higher induced temperature levels. It was suggested that the temperature increase was a result of insufficient flushing and/or drill bit wear /Sjöberg 2004/. The elevated temperatures remain after the end of overcoring, which may affect the resulting stresses. Tests at 415.16, 465.05, 474.25, and 475.34 mbl resulted in extensive core discing of the entire, or almost entire, overcore sample. Debonding and/or large strain drift for several gauges inhibited conventional evaluation of these tests. Biaxial testing was not possible for any of these four tests. However, these tests were analysed using transient strain analysis /see Sjöberg 2004/ but the results indicated varying and therefore uncertain stress estimates.

The core discing was positively identified on the strain versus time plots during overcoring (Table 4-1) in all the cases where the discing occurred close to the strain gauges. Noteworthy is that not only the axial gauges are affected by the core discing, but also the tangential and 45-degree inclined gauges. This effect is likely a result of induced axial fractures (spalling failures) identified using line mapping of thin sections of the pilot hole wall /Lindfors et al. 2004/.

The biaxial testing yielded that the average elastic parameters in borehole KFM01B are equal to $E = 62.8 \pm 13.6$ and $\nu = 0.30 \pm 0.07$ (based on tests of ratings a and b /Sjöberg 2004/; Figure 4-4). One biaxial test, at 412.79 mbl in Level 2, indicated slightly anisotropic rock, but the derived elastic parameters are of the same order of magnitude as the remainder of the tests. Debonding and/or large strain drift for several gauges at Level 2 inhibited evaluation of biaxial test results. A more detailed description of the overcoring and biaxial tests is presented in /Sjöberg 2004/.

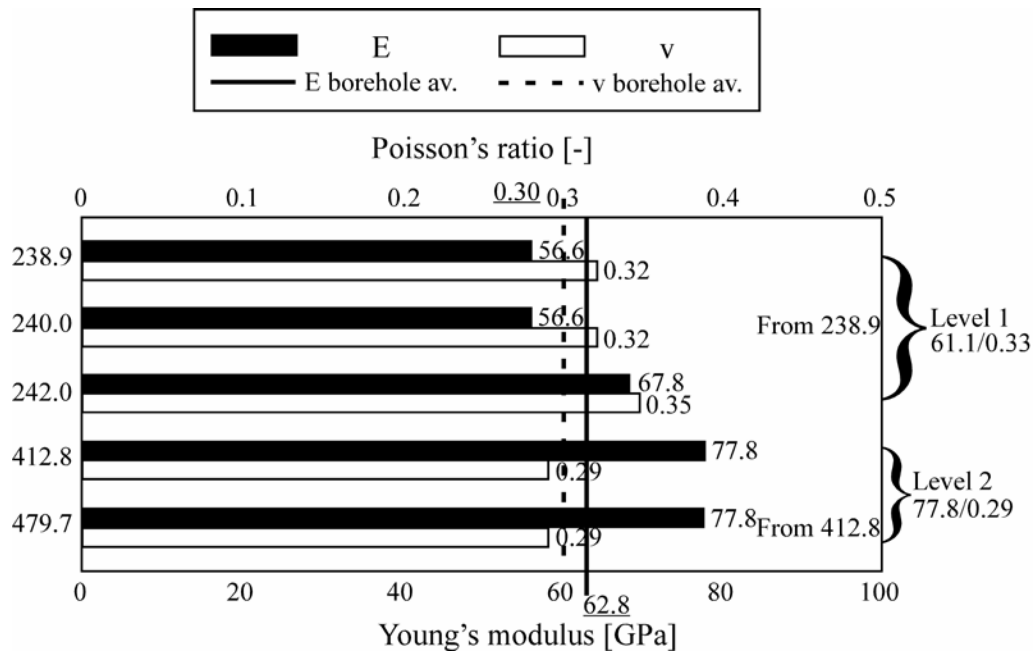


Figure 4-4. Summary of elastic parameters from biaxial tests on cores from KFM01B. Average results are calculated using data of rankings a and b /Sjöberg 2004/.

Table 4-1. Core discing (CD) during overcoring measurements in borehole KFM01B.

Borehole length [m]	Level	Rating ¹	Core discing ²	Visible during overcoring	Positive ident. during overcoring
238.94	1	a	After 34 cm?	After 18 min overcoring?, i.e. after 63 cm	No
240.01	1	a	After 37 cm?	After 14.5 min overcoring, i.e. after 68 cm	No
242.05	1	a	After 36 cm?	After 12 min overcoring, i.e. after 33 cm	Yes?
406.92	2	a	After 19 cm	After 5 min overcoring, i.e. after 18 cm	Yes
412.79	2	a	After 35 cm	After 28 min overcoring, i.e. after 36 cm	Yes
415.16	2	b	Extensive	After 0.5 min overcoring, i.e. after 0.6 cm	Yes
465.05	2	b	Extensive	After 0.5 min overcoring, i.e. after 0.9 cm	Yes
471.69	2	a	Upper 20 cm	After 0 min overcoring, i.e. after 0.1 cm	Yes
472.98	2	a	No	–	–
474.25	2	b	Extensive	After 0 min overcoring, i.e. after 0.1 cm	Yes
475.34	2	b	Extensive	After 0 min overcoring, i.e. after 0.1 cm	Yes

¹Ratings according to /Sjöberg 2004/. ²Core discing based on core photos.

The large scatter in Young's modulus and the large scatter and high values on Poisson's ratio, between 52.6–77.8 GPa and 0.22–0.35, respectively, are unusual for this type of rock. If the observed variations are real, it implies large variations in the stress tensor in the rock mass, rendering an integration of various local stress tensors erroneous. Although no microcracks were visible for the naked eye, the observed scatter is interpreted to be a result of microfracturing of the core, based on the considerably smaller scatter observed (especially for Young's modulus) during axial and triaxial tests on solid cores (Figure 4-5). Naturally, this does not preclude that variations in elastic parameters exist at the locations of the overcoring measurements. More reliable comparisons of the elastic parameters would be obtained if axial or triaxial tests on solid cores were made in the immediate vicinity of the overcoring locations. In this report, in the absence of elastic parameters from laboratory tests close to the overcoring test locations, the biaxial test results are used for stress calculation.

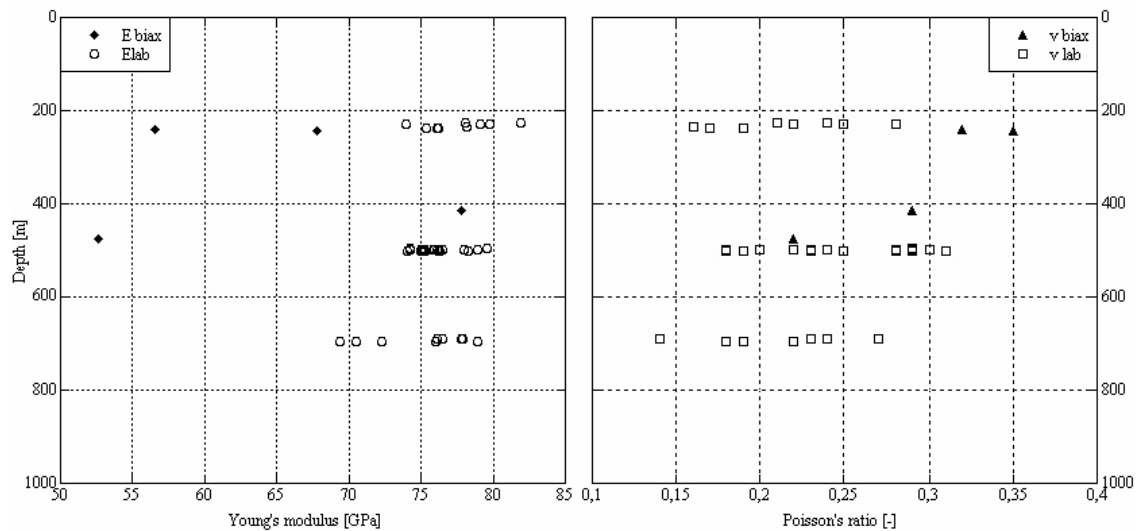


Figure 4-5. Comparison of elastic parameters derived using biaxial tests of overcoring rock cylinders from borehole KFM01B (filled symbols) and uniaxial and triaxial testing on solid cores from borehole KFM01A (unfilled symbols), respectively /Eloranta 2004bc, Jacobsson 2004de/.

Although the number of tests on solid cores is limited, an interesting trend is visible. Similar to observations at the URL, the Young's modulus seems to decrease with depth, whereas no trend can be identified for Poisson's ratio. If the trends are true and not a result of the limited number of samples, it may reflect sample disturbance as a result of stress relaxation after drilling. If so, the results are not representative of the rock mass *in situ* /e.g. Martin and Simmons 1993/.

To conclude the data analysis, the most reliable stress data from overcoring include tests at 238.94, 240.01 (only two strain rosettes), 412.79, and 471.69 mbl. Data at 242.05 mbl are judged less reliable due to influence of core discing, but are still included in the analysis.

The overcoring data have been re-evaluated to minimize the temperature effects and these results are compared with the original data of /Sjöberg 2004/ in Table 4-2, including the most reliable data from transient strain analysis /Sjöberg 2004/. The attempts to minimize the temperature effects involve a final strain reading at stable strain levels between the end of the overcoring process and core break. This effectively reduced the temperature-induced stresses, giving somewhat larger stresses compared with the results of /Sjöberg 2004/.

In the tests at 240.01 and 242.05 mbl, the strains are dropping significantly after the overcoring process, resulting in smaller stress magnitudes for these tests. The dropping strain values are interpreted as a result of relaxation of the stresses due to microfracturing of the core. This is verified by that core discing was initiated some time after completed tests.

4.2.2 Discussion of re-evaluation results

The results indicate that measurements at Level 1 were located in much better rock with a lower fracture frequency and less pronounced development of core discing compared with Level 2. The presence of fractures on Level 2 probably led to lower local stresses, which permitted measurements to be made, whereas the overall stress state at larger depth is likely to have been higher /Lindfors et al. 2005/.

Transient strain analysis indicated the largest discrepancy between measured and calculated strain for the axial gauges, followed by the inclined gauges, whereas the tangential gauges are less affected. These discrepancies are a clear sign of non-ideal behavior and induced microcracks in the axial direction of the core sample, as indicated by the occurrence of core discing, a large vertical stress component, and high values on Poisson's ratio during biaxial

Table 4-2. Magnitudes and orientations of principal stresses determined from temperature corrected overcoring data and comparison with results of /Sjöberg 2004/ without temperature correction (marked¹). Results from transient strain analysis (marked *) are also included /Sjöberg 2004/.

Hole length [m]	Magnitude and Trend/Plunge of principal stresses					
	σ_1 [MPa]	[°]	σ_2 [MPa]	[°]	σ_3 [MPa]	[°]
238.94	50.8	101/45	38.0	319/38	30.4	212/20
238.94 ¹	50.5	102/42	37.4	324/30	29.6	214/23
238.94*	41.3	104/06	21.9	198/34	6.9	006/55
240.01	28.3	285/13	17.7	192/14	12.9	058/71
240.01 ¹	38.7	282/12	22.3	187/19	15.6	043/67
242.05	34.9	279/20	31.0	185/12	19.7	066/67
242.05 ¹	40.2	289/12	32.4	195/17	19.0	053/69
Av. L1	36.2	285/02	28.0	194/48	26.9	017/42
Av. L1 **	39.5	283/05	25.4	191/25	14.6	024/64
412.79	45.4	138/32	28.3	022/35	16.0	258/39
412.79 ¹	42.3	141/28	25.2	030/34	10.3	261/43
471.69	50.3	156/24	19.0	352/66	13.3	249/06
471.69 ¹	46.8	153/23	14.5	011/62	10.0	252/14
Av. L2	49.2	150/24	22.5	047/26	14.5	263/33
Av. L2 ¹	44.1	150/24	19.7	035/43	10.7	261/37

* Data from transient strain analysis (inverse solution). ¹ Data from /Sjöberg 2004/ without temperature correction.

** Average based on inverse solution of 1:4:1 and classical analysis of 1:5:1, 1:7:1.

testing. All tangential strain gauges remain, however, less affected, and the value and orientation of the horizontal stresses can be regarded as more confident. The tangential gauges at Level 1 were almost unaffected, whereas the discrepancy was larger for data at Level 2. This can be correlated to the larger calculated tensile stress at Level 2 compared to Level 1. In fact, the only successful measurements at Level 2 were from those tests in which core discing was less extensive. Thus, it is plausible that these measurements represent a lower bound to the actual stress state. The inferred stress gradients for the horizontal stress components from Level 1 to Level 2 are also small, considering the measured depth range, which further adds to the above hypothesis /Lindfors et al. 2005/. As the basic premises of the overcoring theory are violated, the results in borehole KFM01B, especially for Level 2, must be regarded with skepticism.

Results from analysis of core discing indicated a maximum horizontal stress of around 35 MPa for Level 1, which is in agreement with the stress state obtained from the overcoring measurements. For Level 2, core discing information indicated stresses of at least 40–48 MPa magnitude (for an observed disc thickness of 12 mm). The observations of thinner discs at the locations of the successful measurements, as well as the observations of discing of solid core, point towards local stress magnitudes in excess of 40–48 MPa /Lindfors et al. 2005/.

Examination of thin sections revealed signs of initiating spalling failure at the pilot hole wall. Spalling failure can, in turn, be a possible explanation to the observed premature debonding of strain gauges for several overcoring tests on Level 2. Stress estimations based on the assumption of developed spalling failures indicated a maximum horizontal stress between 43 ± 5 and 53 ± 5 MPa for Level 2, i.e. the total interval 38 to 58 MPa. P-wave velocity measurements partly supported the observed core damage (at large depths), but could not be used to determine stress orientations /Lindfors et al. 2005/.

In conclusion, the stress state in borehole KFM01B is characterized by horizontal stresses reaching 40 MPa or more already from approximately 250 m depth. The major principal stress appears to be oriented E-W to NW-SE and dipping subhorizontally. Even higher stress magnitudes can be expected at larger depth, but this cannot be confirmed conclusively from the reported measurements. Neither can the vertical stress component be estimated with any confidence.

4.2.3 Correlation with geological/geophysical data

The point-wise variation in each measurement level is generally substantial and a detailed investigation around each measurement point is necessary for identifying unreliable data. For example, a test made close to discontinuities in the rock mass may cause a local stress heterogeneity, which is not representative for the regional stress state. Data affected by local stress heterogeneities were determined through comparisons between calculated stresses and the mapped fractures in the core samples and results from borehole radar and BIPS logging. Depending on the stiffness of the fracture and its filling material, the following general classification can be made: (1) if the fracture is stiffer than the surrounding rock, the major principal stress, σ_1 , will be directed parallel with the fracture; (2) if the fracture has a lower stiffness (e.g. open or partly open), σ_1 will be oriented perpendicular to the fracture; and (3) if the stiffness difference is negligible, no re-orientation will take place /Hudson and Cooling 1988/. However, the rotation of the stresses around a discontinuity is also dependent upon the orientation of the in situ stress field in relation to the orientation of the discontinuity.

The data of most interest concerning heterogeneity are tests indicating deviating stress field with respect to the overall trend, e.g. tests with deviating orientations and tests indicating a vertical stress component significantly deviating from the theoretical weight of the overburden. In this report, only the reliable results of the overcoring and transient strain analysis are used for further correlation with geological/geophysical data. These data have been corrected for temperature effects and for the exaggeration of the vertical stress component. Thus, the study aimed at finding explanations to the observed rotation of the stresses from about 108 to 157°N between Levels 1 and 2 as well as to explain why the stress field at Level 1 is more horizontal/vertical compared to Level 2.

At Level 1, there are few fractures and no fracture zones in the vicinity of the test intervals, implying that the average stress at this level may represent the regional stress field (disregarding the problems associated with microfracturing of the core and temperature effects). However, below c. 270 mbl two sub-vertical fracture sets are particularly common. These have orientations around NNW-SSE and NE-SW, respectively. The tests at Level 2 (412.79 and 471.69 mbl) could be affected by nearby-located features detected with borehole radar (at 413.0 and 472.0 mbl). At 412.79 mbl, a feature at 413.0 mbl with dip direction 140°N and dip 29° /Gustafsson and Gustafsson 2004/ nearly coincides with the major principal stress, which is directed 138°N/24°, whereas intermediate and minor principal stresses are located in the plane defined by the fracture. The orientation of the reflector at 472.0 mbl could not be determined, but it is conceivable that the test at 471.69 mbl is affected by this feature.

The tests at Level 2 are located close to an interval that is anomalous with increased fracture frequency and alteration to varying degree (between c. 415 and 460 mbl). The fractures in this interval generally have no aperture and are sealed with laumonite. The most common fractures are oriented NNW with dip towards SW. A laumonite-sealed network of fractures exists between 433 to 443 mbl, which is predominated by fractures with steep dips and strikes NNW or NE. Two ductile shears are also located within this interval at approximately 420 mbl /Berglund et al. 2004/. Moreover, the spalling failures in walls of the pilot hole wall at Level 2, which may explain the observed premature debonding of strain rosettes during overcoring /Lindfors et al. 2005/, indicate that the limit for reliable results using the overcoring technique may have been reached or even passed.

4.3 Overcoring measurements in borehole DBT-1

Borehole DBT-1 was drilled vertically with 76 mm diameter down to c. 500 m vertical depth (mvd) in connection to the projecting of the Forsmark nuclear power plants, Figure 2-1.

Overcoring measurement data from the *SSPB stress cell* (currently known as the *Borre Probe*) have been reported in a measurement report /Ingevald and Strindell 1981/ and in a summary report which includes all conducted borehole investigations /SSPB 1982/. It must be noted that the reported data are not the same in the two reports. Strain differences and, hence, calculated stresses are different in /SSPB 1982/ compared with /Ingevald and Strindell 1981/. The changes are relatively small, a few microstrains in strain difference, resulting in stresses being up to a few MPa higher in /SSPB 1982/. There is no explanation as to why these changes were made /Perman and Sjöberg 2003/.

The reported measurement data in /SSPB 1982/ comprise borehole depth and orientation, probe bearing, elastic constants (E , ν), strain differences (after vs before overcoring) for each of the nine strain gauges, and the resulting stress data (principal stresses and projected stresses onto the horizontal/vertical planes; see report by /Perman and Sjöberg 2003/). Contrary to current procedures, the values of E and ν were determined from both uniaxial and biaxial testing. The cores were first tested uniaxially (concrete-testing machine), giving E and ν in the axial direction, and thereafter tested biaxially, giving E and ν in the horizontal direction. Moreover, for some tests, additional strain gauges were glued on the outside of the core sample. As far as can be seen from /SSPB 1982/, the individual and different values of E and ν in the horizontal and vertical directions of the sample were used in the stress calculation. Calculations made in this report, as well as test calculations made by /Perman and Sjöberg 2003/, indicate somewhat different stresses than those reported in /SSPB 1982/. In most, but not all cases, slightly lower magnitudes were obtained as well as slightly different orientations (within a few degrees). This confirms that stresses were originally calculated slightly differently compared to current procedures, which probably reflects that different values on the elastic parameters were employed for different gauge orientations. The relatively small differences indicate that the anisotropy is insignificant at the site /Perman and Sjöberg 2003/.

The reported overcoring measurements in DBT-1 involve eleven measurement levels with a total of 30 discrete test points between 14 to 502 mvd /Ingevald and Strindell 1981/. Below 300 m depth, Young's modulus and Poisson's ratio were reported to 75 GPa and 0.19, respectively, indicating problems to achieve overcore samples that were sufficiently long for biaxial and/or uniaxial testing. Contacts with some of the personnel involved confirmed severe problems with core discing during measurements. Furthermore, the frequency of induced fractures noted in the core log for DBT-1 is high, which may be taken as an indication of stress-induced damages. However, the frequency of induced fractures is only slightly lower above 300 m depth indicating the core damage may have occurred already at more shallow depth. Transient strain analysis confirmed to a large extent that high tensile strains are present during the measurements /Perman and Sjöberg 2003/.

New stress calculations using overcoring data require measured strains (or strain differences) as well as calculated values on the elastic parameters (and not calculated stresses). The data chosen for the analysis were taken from /SSPB 1982/ and not from /Ingevald and Strindell 1981/, because the former report is the most recent one and presumably data from that report have undergone more scrutiny than data in /Ingevald and Strindell 1981/. Given that different elastic parameters were used for gauges of different directions during stress calculation in /SSPB 1982/, the initial calculation of the present report, in which only one set of elastic parameters were used, will differ slightly from the results in /SSPB 1982/. The *in situ* stress state from overcoring data in the here presented study was calculated using (i) the measured strain difference from /SSPB 1982/, (ii) recorded orientation of strain gauge rosettes in the borehole, and (iii) values on elastic constants determined from biaxial testing.

The stress calculations presented in this report require uncertainty estimates of the position and orientation of the cell, strains, elastic parameters, and uncertainties related to the assumption of linear elasticity, homogeneity, and continuity. The uncertainty related to measured depth is

depending on the precision of the drilling operation, which in general is high (maximum error $< \pm 0.5$ m) and negligible (in terms of calculated stress magnitudes and orientations). The orientation of the strain rosettes is measured using compass in near-vertical boreholes, with a precision of about $\pm 1^\circ$. (Nothing is known regarding possible uncertainties in deviation measurement, cf. discussion about uncertainties in later investigated boreholes in Section 4.2) The relative orientations of the three plastic tongues (separated by 120°), on which the strains rosettes are located, are verified after completed overcoring and biaxial tests. The accuracy of this verification is about $\pm 2^\circ$ (it is assumed that the precision of the *SSPB cell* is the same as for the *Borre Probe*).

The results of the biaxial tests commonly display a scatter in Young's modulus and Poisson's ratio, especially at larger stress magnitudes (depth), which also affects the assumption of linear elasticity, homogeneity, and continuity. As a result, the elastic parameters are the main uncertainty in the stress calculation using overcoring data, which is discussed below.

4.3.1 Results of brief re-evaluation

Because the measurements in DBT-1 using the *SSPB cell* only includes the strain difference before and after completed overcoring, a detailed analysis of strain during the overcoring cycle is not available. Thus, rather crude methods must be applied to distinguish reliable measurements from less reliable/unreliable. The following rules were employed with this respect:

1. Because the hydraulic stress data successfully derived that one principal stress is vertical (see Section 4.5), data indicating principal stresses deviating more than 20° from the horizontal/vertical planes are judged as less reliable data (but they were not excluded at this point). This rule identified eight less reliable points (134.2, 134.7, 136.4, 166.8, 218.9, 219.6, 300.3, and 485.7 mvd).
2. Because the vertical stress was successfully determined to correspond to the theoretical weight of the overburden from the hydraulic stress data (see Section 4.5), overcoring data indicating a vertical stress 4 MPa below this value identified at 31.4, 71.4, 90.0, 195.4, and 378.2 mvd were judged as less reliable. This rule was employed because the common observation of core discing implies that overestimations of the vertical stresses are to be expected, even at shallow depth, and not the opposite.
3. Because the orientation of maximum horizontal stress was fairly reliably determined to 134°N using hydraulic stress measurements (see Chapter 5), results deviating more than 40° were judged less reliable (14 tests).
4. Data from the uppermost 100 m were excluded to avoid effects from sheet joints related to the deglaciation period (7 tests).
5. The results from transient strain analysis /Perman and Sjöberg 2003/ were used to identify tests with high tensile stress. In total, 13 such tests were identified.
6. Finally, tests where only average elastic parameters are presented in /SSPB 1982/ were identified, and judged less reliable (15 tests; Figure 4-6).

The results of application of the crude rules are presented in Figure 4-7 and primarily imply that few data are reliable. The results are however not as drastic as they first appear because only one malfunctioning strain gauge may cause the results to be judged ambiguous according to the crude rules. For this reason, a more thorough investigation is conducted in Section 5.2. Based on all data except for the uppermost 100 m but disregarding other uncertainties at this stage, the results entail:

$$\sigma_v = 18.4 + 0.072(z - 250) \text{ MPa; where } z \text{ is true vertical depth.}$$

$$\sigma_H = 28.1 + 0.128(z - 250) \text{ MPa; where } z \text{ is true vertical depth.}$$

$$\text{Orientation } \sigma_H = 107 \pm 43^\circ\text{N.}$$

Note that the estimate is valid between 0 and 500 mvd.

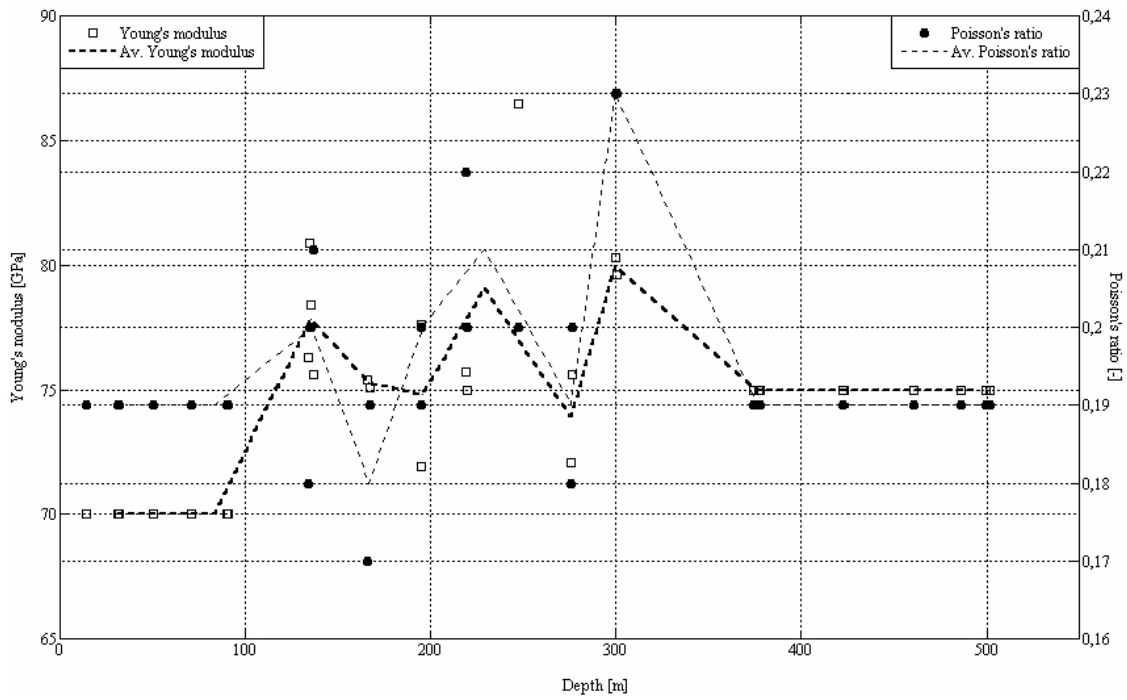


Figure 4-6. Summary of elastic parameters from uniaxial and biaxial testing on cores from DBT-1.

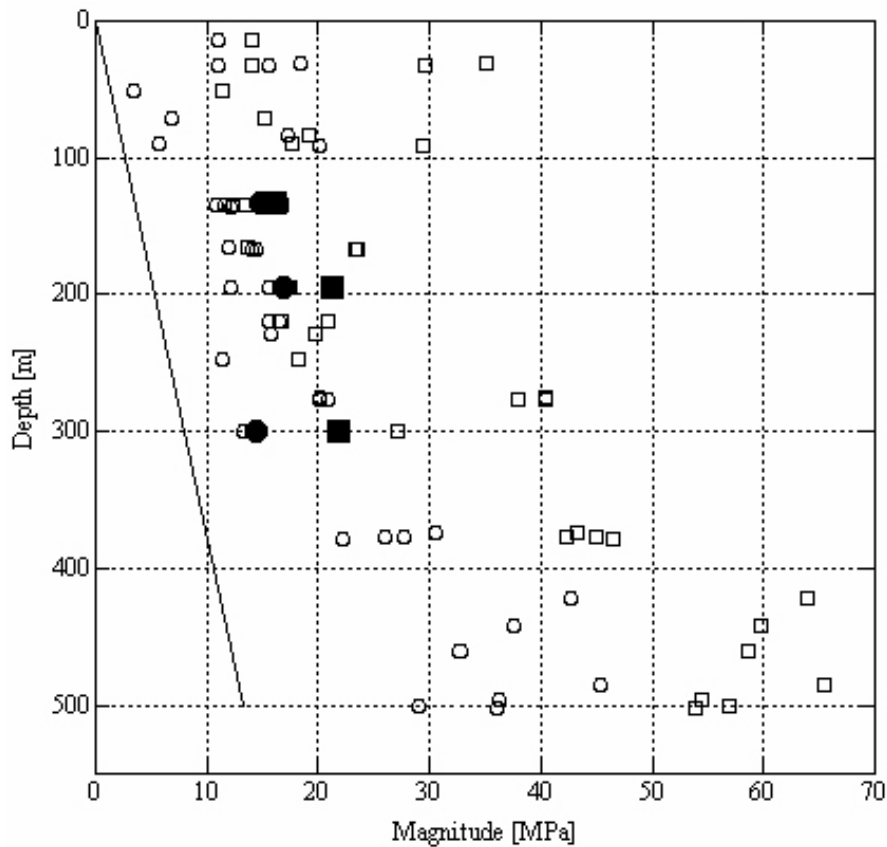


Figure 4-7. Horizontal stresses after identification of less reliable stress data in borehole DBT-1. Unfilled and filled symbols denote ambiguous and unambiguous data, respectively, and circles and squares denote σ_h and σ_{Th} , respectively. The vertical stress is plotted to the left in the figure.

Data analysis indicates that the standard deviations of the strain measurements are fairly low, in average 14 μ strain (range 4–41 μ strain).

Noteworthy about the results in borehole DBT-1 (and DBT-3) is that the vertical component in average is fairly well constrained. This is in disagreement with later applications of the *Borre Probe*, where the vertical component has been greatly exaggerated. The elevated vertical component is believed a result of microfracturing of the core (core discing), which according to the /SSPB 1982/ and field personnel was present also in borehole DBT-1. This misfit may be interpreted as that the raw data from DBT-1 have been corrected with this respect.

4.3.2 Correlation with geological/geophysical data

The analysis of results in borehole DBT-1 has neither been subjected to a point-wise, nor larger scale correlation with geology as a result of the limited material available.

4.4 Overcoring measurements in borehole DBT-3

Borehole DBT-3, located about 120 m NE of DBT-1, was drilled vertically with 76 mm diameter down to c. 250 m vertical depth (mvd) in connection with the projecting of the Forsmark nuclear power plants, Figure 2-1.

Like in borehole DBT-1, the overcoring measurements in borehole DBT-3 were conducted with the *SSPB stress cell* and reported in /Ingevald and Strindell 1981/ and in /SSPB 1982/. Similar to the results in DBT-1, the values of E and ν were determined from both uniaxial and biaxial testing and calculations made in this report, as well as test calculations made by /Perman and Sjöberg 2003/, indicate somewhat different stresses than those reported in /SSPB 1982/. Most likely, this can be correlated to that different values on the elastic parameters were employed for different gauge orientations /Perman and Sjöberg 2003/.

The reported overcoring measurements in DBT-3 involve nine measurement levels with a total of 22 discrete test points between 23 and 249 mvd /Ingevald and Strindell 1981/. As in borehole DBT-1, transient strain analysis confirmed that high tensile strains are present during the measurements in DBT-3 /Perman and Sjöberg 2003/.

The *in situ* stress state from overcoring data in this report was calculated using (i) the measured strain difference from /SSPB 1982/, (ii) recorded orientation of strain gauge rosettes in the borehole, and (iii) values on elastic constants determined from biaxial testing.

The stress calculations presented in this report require uncertainty estimates of the position and orientation of the cell, strains, elastic parameters, and uncertainties related to the assumption of linear elasticity, homogeneity, and continuity. These uncertainties are equivalent with those for DBT-1 (see Section 4.3).

4.4.1 Results of brief re-evaluation

As in borehole DBT-1, the analysis of data from borehole DBT-3 was based on the rather crude rules given in Section 4.3.1. The following results were obtained for each rule:

1. Eight tests were judged less reliable as a result of inclined principal stresses.
2. One test was judged less reliable as a result of a vertical stress component deviation from the theoretical weight of the overburden rock mass.
3. Eight tests were judged less reliable as a result of strongly deviating orientation of maximum horizontal stress.
4. Six tests in the uppermost 100 m were excluded to avoid effects of sheet joints related to the deglaciation period.

5. Two tests were judged less reliable as a result of high tensile stresses.
6. No data were judged less reliable as a result of that only average elastic parameters are presented (Figure 4-8).

The results of application of the crude rules are presented in Figure 4-9 and primarily imply that many data are unreliable. As for DBT-1, the results are not as drastic as they first appear because only one malfunctioning strain gauge may cause the results to be judged ambiguous according to the crude rules. A more thorough investigation is conducted in Section 5.2. Based on all data except those for the uppermost 100 m but disregarding other uncertainties at this stage, the results entail:

$$\sigma_h = 12.8 + 0.026(z - 250) \text{ MPa; where } z \text{ is true vertical depth.}$$

$$\sigma_H = 21.7 + 0.016(z - 250) \text{ MPa; where } z \text{ is true vertical depth.}$$

$$\text{Orientation } \sigma_H = 118 \pm 53^\circ \text{N.}$$

Note that the estimate is valid between 0 and 250 mvd.

Data analysis indicates that the standard deviations of the strain measurements are fairly low, in average 14 μ strain (range 2–33 μ strain).

As in borehole DBT-1, the surprisingly good resolution of the vertical component in borehole DBT-3 despite the known core discing problems may indicate that the raw data have been corrected in this respect.

4.4.2 Correlation with geological/geophysical data

The analysis of results in borehole DBT-3 has neither been subjected to a point-wise, nor larger scale correlation with geology as a result of the limited material available.

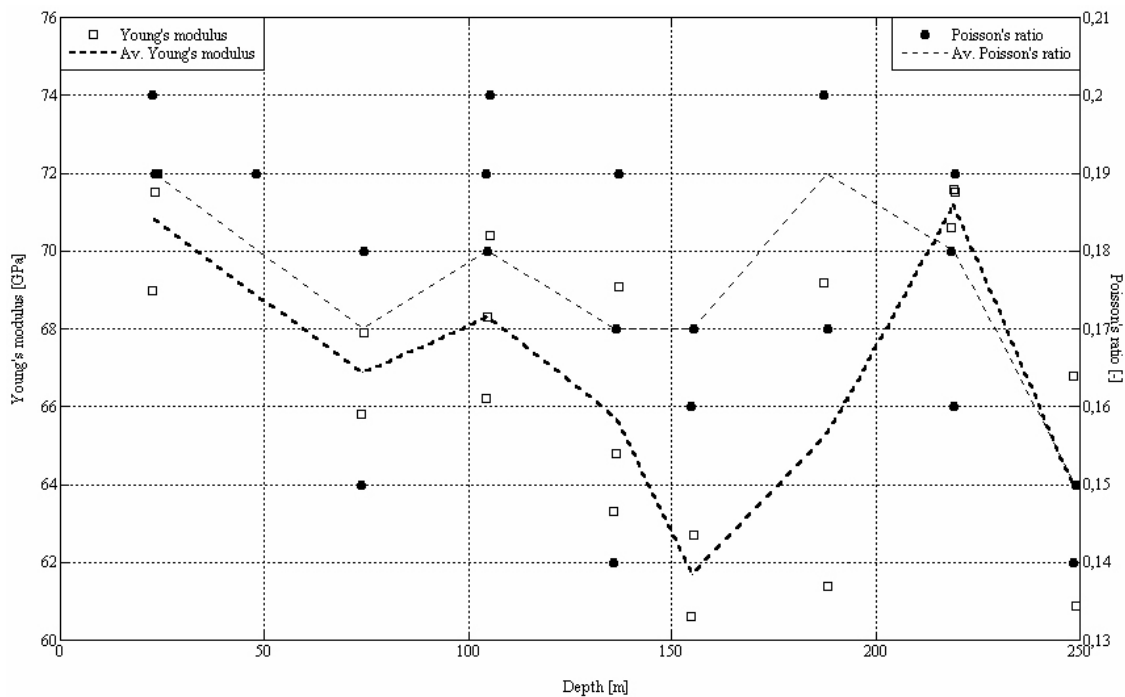


Figure 4-8. Summary of elastic parameters from uniaxial and biaxial testing on cores from DBT-3.

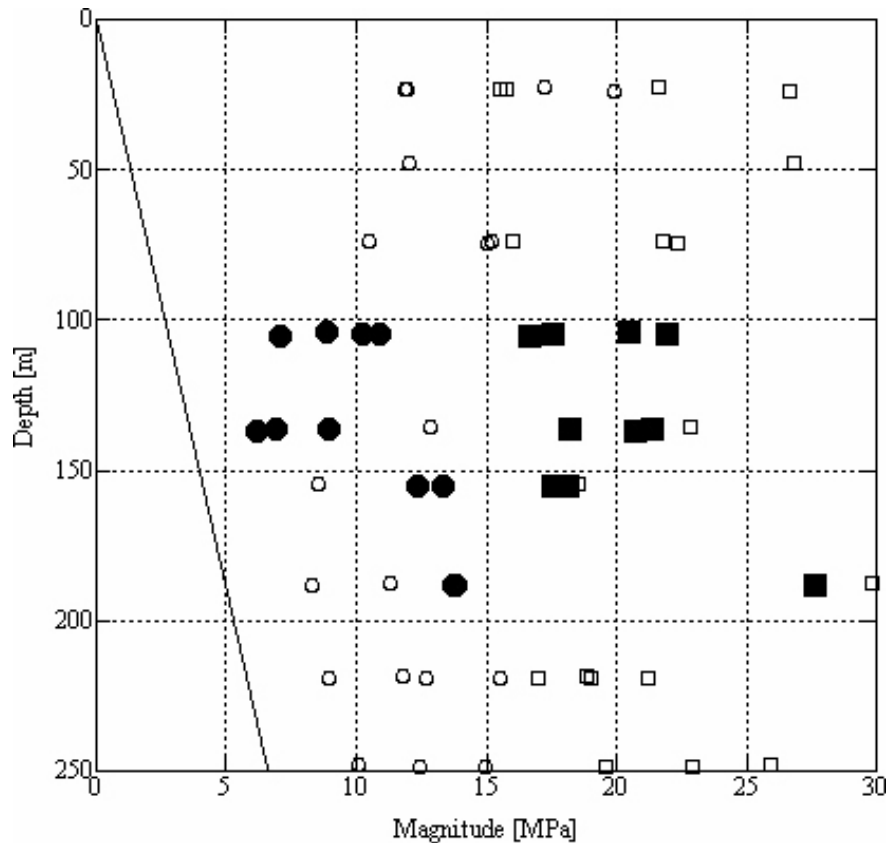


Figure 4-9. Horizontal stresses after identification of less reliable stress data in borehole DBT-3. Unfilled and filled symbols denote ambiguous and unambiguous data, respectively, and circles and squares denote σ_h and σ_H , respectively. The vertical stress is plotted to the left in the figure.

4.5 Hydraulic stress measurements in Forsmark

The hydraulic measurements in boreholes KFM01A, KFM01B, KFM02A, and KFM04A were conducted according to the activity plan AP PF 400-04-023 (SKB internal controlling document). All results are stored in the SKB database Sicada, where they are traceable by the Activity Plan number. The review of the hydraulic data indicates significant discrepancies compared with the results presented by /Klee and Rummel 2004/, which are described below. The following discussion is based on the ISRM suggested methods for rock stress estimation by hydraulic fracturing and hydraulic tests on pre-existing fractures /Haimson and Cornet 2003/.

4.5.1 Borehole information

Boreholes KFM01A and KFM01B, Figure 2-1, were drilled sub-vertically (at approximately 85° and 79° dip, respectively) from the ground surface. Borehole KFM01A is of "telescopic" type with the upper 100 m percussion drilled with larger diameter (250 mm) and cased, whereas the remainder of the borehole was drilled with 77 mm diameter down to a borehole length of c. 1,001 m. KFM01B, which is a conventional core drilled borehole, was drilled with 76 mm diameter from 15.6 m to c. 501 mbl. Hydraulic fracturing (HF) and hydraulic tests on pre-existing fractures (HTPF) were conducted between 249 m and 975 mbl (c. 244–958 m vertical depth) in borehole KFM01A and between 171 m and 476 mbl (c. 165–458 m vertical depth) in borehole KFM01B. In total, 21 hydraulic fracturing and 16 hydraulic tests on pre-existing fractures were planned. However, due to problems to open and stimulate pre-existing fractures, /Klee and Rummel 2004/ concluded that the test campaign resulted in 27 hydraulic fracturing tests. Because one test section was abandoned (fracture could not be induced at 952.0 mbl), only nine tests involved stimulation of pre-existing fractures.

Borehole KFM02A, Figure 2-1, was drilled sub-vertically (at approximately 85° dip) from the ground surface and is, like KFM01A, a telescopic borehole where the upper 100 m are of larger diameter (250 mm) and cased. The remainder of the borehole was drilled with 77 mm diameter down to a borehole length of c. 1,002 m. Hydraulic fracturing (HF) and hydraulic tests on pre-existing fractures (HTPF) were conducted between 150 m and 757 mbl (c. 142–746 m vertical depth). Three tests were performed at an injection pressure around 36 MPa to prevent damage of the packer elements.

Finally, borehole KFM04A, Figure 2-1, was inclined at approximately 60° dip from the horizontal plane and is of telescope type. The upper c. 100 m were drilled with a larger diameter (250 mm) and is cased. The remainder of the borehole was drilled with 77 mm diameter down to a borehole length of c. 1,001 m. Hydraulic fracturing (HF) and hydraulic tests on pre-existing fractures (HTPF) were conducted between 195 m and 594 mbl (c. 161–495 m vertical depth).

4.5.2 Choice of test sections

The planning prior to the field campaign involved choice of suitable fracture free sections for the hydraulic fracturing tests, whereas for the HTPF tests pre-existing fractures were sought.

HTPF measurements are commonly used to constrain the magnitude of primarily σ_H but also σ_v , once σ_h has been solved with hydraulic fracturing technique. Generally, for this type of test, isolated fractures are searched for, distributed with a large variety of dip and dip directions for a reliable resolution of all stress components during stress inversion. If a limited number of fracture orientations exist, fractures with similar orientation should be spaced at least 50 m apart so that a stress gradient can be picked up. Preferably, the chosen fractures should be at least partially opened or coated with weak fracture minerals, which, using a low flow rate test, enhances the possibility for re-opening as the fluid has time to penetrate the fracture plane and add an additional stress component. Finally, individual tests should be separated by c. 2 m to avoid the local stress change caused by the neighboring test as a result of the mechanical opening of a fracture /e.g. Cornet 1993ab, Haimson and Cornet 2003/.

In all boreholes investigated by /Klee and Rummel 2004/, the number of tests on pre-existing sub-horizontal fractures is unusually large. The aim of the large amount of sub-horizontal fractures was to verify/reject the very large vertical component found during overcoring measurements in borehole KFM01B, prior to the hydraulic campaign. Indeed, such a program will resolve the vertical stress with a very high degree of confidence. However, this choice was made at the expense of tests with other fracture orientations, which significantly reduces the chances of obtaining reliable results for the remainder of the unknown stress parameters, as the number of tests constraining these was reduced.

Boreholes KFM01A, KFM01B, and KFM02A involve a large number of hydraulic fracturing tests, especially around 230 and between 400 to 500 mvd, which resolve the minimum horizontal stress and its orientation. The aim of the concentration of measurements around 230 m depth, is that this depth corresponds to the measurement depth of the overcoring data collected in borehole KFM01B. The depth interval 400–500 m corresponds to the planned depth of the future repository. The large number of data should, given that axial fractures are induced, result in a good resolution of the minimum horizontal stress and its variation with depth.

Unfortunately, most of the chosen pre-existing fractures in boreholes KFM01A, KFM01B, and KFM02A were sealed, resulting in problems to open and stimulate them. As a result of these problems, new pre-existing fractures in borehole KFM04A were chosen which involved more pronounced, non-sealed fractures.

The tests conducted in borehole KFM04A, two hydraulic fracturing tests and nine HTPF tests, have a reasonable spread but the amount of data is relatively small with respect to the number of unknown parameters to be resolved. Considering that this borehole also penetrates a geological discontinuity (the border zone of the tectonic lens), with a potential to decouple the stress field,

the amount of data is judged too small for a confident evaluation of the influence of this zone on the prevailing stress field (see section 4.5.3).

4.5.3 Parameterization of the stress field

The parameterization of the stress field in all boreholes at Forsmark involves the vertical and horizontal stresses with depth /Klee and Rummel 2004/. This implies that lateral stress gradients are neglected and that the borehole was assumed vertical with one principal direction aligned with the borehole direction. Furthermore, the stresses are assumed to be following a linear function versus depth, i.e. rotations of the stresses do not occur. Thus, the stress calculations consist of solving six unknown parameters: maximum and minimum horizontal stresses, vertical and horizontal stress gradients with depth, and orientation of maximum horizontal stress. This assumption is based on the result of stress measurements in crystalline rocks all over the world, which demonstrate a linear increase of the *in situ* stresses with depth. Data deviating from the linear trend are therefore neglected in the analysis, and /Klee and Rummel 2004/ therefore conclude that the results characterize the general stress field for the Forsmark area.

The limited variation of fracture orientations of the chosen HTPF test sections implies that it will be problematic to determine σ_H versus depth with accuracy.

The parameterization for borehole KFM02A can be questioned as this borehole penetrates zone ZFMNE00A2, with an interpreted dip of 24° towards SSE /SKB 2005/, between 415–520 mbl. The same is valid for the parameterization for borehole KFM04A, which is located at the border of the tectonic lens at Forsmark (penetrates the lens border at c. 30° angle). Several studies have shown that in the vicinity of discontinuities, lateral stress gradients have been encountered /e.g. McGarr 1980/. The penetration of a discontinuity implies that the collected data may have to be divided into different data sets. The hydraulic data in borehole KFM02A clearly indicate that zone ZFMNE00A2 decouples the stress field and data gathered above the zone should, as a result, not be integrated with data collected below the zone. In borehole KFM04A, the effect of the zone on the stress field is unclear but considering that the borehole penetrates the border zone at c. 30° angle, the assumption of that one principal stress is vertical is doubtful.

4.5.4 Inversion procedure

The inversion method of /Klee and Rummel 2004/ is based on Monte Carlo simulation (MC). MC simulations have a benefit when solving non-linear optimization problems compared to methods that use an iterative approach, because it avoids the need for linearization and does not depend on local information on the gradient of the objective function. The MC method is therefore preferable when strongly non-linear problems are to be solved. The MC method relies on random processes to search the model space and determines the models that minimize a misfit function. The misfit function of /Klee and Rummel 2004/ was based on the difference between calculated and observed normal stress, σ_n , for n number of measurements:

$$AVE = \sqrt{\frac{\sum_{i=1}^n (\sigma_{n,theory} - \sigma_{n,measured})^2}{n-1}} \quad (51)$$

The Monte Carlo method is a memoryless random process, which means that it does not use the information gained from previous models. As a result, the Monte Carlo method is ineffective compared to e.g. Genetic Algorithms /Gallagher et al. 1991/ and always involves a significant exploration of unfavorable regions of the model space. As a result, Monte Carlo methods are often applied at different scales, a global search with relatively large steps of the unknown parameters, followed by successively smaller steps, until a stable solution is obtained. This implies that possible solutions may be missed during the first, large step stages of the analysis.

The collected data during hydraulic measurements involve four measured parameters: the depth of the fracture, the dip direction and dip of the normal to the fracture plane, and the fracture

normal stress. It has been shown that depth does not significantly affect the calculation of the unknown parameters /Cornet and Valette 1984/, but the uncertainties in the orientation of the tested fracture (primarily the fracture azimuth) does. As a result, it is not correct to calculate the unknown parameters based on that measured fracture azimuths and dips are absolute values as conducted by /Klee and Rummel 2004/. This is also explained by that the normal stress often can be determined with a high accuracy, whereas a high accuracy of the fracture plane orientation is more difficult to obtain (few systems exist that can determine fracture orientations within a few degrees).

4.5.5 Hydraulic fracturing tests

In total, 35 hydraulic fracturing tests were planned in boreholes KFM01A, KFM01B, KFM02A, and KFM04A. However, due to problems to open and stimulate pre-existing fractures, many of the hydraulic tests of pre-existing fractures were judged to have induced fractures. Moreover, to reduce possible damage to the packer system, a number of hydraulic fracturing tests were abandoned prior to fracture initiation. Thus, /Klee and Rummel 2004/ concluded that the test campaign in the four boreholes resulted in 57 hydraulic fracturing tests.

The hydraulic fracturing testing procedure should preferably follow the standard of the ISRM /Haimson and Cornet 2003/, which involves permeability inspection, fracturing, re-opening cycles (until reproducible P_s -values are observed), and finally step-rate pressurization (see also Section 3.2.1). On a few aspects, the test procedure of /Klee and Rummel 2004/ differs from this standard. Firstly, the pumping is continued for a period after first breakdown. Secondly, the pore pressure is not allowed to return to its original value during the test cycle, which has great consequences for the reliability of the fracture re-opening pressure, hence for application of the classical /Hubbert and Willis 1957/ equation. Finally, fracture re-opening tests should not be applied for HTPF tests to limit the chances of opening more than one fracture in the test section. These issues will be discussed below. Moreover, in this report, the data dealing with the *in situ* stress field is of primary interest, i.e. the parameters P_b , P_r , and P_s , and the permeability inspection will not be commented further.

Breakdown pressure and fracture re-opening measurement procedure

The breakdown pressure is defined as the maximum pressure observed during the fracturing cycle and was determined from detailed plots of pressure versus time. The re-opening pressure was based on analysis of the stiffness (dP/dV) during pressurization of the test interval. Fracture opening was assumed to occur when a significant deviation of the stiffness from linearity was observed on the pressure versus time plots. However, as stated by /Haimson and Cornet 2003/, it is essential that the tests are conducted with a fast flow rate (to reduce the chances that fluid penetrates the fracture) only when the pore pressure has returned to its original value. Because it is very difficult to ensure this condition, /Haimson and Cornet 2003/ recommended that step-rate tests are conducted instead (see Section 4.5.6). In the Forsmark case, /Klee and Rummel 2004/ have demonstrated, first with the permeability tests, secondly by the difference between injected and recovered volume, that in all tests the pore pressure has not returned to its original value. Hence, none of these tests can be used for evaluating the tangential stress at the borehole, i.e. they cannot be used for evaluating the apparent tensile strength used in the classical /Hubbert and Willis 1957/ determination procedure (Cornet, pers. comm.). Moreover, as described in Section 3.2.2, other factors entail that this method may be questioned because P_r is always close to σ_h and independent of the value of σ_H (and verified by results from Forsmark in Figure 4-10). For these reasons, the magnitude of σ_H of /Klee and Rummel 2004/ using the classical /Hubbert and Willis 1957/ method is not reliable.

/Klee and Rummel 2004/ suggest that most hydraulic tests resulted in the initiation of new fractures, identified by distinct breakdown events with sudden and rapid pressure decrease during pressure build-up in the test section and by a relatively large difference between breakdown pressure and first re-opening pressure, $P_b - P_r$. The difference between $P_b - P_r$ is often regarded as a measure of “*in situ*” tensile strength, $T_{in situ}$. However, because the pore pressure was not allowed

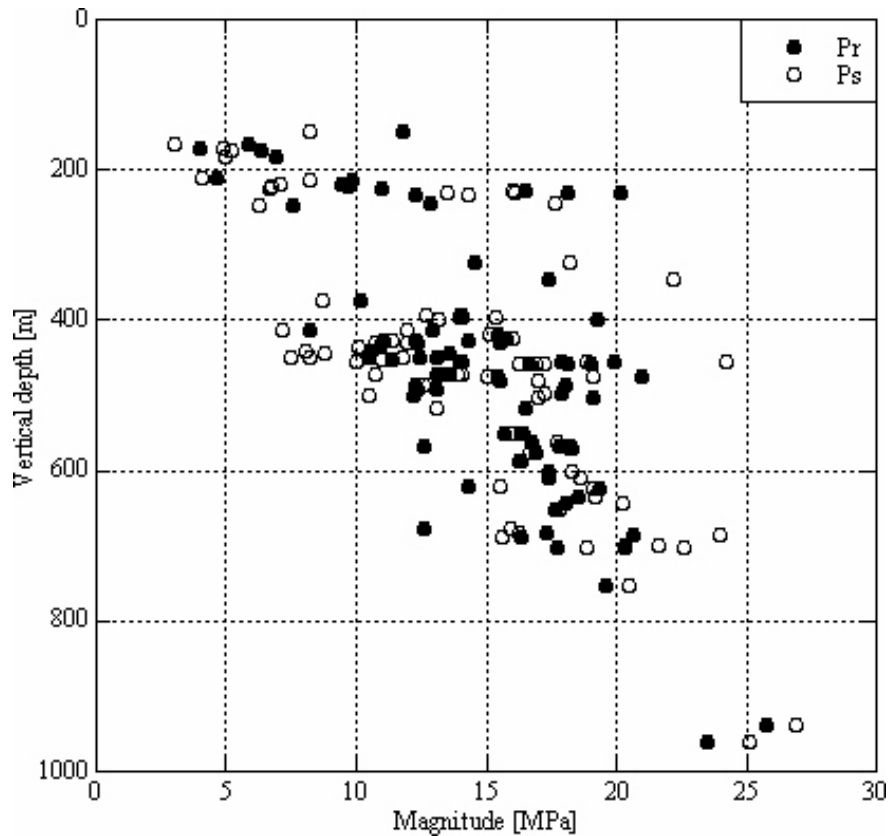


Figure 4-10. Re-opening and shut-in pressures versus depth at Forsmark. Data from /Klee and Rummel 2004/.

to return to its original value, the $T_{in\ situ}$ -values cannot be regarded as true values. The resulting $P_b - P_r (= T_{in\ situ})$ are given in Figure 4-11, including $T_{in\ situ}$ and tensile strength measurements made in laboratory, T_{HF} and T_{LAB} , which are miniature fracturing tests and indirect tensile strength tests on solid cores, respectively. /Hudson 1970/ generally suggests that if the tensile strength is required for some engineering or experimental purpose, it should be measured in the same specimen geometry and loading conditions for which it is required. Thus, minifrac tests are more applicable compared to the indirect tensile strength tests. Furthermore, /Hudson 1970/ proposes that if the test specimen must be on a reduced scale, all dimensions should be equally reduced and an estimate of the volume effect obtained. He also puts forward that the value of the maximum stress may not be relevant because it is not the direct cause of failure.

Shut-in pressure determination

A number of methods exist for determination of the shut-in pressure, of which /Haimson and Cornet 2003/ propose the dt/dP versus P -method /Hayashi and Haimson 1991/, the Muscat method /Aamodt and Kuriyagawa 1981/, and the dP/dt versus P -method /Lee and Haimson 1989/. /Klee and Rummel 2004/ defined an interval within which P_s must lie: the higher limit was specified by the end of pumping (at zero flow); and the lower limit using the Muscat method /Aamodt and Kuriyaga 1981/.

/Klee and Rummel 2004/ did not follow the guidelines of /Haimson and Cornet 2003/ but used the inflection point method /Gronseth and Kry 1983/, although /Guo et al. 1993/ showed that this method is subjective, strongly dependent upon the time scale used, and always gives a high value on P_s . /Guo et al 1993/ recommended the p_w versus $\log Dt$ -method /Doe and Hustrulid 1981/, the p_w versus $\log (t+Dt)/Dt$ -method /McLennan and Rogiers 1981/, and the Muscat method /Aamodt and Kuriyagawa 1981/.

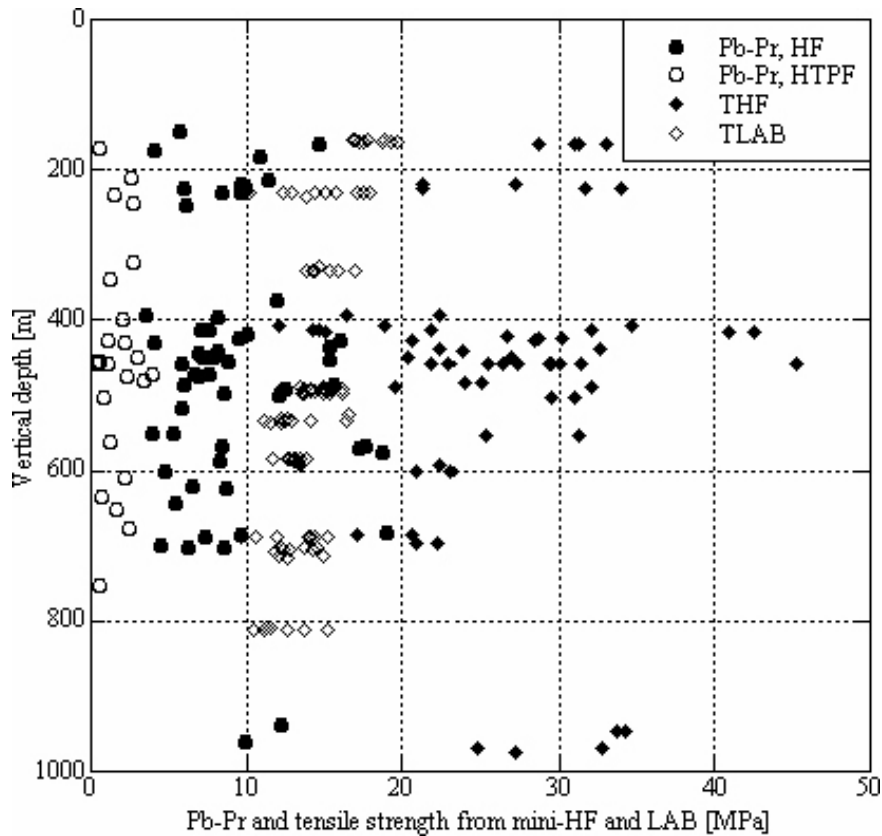


Figure 4-11. Difference between breakdown pressure and re-opening pressure for HF and HTPF tests, results from minifrac tests (THF), and results from indirect tensile strength tests (TLAB) in boreholes KFM01A, KFM02A, and KFM04A /Rummel and Weber 2004, Jacobsson 2004abc, Eloranta 2004a/.

A number of tests involve multiple shut-ins, which could be interpreted as closure of multiple fractures in the test section but are left unmentioned by /Klee and Rummel 2004/. If multiple fractures are indeed found on the imprints, the validity of the test may be questioned when there are no means to determine which fracture has been opened first. The reason for this is that the mechanical opening of a fracture changes the stress field. The interpretation is unambiguous only when one single fracture is opened, for the mechanical opening leaves the normal stress exerted on the fracture plane unchanged. The opening of secondary fractures depends on an unknown stress variation, which cannot be estimated. Hence, tests with multiple fractures do not yield unambiguous results.

The hydraulic fracturing tests were conducted with continuous pumping for a few seconds after obtained breakdown. Some tests involve kinks on the pressure versus time plot (Figure 4-12) whereas some tests display strongly varying pressure (Figure 4-13) during this continued pumping period. Although there is no method to qualitatively exploit this information, they may be interpreted as that thrust regime prevails at the Forsmark site. These tests will be commented upon in the following, but keeping in mind the speculative nature of this procedure.

Hydraulic fracturing in thrust regimes

The hydraulic fracturing test can be generalized by internal pressurization of an infinite rock cylinder. This implies that the test does not generate any stress component parallel with the borehole axis. Hence, in an infinite cylinder, all induced fractures at the borehole wall are perpendicular to the smallest principal stress in the plane perpendicular to the borehole axis, i.e. despite if the vertical stress is the minor principal stress.

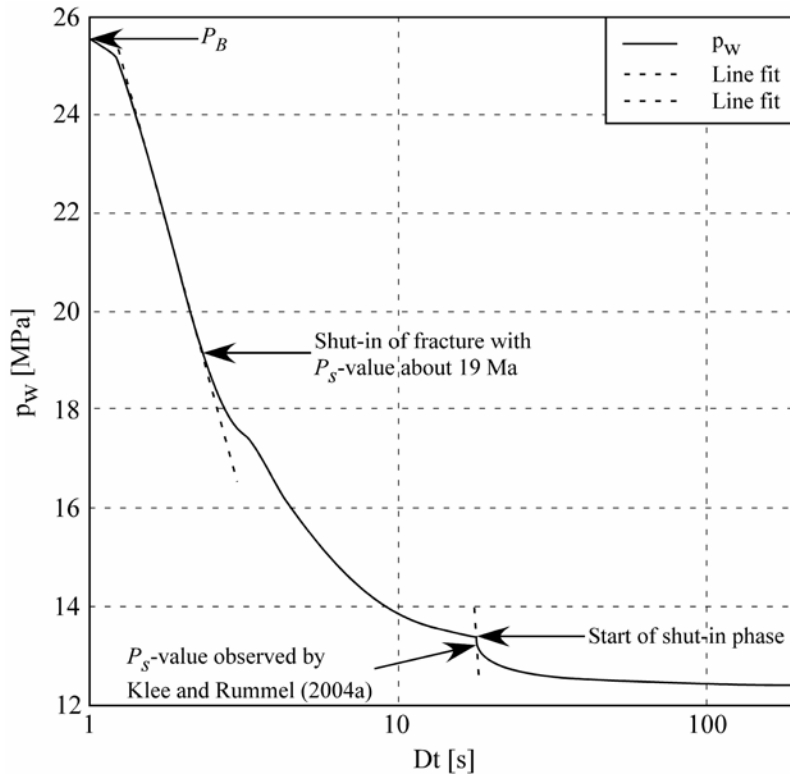


Figure 4-12. Fracturing cycle at 496.00 mbl in borehole KFM01A. Speculation of axial fracture closure prior to the shut-in phase.

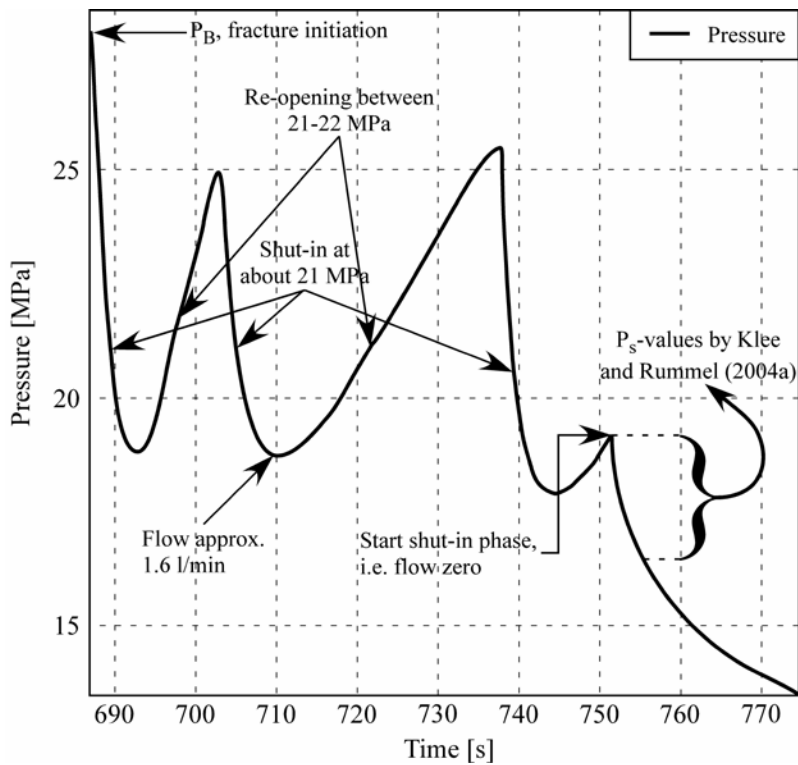


Figure 4-13. Fracturing cycle at 236.00 mbl in borehole KFM01B. Speculation of axial fracture re-openings, and closures prior to the shut-in phase.

Because minor principal stress is vertical in thrust regimes, the axially induced fractures are likely to rotate during subsequent propagation into the rock mass /e.g. Evans et al. 1989/. Whether these fractures propagate back to intersect the borehole, giving traces of both an axial fracture and a fracture perpendicular to the axial direction at the borehole wall, depends on the flow rate, fluid viscosity, packer behavior and tensile strength of the rock. Because the hydraulic fracturing test does not strictly involve an infinite rock cylinder but is restricted by the length of the test section, fractures perpendicular to the axial direction may also be a result of axial stresses exerted by the straddle-packer during testing. However, these packer-induced axial stresses are very small and can only give rise to fractures perpendicular to the axial direction in rocks with low tensile strength or in rocks with weakness planes oriented perpendicular to the borehole axis (Cornet, pers. comm.).

On the pressure versus time records, rotating fractures may be indicated by successively declining shut-in values during the test cycle, but may be difficult to distinguish from the lowering of shut-in values as a result of the necessary propagation of the fracture plane outside the zone of stress concentration around the borehole. Successively declining shut-in values during the test cycle may also be difficult to distinguish in regions where the difference between σ_h - and σ_v -magnitudes is small. Some authors have reported two shut-ins on the pressure versus time records, although only one fracture is visible on imprints /Roegiers et al. 1982, Haimson et al. 1986/, which were interpreted as the closure of the vertical part of the fracture followed by the horizontal part (see also alternative explanation in Section 4.5.7).

In conclusion, when minor principal stress is parallel with the borehole axis, hydraulic fractures are generally perpendicular to the borehole axis, i.e. they rotate from the axial direction to become perpendicular to the borehole axis during the test cycle. In vertical boreholes, fractures rotating from the axial direction to the horizontal direction imply that only σ_v is measured, which may only be regarded as a lower limit of σ_h /e.g. Evans et al. 1989/. Depending on the tensile strength of the rock and how the test is conducted, the fracture indications at the borehole wall may yield a trace of only axial fractures or traces of both an axial fracture and a fracture perpendicular to the axial direction at the borehole wall.

With this introduction to hydraulic fracturing in thrust regimes, we return to the observations in Figures 4-12 and 4-13 and ask if these tests yield some evidence of thrust regime, and if so, do these tests yield some information of minimum horizontal stress during the pumping phase? The conceivable interpretation would then be that an axial fracture was first initiated, which later rotated to become horizontal as it propagated away from the wellbore. The axial fracture would then close first as a result of the stress concentration around the borehole, whereas the horizontal fracture would close during the shut-in phase. This tempting interpretation is though based on several unknown factors: (1) considering that the configuration of a hydraulic fracturing test yields axial fractures, not all imprints include axial fractures and many existing axial fractures are poorly defined; (2) the size of the presumably axial fracture is not known which may result in an overestimation of the σ_h -magnitude if the fracture does not extend beyond the zone of stress concentration around the borehole; (3) as stated above, the opening of more than one fracture in the test section does not yield unambiguous results.

4.5.6 Hydraulic tests on pre-existing fractures (HTPF)

In total, 50 hydraulic tests of pre-existing fractures were planned in boreholes KFM01A, KFM01B, KFM02A, and KFM4A. However, of these attempts /Klee and Rummel 2004/ estimated that only 24 tests stimulated pre-existing fracture planes.

The hydraulic tests on pre-existing fractures are normally associated with the step-rate pressurization test (sometimes denominated hydraulic jacking test). This test is preceded by a breakdown test, aiming at opening a pre-existing fracture in the test section. Different strategies of the breakdown phase exist, but it is the author's opinion that in low-permeability rocks, as at Forsmark, the pressurization should be conducted at a low flow rate /see also Cornet and Valette 1984/. This enhances the possibility to open sealed or partly sealed fractures as the fluid

has time to penetrate the fracture plane and add an additional stress component. This may have produced more true HTPF tests at Forsmark, where most HTPF tests indicate that instead new fractures were induced.

Unlike during hydraulic fracturing, no re-opening tests should be conducted after the breakdown cycle /Haimson and Cornet 2003/. This is to limit the chances of inducing fractures in the test section. Regrettably, /Klee and Rummel 2004/ made several re-opening cycles and multiple fractures were indeed found in 31 out of 49 test sections where imprints were made.

Instead of re-opening cycles after the breakdown test, step-rate tests should be conducted, including either an opening or opening/closing phase, i.e. a cyclic step-rate test (Figure 3-5 and Figure 3-6). During the step-rate test, the flow rate is first brought up to a very low level and maintained constant while the pressure increases and reaches a constant plateau. This is repeated in the following steps, and the pressure is allowed to equilibrate at a constant level (Figure 3-5). This yields an array of constant pressure levels at different flow rates (Figure 3-6). When the fracture is fully open, there are two options: (1) the injection is stopped and the test section shut-in, giving an additional shut-in pressure value; or (2) a cyclic step-rate test is conducted, in which the flow is also reduced in a stepwise manner. Disregarding choice of method, at least three P_s -values should be produced for each test section /Haimson and Cornet 2003/.

/Klee and Rummel 2004/ used alternative 1 but with only a few steps and with very large flow/pressure increments. The first step generally involves a high flow rate, which nearly corresponds to the P_s -value. As a result, the following steps involve further fracture propagation, indicated by unstable pressure versus flow rate curves (Figure 4-14). Further propagation is not necessary, especially considering that at least four cycles were conducted prior to the step-rate test. In fact, this introduces new uncertainties as the fracture plane may rotate when propagating further into the rock mass or intersect with other fractures in the rock mass with different hydraulic properties, or new fractures may be opened. Moreover, equilibrium condition was not reached at each level (Figure 4-15), implying that the evaluated P_s -value will be overestimated.

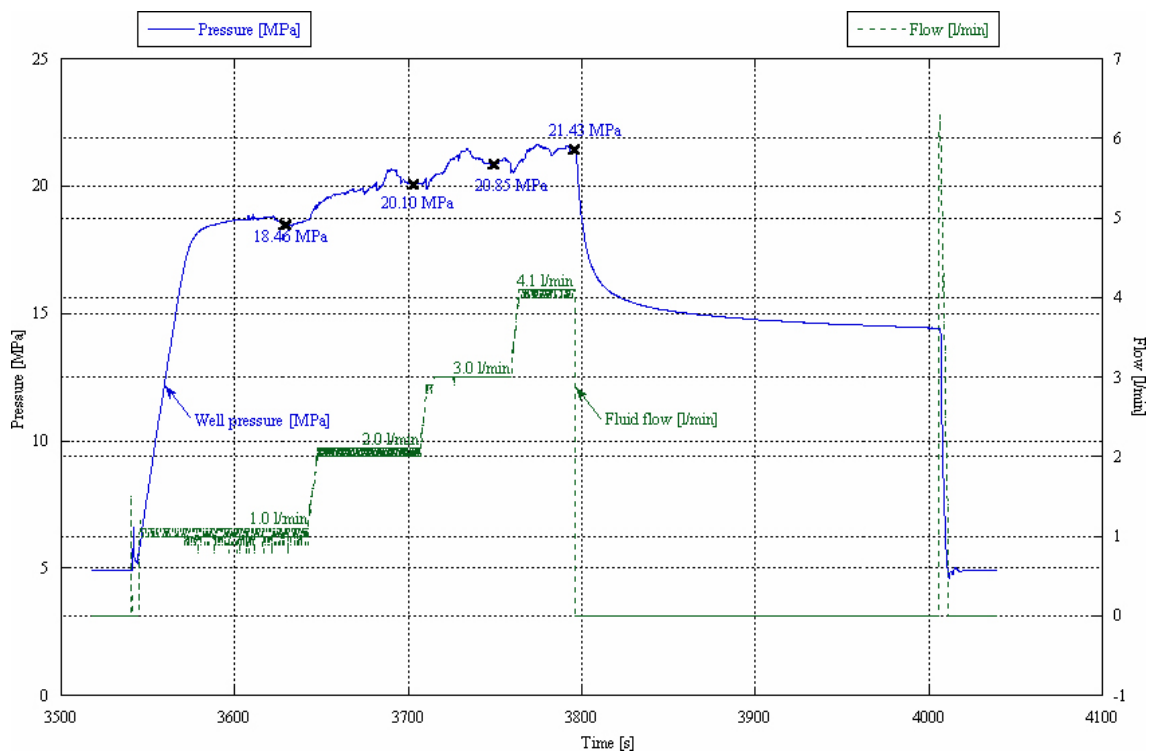


Figure 4-14. Step-rate test at 502.0 mbl in borehole KFM01A. The first step involves a too high flow rate indicated by fracture propagation already at the first step making the interpretation work troublesome /after Klee and Rummel 2004/.

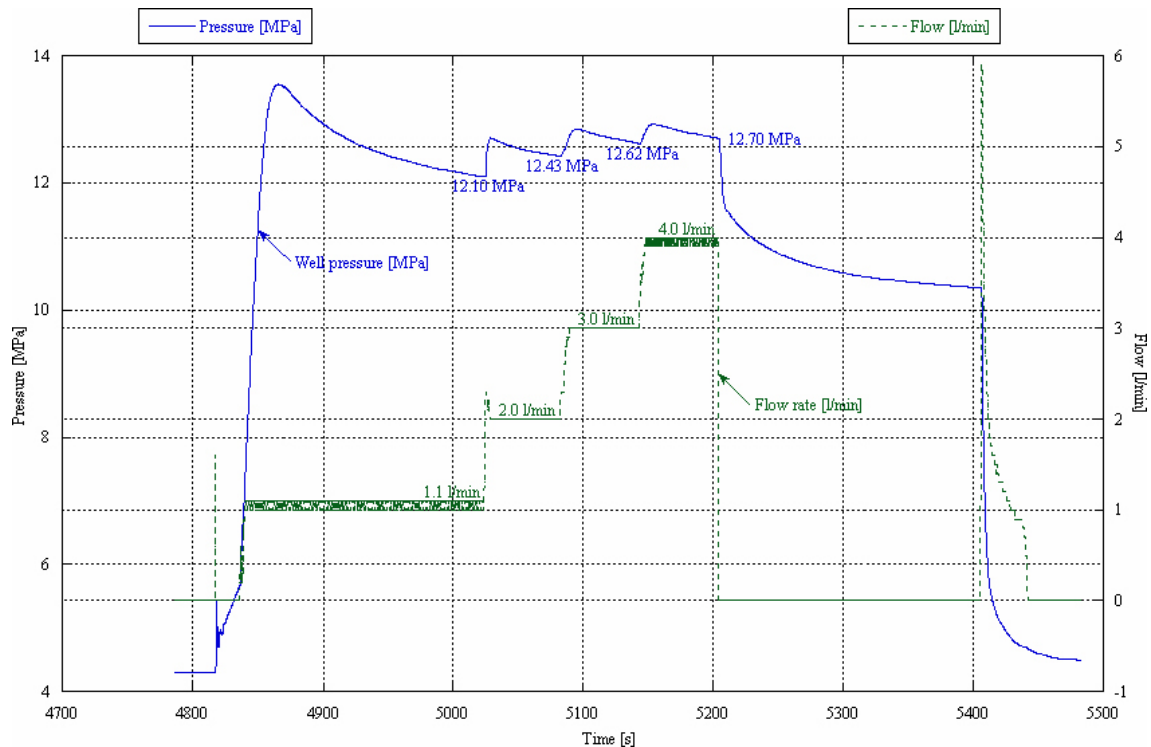


Figure 4-15. Step-rate test at 433.4 mbl in borehole KFM01A. The pressure does not reach equilibrium at each flow rate level, resulting in overestimations of the P_s -value /after Klee and Rummel 2004/.

A serious constraint during step-rate tests was recently presented by /Cornet et al. 2003/, stating that the P_s -value may be overestimated for mean fracture openings of less than 15–20 μm and for channeling-controlled fluid flow. In those cases, /Cornet et al. 2003/ concluded that step-rate tests should discard results from the opening phase.

It is conceivable that the stress situation at Forsmark, with relatively large stress magnitudes, may lead to residual fracture apertures below 20 μm . Determination of fracture apertures was, though, outside the scope of the field tests at Forsmark, and the effect of this phenomenon was not investigated.

4.5.7 Determination of fracture orientations

The fracture orientations were determined using two systems; an oriented impression packer and the Boremap system. The impression packer was only applied in 49 of the 85 test locations, and in the remaining 36 test sections the Boremap system was used.

The obtained imprints indicate relatively poorly defined fractures, especially for borehole KFM01A, and with multiple fractures in 31 out of 49 test sections. Because it is not possible to determine, based on the imprint record, which fracture that has been tested when multiple fractures appear, different fracture alternatives must be tested. This means that, assuming that all tests are used for stress calculation, 432 fracture combinations have to be tested in borehole KFM01A, 96 in borehole KFM01B, 256 in borehole KFM02A, and 1,152 in borehole KFM04A, during stress calculations at the single borehole scale. In three hydraulic fracturing measurements, imprints were not made and the data cannot be used.

The ISRM suggested method /Haimson and Cornet 2003/ explicitly states that tests should involve only one single fracture per test section. When multiple fractures are opened, only the first fracture opening may be used for stress evaluation. This implies that borehole examination is required at the end of each hydraulic test. In the Forsmark case, all hydraulic tests have not been associated with an imprint taken at the end of the test and hence, according to /Haimson

and Cornet 2003/, should not be integrated in the stress evaluation process. It may be argued that the Boremap system may be used although this system is based on logging prior to the hydraulic tests. However, because most tests indicate that fractures have been induced, significant errors may be introduced as fractures of unknown orientation are likely to exist in the test section. Moreover, /Klee and Rummel 2004/ stated that the relative depth error is 13 to 24 cm within a 100 m depth interval, which may lead to misplacement of the straddle packer over the chosen fracture. Possibly, this may be the cause of the poor match of fractures between the two systems used.

Another important factor is that the fracture orientations based on Boremap and impression packer systems are rather imprecise. For Boremap, the precision of the fracture orientations using a gravity sensor is of the order of 1° , but it is dependent on the operator, which manually records the orientation of the system downhole during BIPS-logging. (Stenberg pers. comm.) estimated the imprecision in orientations to $2\text{--}3^\circ$ during logging. To this, the imprecision of the borehole orientation in space should be added, giving a total imprecision of approximately $4\text{--}8^\circ$ (Stenberg, pers. comm.). For the impression packer technique, the uncertainty in the fracture orientations is a function of the precision of the magnetic compass, the condition of the impression packer, and the transfer of fractures on the impression packer to a plastic film. For vertical boreholes, the imprecision of the dip is smaller than the imprecision of the strike or dip direction. It is estimated that in the optimal case (optimal handling and the packer is a perfect cylinder), the imprecision is about 2° and 6° for the dip and dip direction, respectively. However, even e.g. the slightest wear of the impression packer (i.e. when it is no longer perfectly cylindrical) changes the situation drastically. Moreover, inclined boreholes also require information of the borehole orientation in space. Hence, in inclined boreholes, the optimal case (the packer is a perfect cylinder) implies a total imprecision for the dip and dip direction for inclined boreholes in the order $4\text{--}7^\circ$ and $8\text{--}13^\circ$, respectively.

Out of 49 impression tests with a total of 77 fractures, only 13 imprint fractures were positively correlated with fractures on the Boremap file and for another 10, the correlation is regarded as uncertain (depth error, deviation in strike and dip angles more than 25° and 10° , respectively). In other words, 20 test sections include one or two fractures that were positively or possibly correlated with fractures on the Boremap file, whereas in 29 test sections no correlation could be found. Moreover, a large amount of the non-identified fractures are likely induced, which indicates that most hydraulic tests have resulted in multiple fractures. Traces of 12 additional fractures were found on the imprints, which were not reported by /Klee and Rummel 2004/. Most of these traces are though too limited for a reliable determination of their orientation.

4.5.8 Correlation with geological/geophysical data

Because the P_s -values using the Muscat method /Aamodt and Kuriyagawa 1981/ follow a well-defined trend with depth, which suggests that influence of discontinuities in the rock mass is negligible, no attempts were made to correlate data with known discontinuities for boreholes KFM01A, KFM01B, and KFM04A.

The data collected in borehole KFM02A display significantly reduced normal stresses between 412 and 518 mvd and at 753.8 mvd, and slightly reduced normal stresses at 653.2 and 703.8 mvd. These heterogeneous data may be interpreted as a result of rock local heterogeneities in the rock mass or a results of that fractures have propagated and reached across one of the packers, inducing some by-pass that closes when the pressure becomes low enough. The water level in the borehole was continuously monitored in the field and the test section was shut during the shut-in phase and the pressure increase was monitored (Klee and Rummel, pers. comm.). However, water level variations will be observed only if the well is perfectly tight. If e.g. a highly conductive fracture exists close to the surface, one may not observe changes in the water level. Moreover, if the short-circuit is with the lower packer, water level changes will not be detected. For the return flow test, which was employed continuously during the field campaign, it is not always an indication that the test has been successful without short-circuiting. This may be the case when the formation fluid has a higher density compared with that of the

injection fluid. In such cases, the pore pressure at a particular depth is larger in the formation than in the hose/tubing filled. Such conditions will result in what appears to be a nice water return, although there may have been a major leak. This phenomenon was identified at e.g. Soultz /e.g. Evans et al. 1998/. However, in borehole KFM02A, the density difference between the formation and injection fluid (from borehole HFM05) is small (about 2 kg/m³), and the effect is hence negligible.

The observed normal stresses are lower than the anticipated minor principal stress (the vertical stress). If these values are true and not a result of short-circuiting around the packers, they represent anomalies in the prevailing stress field. When the minimum principal stress component is vertical, its value may be smaller than the weight of the overburden because of various structural effects, as was observed for example at the Bure sedimentary site, France /Wileveau et al. 2007/.

A closer look at the data between 412 and 518 m depth entails that the data are located near/ within a deformation zone. The wide zone, denominated ZFMNE00A2 with an interpreted dip of 24° towards SSE /SKB 2005/, involves increased fracture frequency of both open and sealed fractures, predominantly coated with chlorite and/or calcite, between 415 to 520 mbl (414–518 mvd; /Carlsten et al. 2004/). *(After completion of this study, this zone has been identified to be composed of two deformation zones, ZFMNE00A2 (later abbreviated to ZFMA2) with strike/dip 080/24 and intersecting borehole KFM02A at 417–442 mbl, and KFMF1 with strike/dip 070/10 and intersecting KFM02A at 476–520 mbl /Stephens et al. 2007/).* The hydraulic data indicate both reduced stress magnitudes and rotating stress directions. Above and below the zone, based on orientations of axial fractures dipping more than 70° on imprints, σ_H is orientated 116 ± 8°N (three tests) and 136 ± 6°N (4 tests), respectively. However, data between 376 and 457 mbl indicate a σ_H -orientation of 24 ± 4°N (three imprints available with axial fractures dipping more than 70°). Furthermore, the test at 413.50 mbl has one sub-axial fracture inclined less than 70° (strike/dip 31°N/68° with dip direction 301°N). Thus, these data suggest that σ_H rotates when approaching zone ZFMNE00A2. The test at 413.50 mbl suggests that minimum horizontal stress is approximately perpendicular to the zone. The number of tests is however small and further tests are required for a more reliable evaluation of the effect of zone ZFMNE00A2 on the stress field at the Forsmark site.

5 New stress estimations

A new stress estimation using unambiguous or partly unambiguous hydraulic stress data of /Klee and Rummel 2004/ was undertaken using two approaches: (1) profiling approach; and (2) cluster approach.

5.1 New stress inversions using all available unambiguous or partly unambiguous hydraulic data

The inversions are based on unambiguous and partly unambiguous data, i.e. data that are judged to have reliable normal stress (from the shut-in phase) and fracture orientation (clear imprints of planar, primarily single, fractures; Table 5-1). The normal stress and fracture orientation data are taken directly from the report of /Klee and Rummel 2004/. In total, there are 11 completely unambiguous hydraulic tests distributed in the four boreholes, and another 14 tests with a reliable normal stress estimate but with multiple fractures identified on the imprint or pressure-versus time record. In borehole KFM02A, all acceptable tests yield sub-parallel vertical fractures, which is a strong constraint of the local minimum horizontal principal stress direction (N40°E) as well as a fair constraint on its magnitude. The data also suggest that the vertical direction is within 15° of the principal direction in the absence of en echelon fractures (Cornet, pers. comm.). However, as pointed out above, the zone ZFMNE00A2 influences the stress field and data above and below the zone should not be integrated. In the inversions, data located above the ZFMNE00A2 zone in KFM02A were excluded as well as data from borehole KFM04A, which are sampled near the border of the tectonic lens (with unknown affect on the regional stress field).

Two approaches were applied; profiling and cluster approaches. In the first approach, attempts were made to use all unambiguous and partly unambiguous data (11+14 data) with investigation of all possible fracture alternatives (96 combinations). This proved to be very problematic as the data set was strongly heterogeneous. To improve the results, three constraints were used to reduce the number of unknowns: (1) one principal stress is vertical; (2) the vertical principal stress is consistent with the theoretical weight of the overburden rock mass; and (3) maximum horizontal stress is directed 134°N. These assumptions are based on the results of /Klee and Rummel 2004/ and reduce the number of unknowns to 4 (σ_v , σ_H and their variation with depth).

The cluster approach was applied because of the problems to invert data using the profiling method. In the cluster method, closely located measurement points were chosen so that, with the constraints described above, the number of model parameters can be reduced to two (as the stress gradients can be neglected). Again, all possible fracture combinations were used. For example, the first cluster involves the tests at 167.07, 183.46 – fracture one, and 211.13 mbl in KFM01B. The second cluster involves the tests at 167.07, 183.46 – fracture two, and 211.13 mbl, whereas the third cluster involves the tests at 183.46 – fracture one, 211.13, and 228.97 mbl – fracture one. Thus, the approach involves a step-wise movement downhole with a replacement of the shallowest measurement at each cluster with the test located immediately below the cluster until all possible clusters have been tested.

Table 5-1. Completely and partly unambiguous hydraulic tests by /Klee and Rummel 2004/ at Forsmark.

Borehole	Vertical depth [m]	Fracture orientation			Normal stress [MPa]
		Strike [°N]	Dip direction [°N]	Dip [°]	
KFM01A	427.40	136	226	35	12.3
KFM01A	452.87	9	279	18	11.0
		<i>121*</i>	<i>31</i>	<i>87</i>	
		?	?	?	
KFM01A	472.27	147	237	18	10.8
KFM01A	492.11	46	136	21	12.4
		159	249	14	
		<i>140*</i>	<i>230</i>	<i>88</i>	
KFM01B	167.07	18	288	19	3.0
KFM01B	183.46	85	175	3	5.0
		77	347	87	
KFM01B	211.13	118	28	7	4.1
KFM01B	228.97	141	231	39	16.0
		152	242	35	
KFM01B	229.94	161	251	23	16.1
		174	264	37	
KFM01B	230.90	128	218	24	13.5
KFM01B	397.00	5	95	13	15.3
		3	273	72	
KFM01B	399.18	137	227	26	13.2
KFM01B	454.68	144	234	76	24.2
KFM01B	457.33	101	191	38	16.9
		?	?	?	
KFM01B	459.32	124	214	41	17.2
		?	?	?	
KFM02A	220.09	110	20	90	7.1
		131	221	40	
KFM02A	549.53	128*	218	89	16.4
		?	?	?	
KFM02A	600.58	137*	227	88	18.3
		?	?	?	
KFM02A	698.30	142*	232	88	21.6
KFM02A	701.08	136*	226	89	22.6
KFM04A	171.43	172	82	15	4.9
KFM04A	322.95	140	50	17	18.2
		13	103	32	
		145	55	41	
KFM04A	471.33	99	189	9	14.0
		?	?	?	
KFM04A	474.84	46	316	78	15.0
KFM04A	479.34	114	204	12	17.0

Data in italic are doubtful because of secondary fractures. “?” denotes fractures with unknown orientation. “*” denotes data used for orientation of σ_H .

5.1.1 The profiling approach

The inversions using the profiling method proved to be problematic because the data set was strongly heterogeneous. As a result, only six measurement points are included in the best model when considering the resolution of solely σ_h . For σ_H , the number of constraining fractures is very small and it is therefore left almost unresolved (Figure 5-1; Table 5-2). Maximum horizontal stress was also determined using the relationship $\sigma_H = T + 3\sigma_h - P_b$, where T was determined to 5.6 MPa by /Rummel and Weber 2004; Figure 5-1; Table 5-2/. The results indicate that between 400 and 750 mvd:

$$\sigma_h = 16.9 + 0.035(z - 560) \text{ MPa; where } z \text{ is true vertical depth.}$$

$$\sigma_H = 50.9 + 0.014(z - 560) \text{ MPa; where } z \text{ is true vertical depth.}$$

$$\text{or when using the relationship } \sigma_H = T + 3\sigma_h - P_b$$

$$\sigma_H = 32.3 + 0.104(z - 560) \text{ MPa; where } z \text{ is true vertical depth.}$$

5.1.2 The cluster approach

The results using the cluster approach provided strongly varying results. Because the resolution of σ_H is generally very poor, only values of σ_H evaluated using the relationship $\sigma_H = T + 3\sigma_h - P_b$ are presented.

At about 220 mvd, σ_h varies between 17.0 and 41.7 MPa with an average of 33.1 ± 6.3 MPa. For σ_H , the corresponding variation is between 37.9 and 107.8 MPa with an average of 80.4 ± 18.6 MPa (Figure 5-2).

At about 450 mvd, σ_h varies between 12.6 and 20.6 MPa with an average of 16.9 ± 3.3 MPa. For σ_H , the corresponding variation is between 17.0 and 41.6 MPa with an average of 32.1 ± 9.4 MPa (Figure 5-2).

Table 5-2. The best model using hydraulic data.

Borehole	Vert. depth [m]	Dip direction [°N]		Dip [°]		Normal stress [MPa]	
		Measured	Calculated	Measured	Calculated	Measured	Calculated
KFM01A	427.27	226	226.2	35	35.0	10.8	11.6
KFM01B	457.33	191	190.5	38	38.1	16.9	16.8
		?	–	?	–	16.9	–
KFM02A	549.53	218	218.7	89	89.0	16.4	16.4
		?	–	?	–	16.4	–
KFM02A	600.58	227	226.9	88	88.0	18.3	18.3
		?	–	?	–	18.3	–
KFM02A	698.30	232	230.9	88	88.0	21.6	22.1
KFM02A	698.30	226	226.6	89	89.0	22.6	21.8

“?” denotes fractures with unknown orientation.

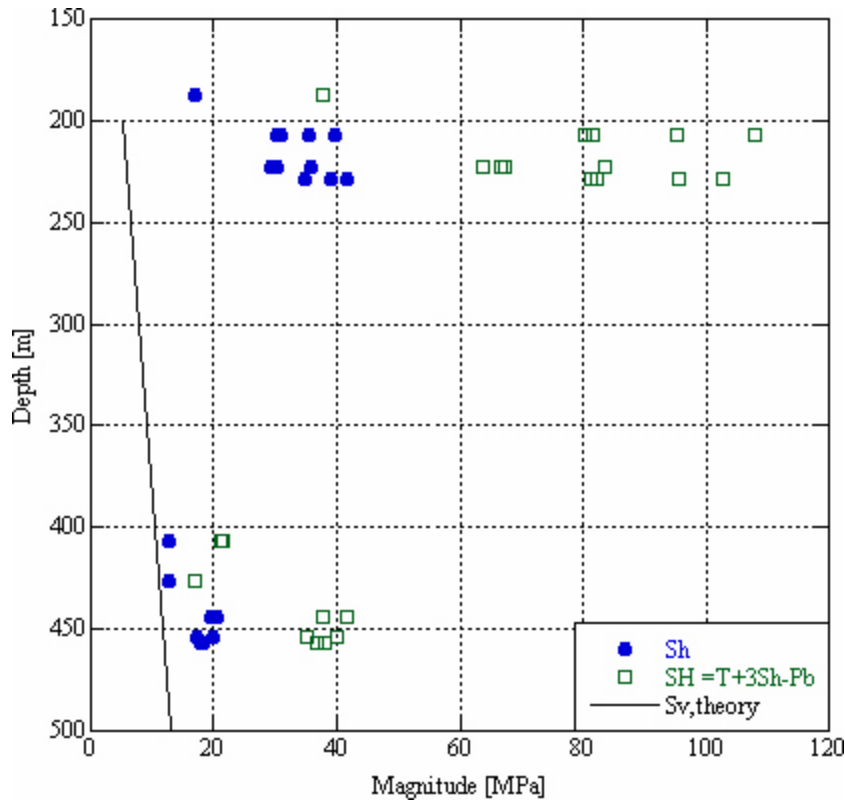


Figure 5-1. Estimates of horizontal stresses at the Forsmark site using profiling approach with unambiguous and partly unambiguous hydraulic stress data. S in the figure corresponds to σ in the text.

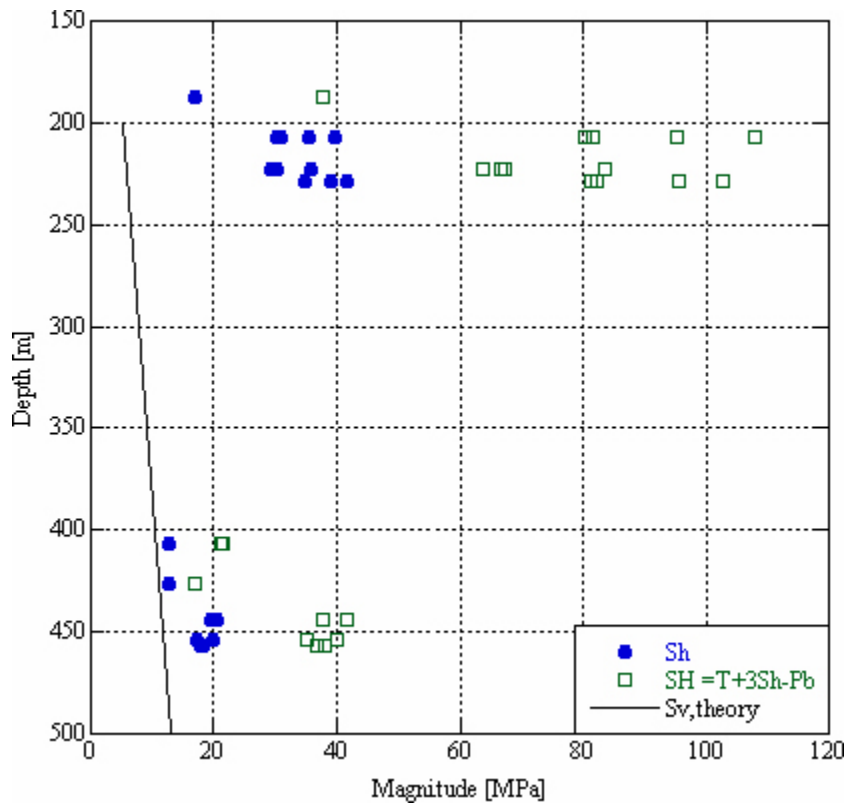


Figure 5-2. Estimates of horizontal stresses at the Forsmark site using cluster approach with unambiguous and partly unambiguous hydraulic stress data. S in the figure corresponds to σ in the text.

5.2 Forced overcoring stress calculations

Overcoring results depend linearly on the value of the measured elastic Young's modulus and on the Poisson's ratio. Both quantities depend strongly on the development of micro-cracks that affect samples on which measurements are being conducted. True HF tests often yield good constraints on principal stress directions and on the magnitude of the minimum principal stress, but only poor values for the maximum horizontal principal stress component. Hence, combining both methods should provide means to constrain the complete stress tensor.

The obtained results with re-interpreted hydraulic and overcoring stress techniques at the Forsmark site demonstrate a fairly consistent magnitude of minimum horizontal stress and orientations of the horizontal stresses. However, in many overcoring tests, none of the principal stresses is vertical whereas the hydraulic data clearly demonstrated that one principal stress is vertical. Moreover, the hydraulic stress data clearly reveal that the vertical component closely resembles the theoretical weight of the overburden rock mass. Maximum horizontal stress, although somewhat less certain compared with that the vertical stress is equal to the theoretical weight of the overburden, is directed about 134°N. As a result of these findings, it was decided to make new overcoring stress calculations in which the hydraulic stress data help constrain the stress field as determined by overcoring strain data. The objective of such an approach is to investigate whether the hypothesis of continuity of the stress field is reasonable; it is not to produce a complete evaluation of the stress field over a multi km³ volume.

It is emphasized that, at this stage, the approach does not include a joint inversion of both data sets. Such an approach is attempted in Section 5.4. The approach involved the following five steps:

Constraint 1). One principal stress was forced to be vertical.

Constraint 2). The vertical stress was forced to be consistent with the theoretical weight of the overburden rock mass.

Constraint 3). The maximum horizontal stress was forced to be oriented 134°N.

Constraint 4). The minimum horizontal stress was forced to be consistent with the solution for hydraulic stress data (the profiling solution) in Section 5.1.1.

In each stress calculation, the most deviating strain gauge was removed until all remaining gauges fitted the 99% confidence interval of the corresponding strain reading. Thus, this semi-integrated stress determination procedure progressively takes advantage of the results from the hydraulic data. The resulting forced overcoring stress profile yields a reasonable estimate of the maximum horizontal principal stress component, which could not be estimated unambiguously using the collected hydraulic data at the Forsmark site.

The inversions are made in two steps, using single measurement points and integration of all overcoring data in each borehole.

Prior to these inversions, the data in borehole KFM01B were temperature corrected. The original interpretation of all data prior to the temperature correction and forced calculations are presented in Figure 5-3, which will be used hereafter for comparisons with the results of the forced calculations.

The original result yields (single measurement points):

$$\sigma_h = 17.5 + 0.036(z - 250) \text{ MPa; where } z \text{ is true vertical depth.}$$

$$\sigma_H = 30.5 + 0.074(z - 250) \text{ MPa; where } z \text{ is true vertical depth.}$$

$$\sigma_v = 10.5 + 0.034(z - 250) \text{ MPa; where } z \text{ is true vertical depth.}$$

$$\text{Orientation } \sigma_H = 115 + 0.09(z - 250)^\circ\text{N; where } z \text{ is true vertical depth.}$$

5.2.1 Results using Constraint 1

Single measurement points

The results indicate that all strain data in borehole KFM01B, 98% of the strain data in borehole DBT-1, and 96% of the strain data in borehole DBT-3 are consistent with Constraint 1. This exceptionally good agreement is interpreted as a verification of that a principal stress is indeed vertical. The resulting stress magnitudes for the three boreholes indicate small differences between the original results (Figure 5-4).

The uppermost 100 m show a large scatter for both horizontal stresses, whereas the large scatter of the orientation of maximum horizontal stress extends down to 250 m depth. Between 100 to 200 m depth, the magnitudes of maximum horizontal stress seem reduced compared with the general trend, especially for borehole DBT-1. The scatter for the vertical stress is large and is considerably overestimated by primarily the data in borehole KFM01B (Figure 5-4).

The result using Constraint 1 yields:

$$\sigma_h = 17.6 + 0.036(z - 250) \text{ MPa; where } z \text{ is true vertical depth.}$$

$$\sigma_H = 30.3 + 0.073(z - 250) \text{ MPa; where } z \text{ is true vertical depth.}$$

$$\sigma_v = 10.5 + 0.036(z - 250) \text{ MPa; where } z \text{ is true vertical depth.}$$

$$\text{Orientation } \sigma_H = 113 + 0.08(z - 250)^\circ \text{N; where } z \text{ is true vertical depth.}$$

Single boreholes

The borehole scale involves the additional assumption of a homogeneous and continuous rock mass. As a result, the number of consistent strain data is somewhat reduced. The results indicate that 75% of the strain data in borehole KFM01B, 77% of the strain data in borehole DBT-1, and 77% of the strain data in borehole DBT-3 are consistent with Constraint 1. The results indicate a good agreement for σ_v and σ_H between DBT-1 and DBT-3 and for orientation of σ_H for all boreholes, whereas the remainder of data show a considerable scatter (Figure 5-5).

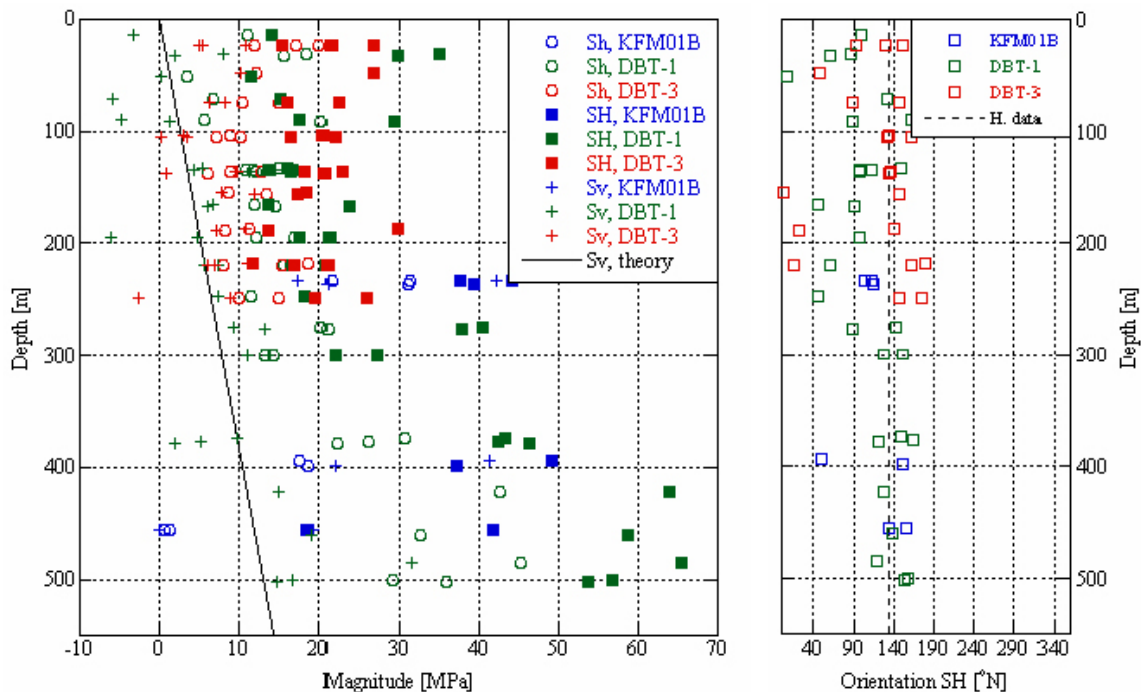


Figure 5-3. Summary plots displaying original results from boreholes KFM01B, DBT-1, and DBT-3. These plots are used for comparison with results from forced inversions. *S* in the figure corresponds to σ in the text.

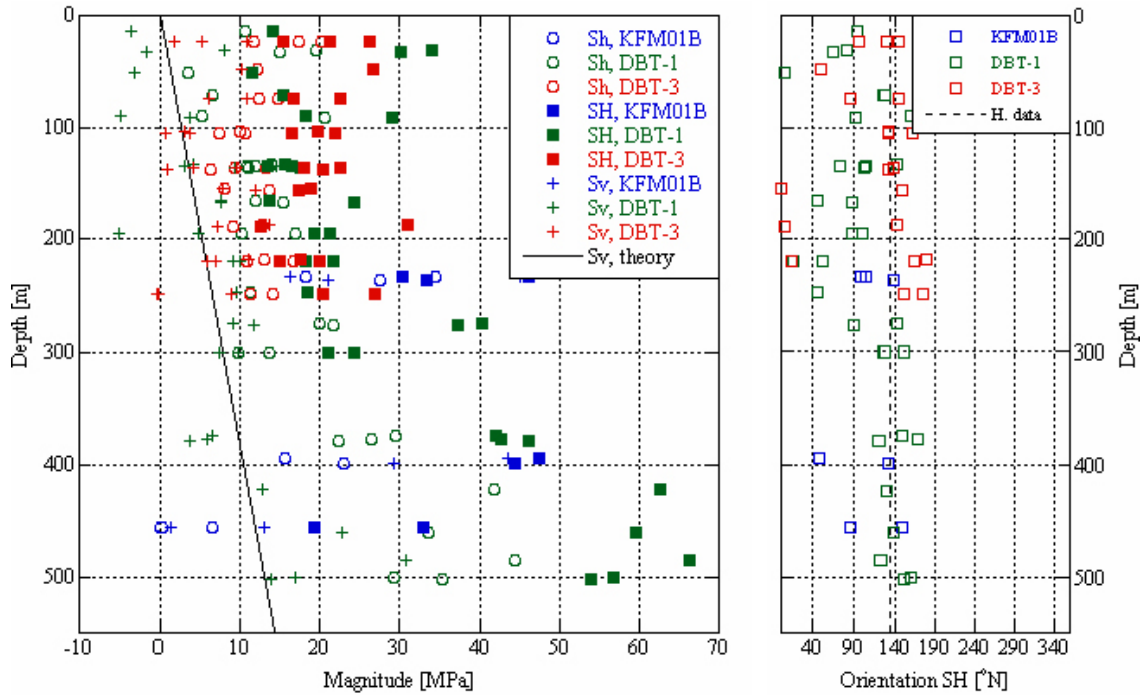


Figure 5-4. Summary plots displaying results using Constraint 1 for boreholes KFM01B, DBT-1, and DBT-3 using single measurement points. S in the figure corresponds to σ in the text.

5.2.2 Results using Constraints 1 and 2

Single measurement points

The results indicate that 98% of the strain data in borehole KFM01B, 94% of the strain data in borehole DBT-1, and 96% of the strain data in borehole DBT-3 are consistent with Constraints 1 and 2. This exceptionally good agreement is interpreted as a verification of that the vertical principal stress is indeed equal to the theoretical weight of the overburden rock mass. The resulting stress magnitudes for the three boreholes again display small differences between the original results (Figure 5-3). The uppermost 100 m still show a large scatter for both horizontal stresses and the large scatter of the orientation of maximum horizontal stress still extends down to 250 m depth (Figure 5-6). Moreover, the magnitudes of maximum horizontal stress between 100 to 200 m depth seem reduced compared with the general trend, especially for borehole DBT-1.

The result using Constraints 1 and 2 yields:

$$\sigma_h = 17.1 + 0.035(z - 250) \text{ MPa; where } z \text{ is true vertical depth.}$$

$$\sigma_H = 29.6 + 0.070(z - 250) \text{ MPa; where } z \text{ is true vertical depth.}$$

$$\sigma_v = 6.6 + 0.0265(z - 250) \text{ MPa; where } z \text{ is true vertical depth.}$$

$$\text{Orientation } \sigma_H = 113 + 0.08(z - 250)^\circ\text{N; where } z \text{ is true vertical depth.}$$

Single boreholes

The results indicate that 68% of the strain data in borehole KFM01B, 75% of the strain data in borehole DBT-1, and 88% of the strain data in borehole DBT-3 are consistent with Constraints 1 and 2. The results indicate a relatively large scatter apart from the orientation of σ_H (Figure 5-7).

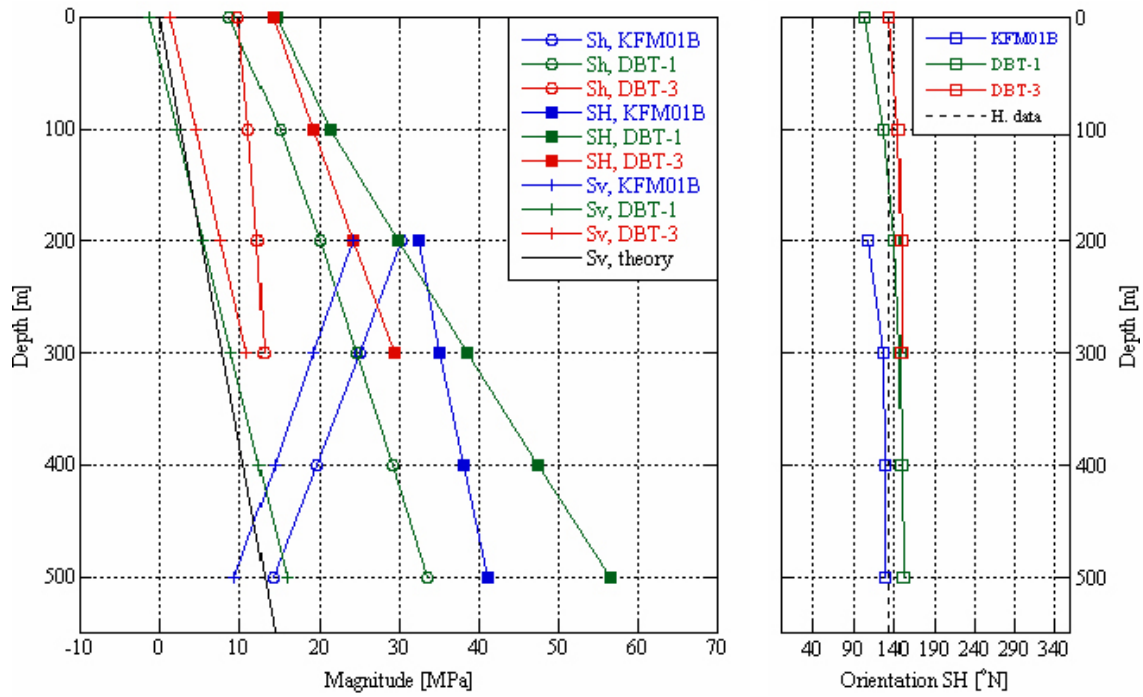


Figure 5-5. Summary plots displaying results using Constraint 1 for boreholes KFM01B, DBT-1, and DBT-3 at the borehole scale. S in the figure corresponds to σ in the text.

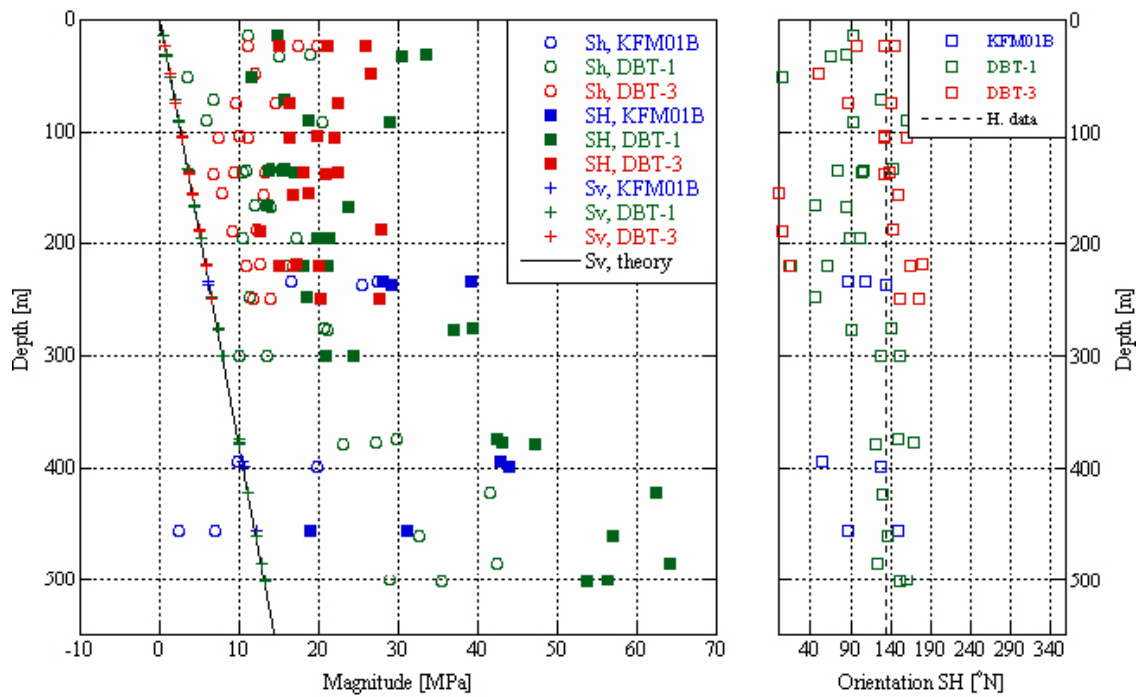


Figure 5-6. Summary plots displaying results using Constraints 1 and 2 for boreholes KFM01B, DBT-1, and DBT-3 using single measurement points. S in the figure corresponds to σ in the text.

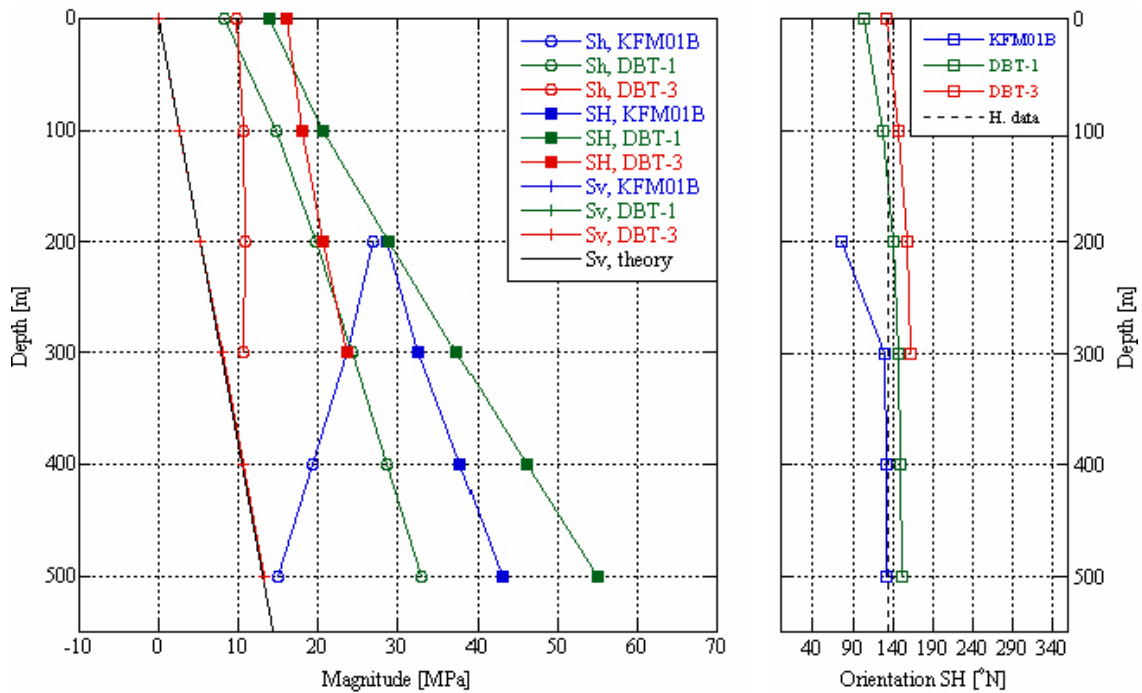


Figure 5-7. Summary plots displaying results using Constraints 1 and 2 for boreholes KFM01B, DBT-1, and DBT-3 at the borehole scale. *S* in the figure corresponds to σ in the text.

5.2.3 Results using Constraints 1, 2, and 3

Single measurement points

The results indicate that 70% of the strain data in borehole KFM01B, 67% of the strain data in borehole DBT-1, and 67% of the strain data in borehole DBT-3 are consistent with Constraints 1, 2, and 3. The quite reduced consistency is due to that 2 tests (out of 7 or 29%) in borehole KFM01B, 9 tests (out of 30 or 30%) in borehole DBT-1, and 6 tests (out of 20 or 30%) in borehole DBT-3 are non-consistent with the orientation of 134°N of maximum horizontal stress. However, when excluding these data, the overwhelming majority of tests are consistent with Constraints 1, 2, and 3 (98% in borehole KFM01B, 96% in borehole DBT-1, and 96% in borehole DBT-3).

Although several tests are not consistent with the constraints, the results are judged as a verification of that maximum horizontal stress is oriented close to 134°N (and that the vertical principal stress is equal to the theoretical weight of the overburden rock mass). The resulting stress magnitudes for the three boreholes again display small differences between the original results (Figure 5-3). The scatter in stress magnitude data has now been significantly reduced, especially for minimum horizontal stress (Figure 5-8). The result using Constraints 1, 2, and 3 yields:

$$\sigma_h = 20.1 + 0.048(z - 250) \text{ MPa; where } z \text{ is true vertical depth.}$$

$$\sigma_H = 29.9 + 0.083(z - 250) \text{ MPa; where } z \text{ is true vertical depth.}$$

$$\sigma_v = 6.6 + 0.0265(z - 250) \text{ MPa; where } z \text{ is true vertical depth.}$$

$$\text{Orientation } \sigma_H = 134^\circ\text{N.}$$

Single boreholes

The results indicate that 67% of the strain data in borehole KFM01B, 74% of the strain data in borehole DBT-1, and 77% of the strain data in borehole DBT-3 are consistent with Constraint 1, 2, and 3. The results indicate significant discrepancies between boreholes (Figure 5-9).

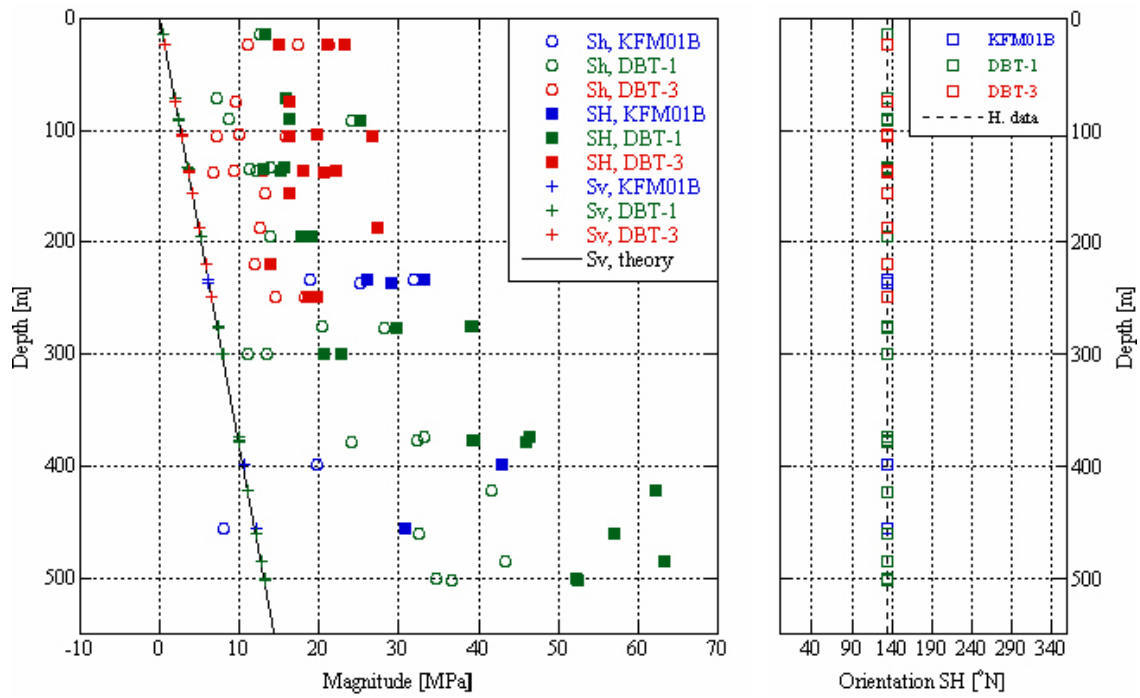


Figure 5-8. Summary plots displaying results using Constraint 1, 2, and 3 for boreholes KFM01B, DBT-1, and DBT-3 using single measurement points. S in the figure corresponds to σ in the text.

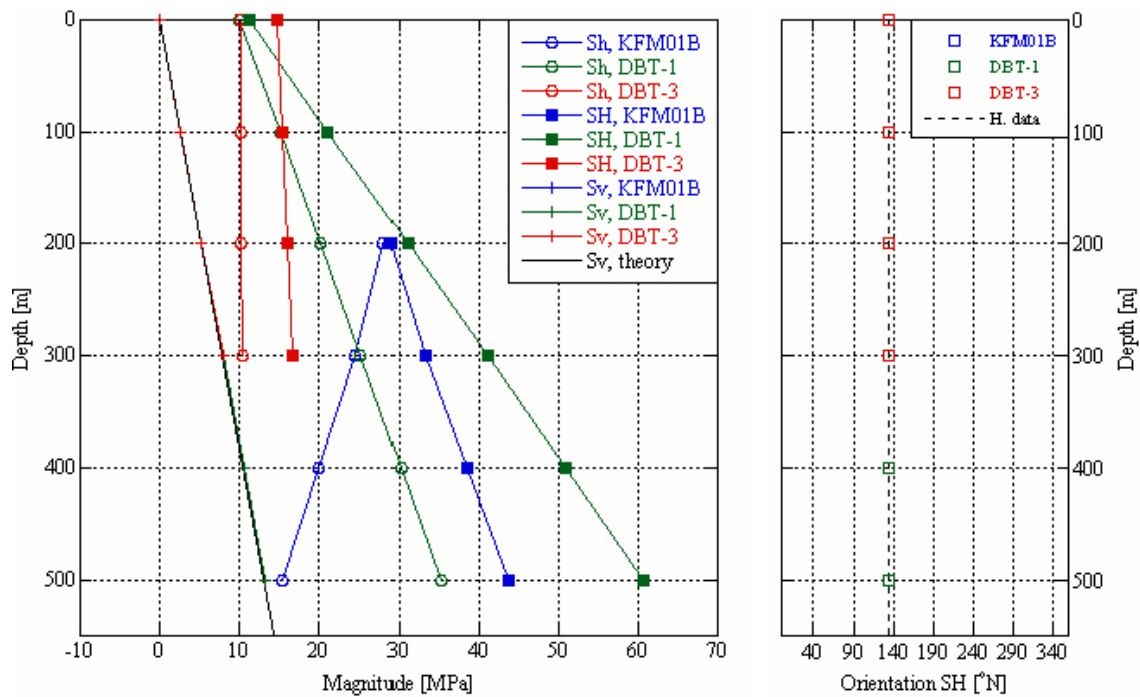


Figure 5-9. Summary plots displaying results using Constraint 1, 2, and 3 for boreholes KFM01B, DBT-1, and DBT-3 at the borehole scale. S in the figure corresponds to σ in the text.

5.2.4 Results using Constraints 1, 2, 3, and 4

Single measurement points

Constraint 4 involves σ_h based on the profiling approach using hydraulic stress data. This profile is valid between 400 to 750 mvd and the number of data within this interval is therefore quite small. To increase the number of tests, the profile was assumed valid between 350 to 750 mvd. In total, the overcoring tests within this interval involve 4 tests in KFM01B (394–456 mvd) and 8 tests in DBT-1 (375–502 mvd).

The results indicate that 50% of the strain data in borehole KFM01B and 85% of the strain data in borehole DBT-1 are consistent with Constraints 1, 2, 3, and 4. The quite reduced consistency for borehole KFM01B is due to that 2 tests (the unreliable tests at 406.92 and 472.98 mbl, see Section 4.2) are not consistent with the orientation of 134°N of maximum horizontal stress. However, the other two tests in borehole KFM01B are completely consistent with Constraints 1, 2, 3, and 4.

The relatively large number of strain data that are consistent with the constraints is judged as a verification of that minimum horizontal stress is indeed close to $6.2+0.035(z-250)$ MPa, where z is true vertical depth (and that the vertical principal stress is equal to the theoretical weight of the overburden rock mass, and that σ_H is oriented 134°N). The results indicate a large gradient of σ_H with depth in borehole DBT-1, whereas the gradient of σ_H in borehole KFM01B is significantly smaller (Figure 5-10).

The result using Constraints 1, 2, 3, and 4 yields:

$\sigma_h = 14.3+0.035(z-500)$ MPa; where z is true vertical depth.

$\sigma_H = 53.4+0.101(z-500)$ MPa; where z is true vertical depth.

$\sigma_v = 13.2+0.0265(z-500)$ MPa; where z is true vertical depth.

Orientation $\sigma_H = 134^\circ\text{N}$.

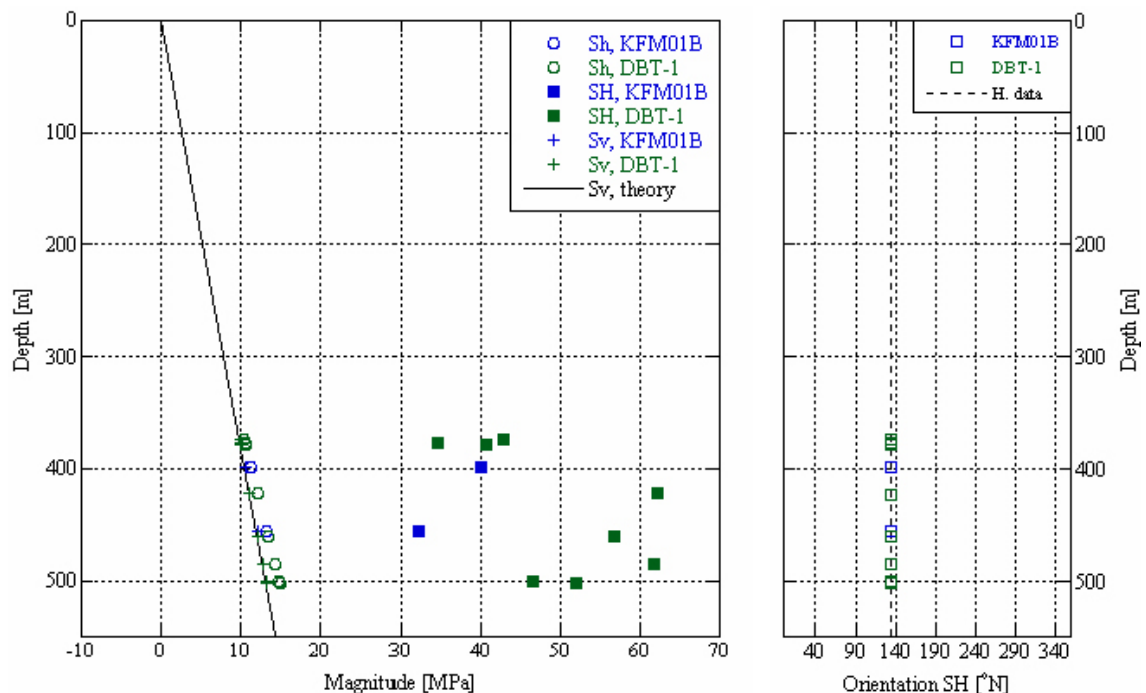


Figure 5-10. Summary plots displaying results using Constraints 1, 2, 3, and 4 for boreholes KFM01B, and DBT-1 using single measurement points. S in the figure corresponds to σ in the text.

Single boreholes

Because Constraint 4 is valid only between 400 to 750 mvd, only results from the deeper sections of boreholes KFM01B and DBT-1 are displayed. The results indicate that 58% of the strain data in borehole KFM01B and 63% of the strain data in borehole DBT-1 are consistent with Constraint 1, 2, 3, and 4. The results indicate a fair agreement of σ_H between the boreholes (Figure 5-11).

5.3 Summary of results using overcoring stress data and comparisons with hydraulic solutions

The results above illustrate the benefits of using a semi-integrated approach to derive a complete stress tensor. The primary result of the forced overcoring inversions is that almost all strain data are consistent with one vertical principal stress equal to the theoretical weight of the overburden rock mass (Constraints 1 and 2). Thus, it may be concluded that the stress field at the Forsmark site is horizontal/vertical. Exceptions to this general rule may however be found locally in connection to fractures or fracture zones.

The results also indicate that the orientation of σ_H is indeed close to 134°N, as about 70% of the collected strain data are consistent with this orientation. Moreover, 50% of the strain data in borehole KFM01B and 85% of the strain data in borehole DBT-1 are consistent with Constraints 1, 2, 3, and 4. The quite reduced consistency for borehole KFM01B is due to that 2 tests (the unreliable tests at 406.92 and 472.98 mbl, see Section 4.2) are not consistent with the orientation of 134°N of maximum horizontal stress. However, the other two tests in borehole KFM01B are completely consistent with Constraints 1, 2, 3, and 4.

At the borehole scale, the results are not satisfactory and often involve a considerable scatter between boreholes. This is primarily a result of the standard deviations of the strains (note that this does not affect results at the single test scale). The standard deviations were determined using the average difference between measured (*a priori*) and calculated (*a posteriori*) strains

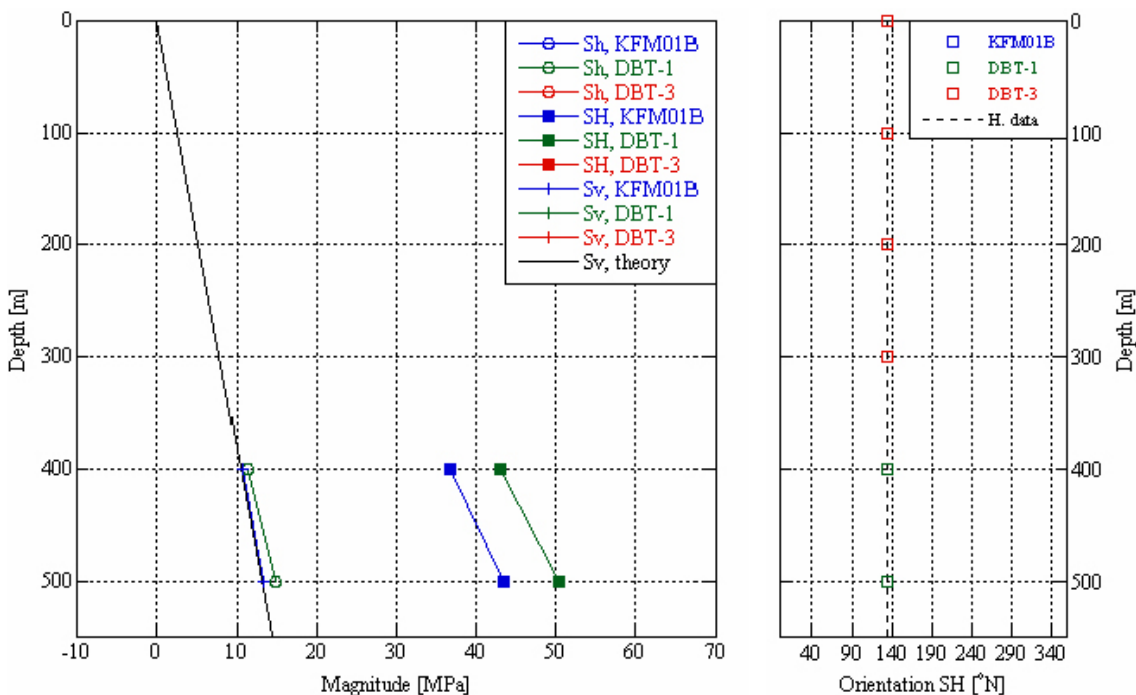


Figure 5-11. Summary plots displaying results using Constraints 1, 2, 3, and 4 for boreholes KFM01B, DBT-1, and DBT-3 at the borehole scale. *S* in the figure corresponds to σ in the text.

using conventional least squares approach. This implies that data with small differences between *a priori* and *a posteriori* strains are given higher weight compared with data with large differences during inversion. However, the determination of standard deviations may be questioned for two reasons: (1) the method mixes two sorts of errors – those associated with the measurement process and those associated with the interpretative model – which is not a rigorous method; and (2) because strain versus time data in boreholes DBT-1 and DBT-3 are not available, it is not possible to verify if one test is more reliable/accurate than other. For this reason, the strain data in the joint inversions in the next section (5.4) are given the same weight.

Another outcome of the study is that most overcoring results are changed considerably when applying constraints, despite that an overwhelming majority of the strain gauges are consistent with the constraint in question. This implies, in theory, that stress calculations based solely on overcoring data require additional information for reliable solutions. This, rather drastic, interpretation can be explained by the relatively large scatter of the measured strains in overcoring measurements combined with the mathematical algorithm used in the stress calculation, i.e. the least squares (LS) criterion. The LS criterion, in which the misfit is based on the l_2 -norm, is known to be sensitive to non-distinct and atypical data (i.e. data with large variance and outliers, respectively; e.g. /Parker and McNutt 1980/). For such data, a more robust method is to use a misfit function based on the l_1 -norm.

Shifting focus to more details, it was clear that a quite large number of overcoring data were not consistent with Constraint 3 (about 30%), i.e. that maximum horizontal stress is oriented 134°N . These data, which also involve the majority of rejected data when applying Constraint 4, are considered as local deviations as general trends are not visible. Whether these localized data are a result of shortcomings during measurement or a result of local geology has not been investigated further.

The application of Constraints 1 to 3 may be regarded as the best solution obtained for stress magnitudes when using only overcoring data because the later application of Constraint 4 involves constraining the overcoring data towards the hydraulic stress magnitudes. The results when using Constraints 1–3, when plotted with the hydraulic solution, indicate that overcoring suggests a considerably larger σ_H -magnitude compared with the hydraulic data. The hydraulic solution for σ_H is completely unresolved and comparisons are pointless (Figure 5-12; single test scale).

The application of Constraint 4 indicates that the magnitude of maximum horizontal stress is indeed high between 350 and 550 m depth (ranges between 32 to 62 MPa; Figure 5-13), however, the scatter is considerable. The application of Constraint 4 implies that the overcoring data are insensitive to changes in minimum horizontal stress.

5.4 Integrated approach – Joint overcoring and hydraulic stress calculations

The final step of the stress calculations involves a joint inversion of both data sets. The purpose of the joint inversion is twofold: (1) to identify the data set that provides the best solution of the prevailing stress field; and (2) because it is the author's opinion that the elastic parameters are the primary source of uncertainty for the overcoring method, to determine the elastic parameters *in situ*. However, prior to solving the elastic parameters *in situ*, calculations were also made using the average values for all overcoring data ($E = 71.0$ GPa, $\nu = 0.20$).

Based on the results of the hydraulic and overcoring data sets, the parameterization was reduced to include the horizontal stresses and their variation with depth and the elastic parameters. Thus, it was assumed that one principal stress is vertical and equal to the theoretical weight of the overburden rock mass and that maximum horizontal stress is oriented 134°N . This leaves 6 unknown parameters to be solved. The joint inversion was made without weighting factors of the two data sets.

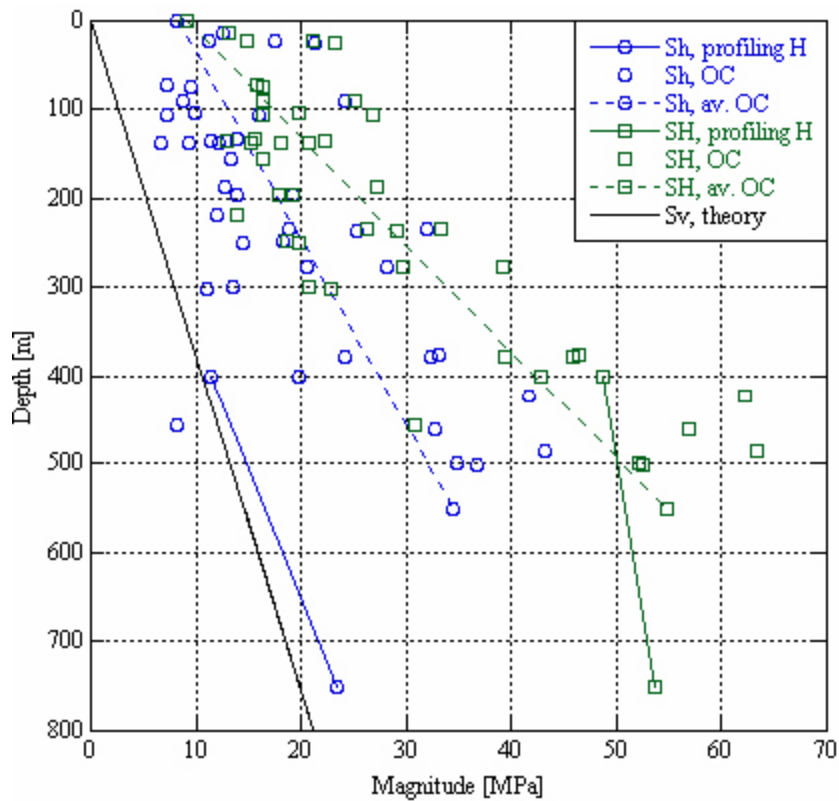


Figure 5-12. Summary plot displaying results from application of Constraints 1 to 3 together with results from hydraulic solutions. S in the figure corresponds to σ in the text.

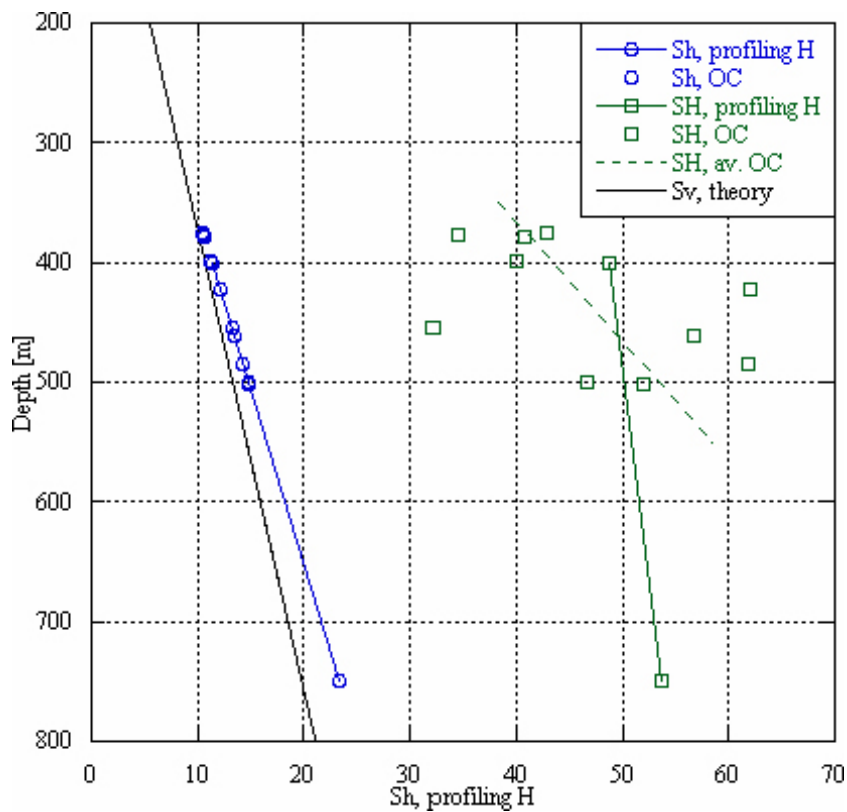


Figure 5-13. Summary plot displaying results from application of Constraints 1, 2, 3, and 4 together with results from hydraulic solutions. S in the figure corresponds to σ in the text.

5.4.1 Joint inversion

The total number of unambiguous or partly unambiguous data used for the joint inversion involves 19 hydraulic tests (when excluding data in the vicinity of the A2 zone in borehole KFM02A and all data in borehole KFM04A, see Section 5.1). This very low number of data in relation to the number of overcoring data (519 strain data) implies that the overcoring data will constrain the solution completely when the average elastic parameters are used. For the case when the elastic parameters are solved *in situ*, the hydraulic data completely constrain the elastic parameters and thus have a greater impact on the solution.

The result when using the average elastic parameters ($E = 71.0$ GPa, $\nu = 0.20$) is consistent with 8 hydraulic tests and 375 overcoring strains (i.e. 42% and 72%, respectively). Compared with the individual overcoring and hydraulic solution, σ_h of the joint solution is in fair agreement with the hydraulic profiling approach, whereas the individual overcoring solution indicates a significantly larger magnitude. For σ_H , the joint solution indicates smaller magnitudes compared to all individual results (Figure 5-14), whereas the gradient is similar.

The result when solving the elastic parameters *in situ* yielded $E = 42.0$ GPa and $\nu = 0.243$ and is consistent with 9 hydraulic tests and 385 overcoring strains (i.e. 47% and 74%, respectively). The *in situ* value of Young's modulus is not in accordance with results from laboratory tests, nor with estimations of rock mass Young's modulus using RMR-ratings and Q-indexes (Figure 5-16 and Figure 5-17; /SKB 2004/). Because stress magnitudes in the joint solution with *in situ* elastic parameters are controlled by the hydraulic data, the result indicates that there is a marked difference between the two data sets. In such cases, the deviation between *in situ* Poisson's ratio and laboratory results may still be fair, but the difference between *in situ* Young's modulus and lab results is pronounced, as this parameter is a linear function of stress magnitudes.

Compared with the individual overcoring and hydraulic solution, σ_h of the joint solution with the elastic parameters as unknowns is in fair agreement with the hydraulic profiling approach. However, the individual overcoring solution indicates significantly larger σ_h and σ_H magnitudes, whereas the gradient is similar (Figure 5-15).

It should be noted that the data sets are not optimal for *in situ* determination of elastic parameters as most hydraulic data are located between 400–700 mvd, whereas most overcoring data are located above 300 mvd.

A sound physical interpretation of the derived low elastic parameters could be fruitful, e.g. by re-evaluating the method for measuring elastic moduli from cores. Another possibility is that non-linearity effects are strong. Indeed, while the maximum biaxial load applied on overcore samples reaches about 10 MPa with full freedom to move in the axial direction, the *in situ* stress field is such that the radial stress component is zero, while the tangential stress is many times larger than that applied on the cores. This topic is though outside the scope of this report and is hence not discussed further.

5.4.2 Summary of results using joint inversions

The solutions based on the joint inversion are judged as the most reliable because of the large amount of data involved and because the major uncertainty in the overcoring data, the elastic parameters, can be solved *in situ* (despite the unanticipated result). However, as both data sets involve uncertainties, in some cases large, the solutions are not to be used for design purposes but merely as guidelines of the prevailing stress field. Hence, for design purposes, new and reliable data should be collected at the Forsmark site.

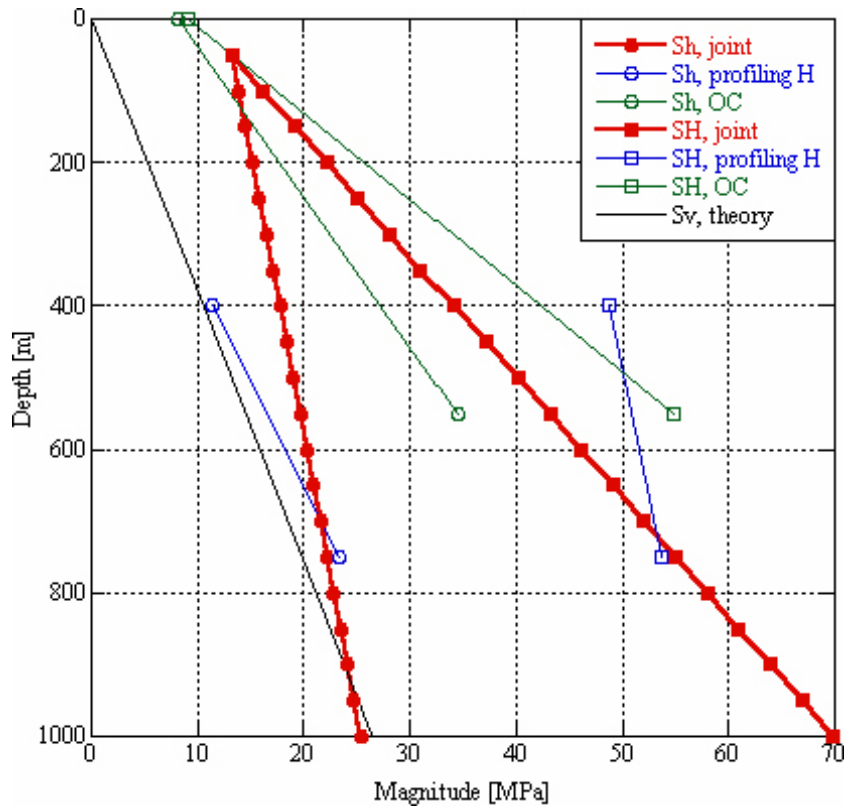


Figure 5-14. Results using joint inversion of hydraulic and overcoring stress data. The average elastic parameters are used ($E = 71.0 \text{ GPa}$, $\nu = 0.20$). S in the figure corresponds to σ in the text.

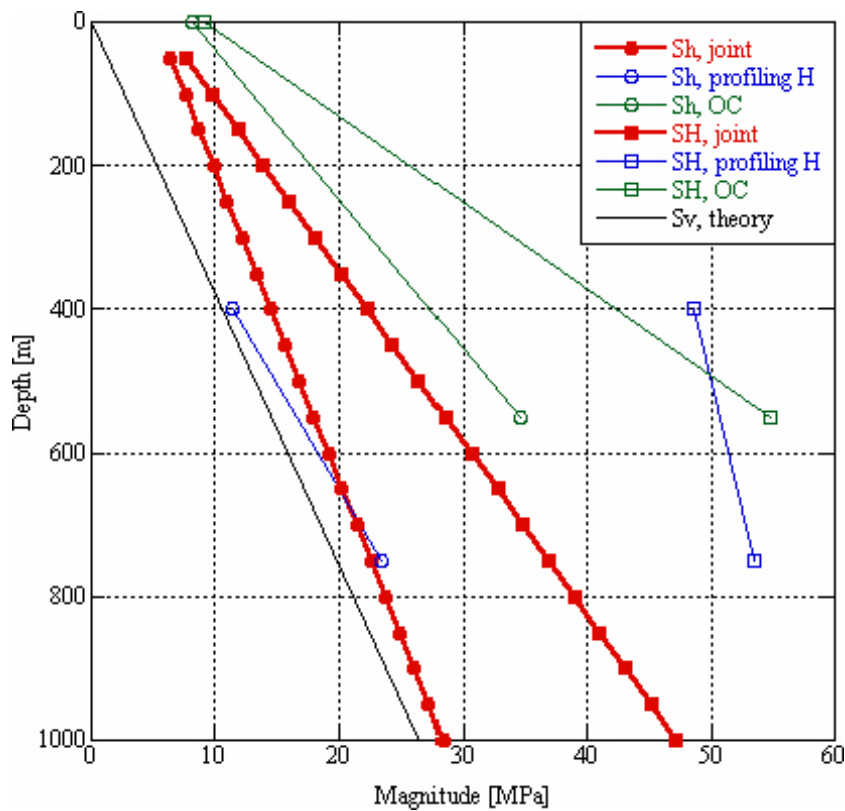


Figure 5-15. Results using joint inversion of hydraulic and overcoring stress data. The elastic parameters were solved in situ and equal $E = 42.0 \text{ GPa}$ and $\nu = 0.243$, respectively. S in the figure corresponds to σ in the text.

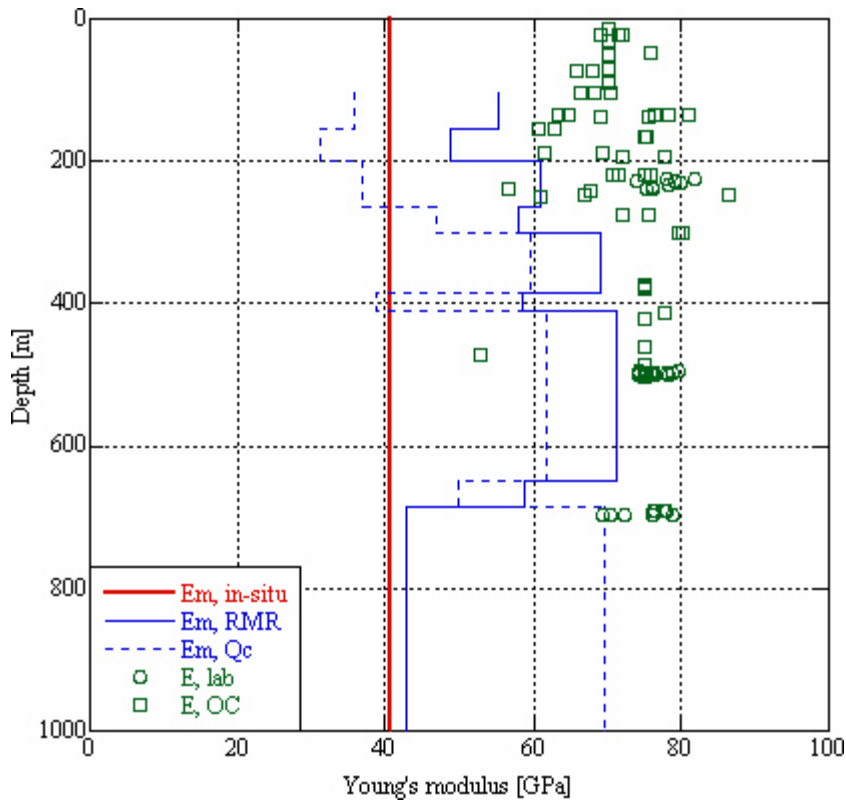


Figure 5-16. Rock mass Young's modulus determined in situ, using RMR-rating and Q -indexing, together with lab results and results from biaxial testing. The in situ value corresponds to 42.0 GPa. S in the figure corresponds to σ in the text.

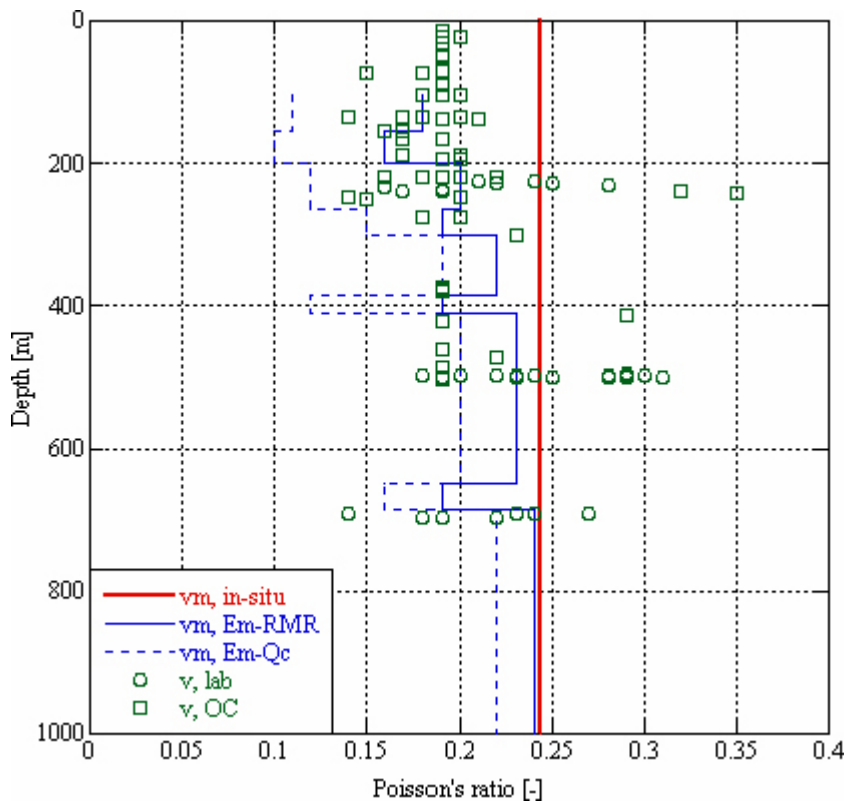


Figure 5-17. Rock mass Poisson's ratio determined in situ, using RMR-rating and Q -indexing, together with lab results and results from biaxial testing. The in situ value corresponds to 0.243. S in the figure corresponds to σ in the text.

6 Discussion and conclusions

6.1 Overcoring data

The findings from overcoring data analysis in borehole KFM01B can be summarized according to the following:

- 33 and 21 overcoring strains are reliable and less reliable, respectively.
- Eleven biaxial strain rosettes are doubtful (and were excluded).
- Although the temperature effect during overcoring is pronounced, the effect on final strain readings are small (generally within 1°C) as the core sample has been allowed to cool down close to its original temperature when the final strain values were selected. One exception to this is the tests at 471.69 and 472.78 mbl.
- Core damage was abundant for all tests and the strain data were therefore adjusted for exaggeration of the vertical stress.
- The average elastic parameters are equal to $E = 62.8 \pm 13.6$ and $\nu = 0.30 \pm 0.07$ (Figure 4-4). The values on Poisson's ratio are relatively high, which may be a result of microfracturing of the core.
- The spalling failure of the pilot hole at Level 2, revealed through examination of thin sections, significantly reduces the reliability of the stress estimates.
- The tests at Level 2 are located close to an interval that is anomalous with increased fracture frequency and alteration to a varying degree (between c. 415 and 470 mbl). Besides, the test at 412.79 mbl could be positively correlated with features detected with borehole radar (at 413.0). Furthermore, a reflector of unknown orientation at 472.0 mbl may influence the test at 471.69 mbl.

The overcoring data in DBT-1 and DBT-3 are, despite the relatively consistent results, regarded as more unreliable because there are no means to verify the time versus strain response during drilling. Moreover, both wells are located outside the tectonic lens and it has not been ascertained that they measure the same stress field as prevailing inside the lens. The discrepancies in the two reports presented /SSPB 1982, Ingevald and Strindell 1981/ imply that strain data have been changed, but in an unknown manner. Primarily the relatively good agreement between calculated vertical stress and theoretical weight of the overburden rock mass implies, because core discing problems were abundant, that the data have been corrected with this respect. Moreover, the elastic parameters were determined by both biaxial and uniaxial testing but with unknown approach.

Although the results from a limited number of laboratory tests on solid cores were reviewed in connection to the preparation of this report, some interesting trends are visible which suggest sample disturbance as a result of stress relaxation /e.g. Martin and Simmons 1993/. Uniaxial compression tests indicate that Young's modulus and tensile strength of solid cores decrease with depth (Figure 4-5 and Figure 4-11). The commonly observed core discing resulting in a significantly overestimated vertical stress and large scatter in elastic parameters of the overcoring tests clearly speak in favour of sample disturbance. Although efforts are made to correct this adversary, it will always leave some uncertainty on the real values. The observed spalling fractures cannot be corrected for, and results at Level 2 therefore include an additional source of uncertainty. The fact that the calculated stress field is more horizontal/vertical at Level 1, which has been established by the hydraulic stress data, compared to Level 2, also speak in favor of that results from Level 1 are more reliable.

It should also be mentioned that all the overcoring stress measurements were collected in a near vertical borehole, which is the most unfavorable direction with respect to stress related

microfracturing /Martin and Christiansson 1991/. At URL, overcoring measurements conducted in boreholes not perpendicular to maximum horizontal stress yielded reliable results, and it may therefore be proposed that overcoring measurements are conducted in boreholes that are oriented to minimize the microfracturing effect. For example, core discing or microfractures were not detected in the pilot core or in the hollow cylinder during drilling tests in borehole KFM08A, which is oriented approximately parallel to maximum horizontal stress and inclined about 60° (at ground surface) from the horizontal plane. Thus, overcoring measurements in surface drilled boreholes may provide more reliable results if the boreholes are inclined and directed approximately parallel with maximum horizontal stress.

6.2 Hydraulic data

In this report, the general approach for hydraulic stress measurements is outlined. The approach is to be regarded as the opinion of the author, although it has also been reviewed and complemented by Prof. Francois Cornet, IGP, who is one of the leading scientist in the field.

Regrettably, the results of the hydraulic stress measurements are not optimal. The primary reason can be correlated to the lack of reliable fracture orientation data. This study has revealed that only 11 tests involve unambiguous data and another 14 tests partly unambiguous data. These defeats aside, a few important conclusions may be drawn from the hydraulic data: (1) the vertical direction is a principal direction; (2) the vertical stress closely reflects the theoretical weight of the overburden rock mass; and (3) maximum horizontal stress is oriented approximately 134°N. The stress magnitudes are discussed below.

Heterogeneous data primarily involve the depth section 412 to 518 mvd in borehole KFM02A. These data can be correlated with a major deformation zone denominated ZFMNE00A2, which is dipping about 24° towards SSE. The low normal stress values may also be explained by that fractures have propagated and reached across one of the packers, inducing some by-pass that closes when the pressure becomes low enough.

6.3 New stress estimation

Numerous attempts have been made to derive a new stress estimation based on hydraulic data, overcoring data, and joint inversions using both data sets. For all attempts, the solutions cannot be more reliable than the accuracy of the measurements themselves. Because most data involve uncertainties, in many cases significant, the results should not be used for e.g. design purposes but merely as guidelines until new and reliable data have been collected at the Forsmark site.

What can be appreciated with the existing data sets, however, is in what direction these data sets point with respect to stress magnitudes and orientations. Thus, at this stage, discussions of the accuracy of the different solutions are pointless. The results clearly show that the hydraulic and overcoring data indicate two widely different states of stress. A more in-depth analysis of e.g. measurement-related uncertainties is required to resolve this issue. At this stage we can conclude however, that one principal stress is vertical and closely resembles the theoretical weight of the overburden. Moreover, maximum horizontal stress is oriented about 134°N, although this needs to be confirmed as the amount of data is sparse. An overwhelming majority of the overcoring strain data support these conclusions as described with the constrained overcoring calculations.

Because both data sets involve uncertainties, the results from the joint inversions are judged to best represent the anticipated intervals for the horizontal stresses. The reason for this is twofold; the results involve the maximum amount of data and the major uncertainty involved in the overcoring data can be handled by solving the elastic parameters *in situ* (despite the unanticipated result).

7 Acknowledgements

The Swedish Nuclear Fuel and Waste Management Co. (SKB) supported this work. Review comments from Francois Cornet, Jonny Sjöberg, Lennart Ekman, and Rolf Christiansson helped me focus the manuscript. Allan Strähle is acknowledged for help with various deliveries of data from Sicada and for several figures in the report.

8 References

Aamodt RL, Kuriyagawa M, 1981. Measurement of instantaneous shut-in pressure in crystalline rock. *Proc. Workshop on Hydraulic Fracture Stress Measurements* (Eds. Zoback, M.D., Haimson, B.C.), Monterey, USA. USGS, pp. 139–42.

Amadei B, 1983a. *Rock anisotropy and the theory of stress measurements*. Lecture notes in Engineering, Springer-Verlag.

Amadei B, 1983b. Number of boreholes to measure the state of stress in-situ by overcoring. *Proc. 24th US Rock Mech. Symp.*, College Station, USA. Ass. Eng. Geologists Publ., pp. 87–98.

Amadei B, Stephansson O, 1997. *Rock Stress and Its Measurements*, Chapman and Hall Publ., London.

Ask D, 2001. Inversion and interpretation of hydraulic and overcoring rock stress data in the Äspö region, Sweden. Licentiate Thesis, Royal Institute of Technology, Stockholm.

Ask D, 2003a. Evaluation of measurement-related uncertainties in the analysis of overcoring rock stress data from Äspö HRL, Sweden: a case study. *Int. J. Rock Mech. Min. Sci.*, 40, pp. 1173–87.

Ask D, 2003b. Hydraulic rock stress measurements in borehole BJO01, Björkö Island, Lake Mälaren, Sweden. Internal Report, Div. Engineering Geology and Geophysics, Royal Institute of Technology, Stockholm.

Ask D, 2004a. New developments of the Integrated Stress Determination Method and application to rock stress data at the Äspö Hard Rock Laboratory. Doctoral Thesis, Royal Institute of Technology, Stockholm.

Ask D, 2004b. New developments of the Integrated Stress Determination Method and application to rock stress data at the Äspö HRL, Submitted to *Int. J. Rock Mech Min. Sci.*

Ask D, 2008. Evaluation of hydraulic and overcoring stress measurements and application of the Integrated Stress Determination Method (ISDM) in boreholes KSH01A and KAV04A at the Simpevarp site. SKB P-report in prep.

Baumgärtner J, Rummel F, 1989. Experience with fracture pressurization tests as a stress measuring technique in a jointed rock mass. *Int. J. Rock Mech. Min. Sci. & Geomech. Abstr.*, 26, pp. 661–71.

Berglund J, Petersson J, Wägerud A, Danielsson, P, 2004. Boremap mapping of core drilled borehole KFM01B. SKB P-04-114, Svensk Kärnbränslehantering AB.

Bredehoeft JD, Wolff RG, Keys WS, Schuter E, 1976. Hydraulic fracturing to determine the regional stress field, Piceance Basin, Colorado. *Bull. Geol. Soc. Am.*, 87, pp. 250–8.

Brudy M, 1995. Determination of in-situ stress magnitude and orientation to 9 km depth at the KTB site. Doctoral Thesis, University of Karlsruhe, Karlsruhe.

Carlsten S, Petersson J, Stephens M, Mattson H, Gustafsson J, 2004. Geological singlehole interpretation of KFM02A and HFM04-05 (DS2). Forsmark site investigation. Revised October 2006. SKB P-04-117, Svensk Kärnbränslehantering AB.

Cornet, FH, 1993a. The HTPF and the integrated stress determination methods. In: *Comprehensive Rock Engineering*, 3, (J. Hudson, Ed.). Pergamon Press, Oxford pp. 413–32.

Cornet FH, 1993b. Stresses in rock and rock masses. In: *Comprehensive Rock Engineering*, 3, (J. Hudson, Ed.). Pergamon Press, Oxford, pp. 297–327.

- Cornet FH, Valette B, 1984.** *In situ* stress determination from hydraulic injection test data. *J. Geophys. Res.*, 89, pp. 11527–37.
- Cornet FH, Li L, Hulin JP, Ippolito I, Kurowski P, 2003.** The hydromechanical behaviour of a fracture: an *in situ* experimental case study. *Int. J. Rock Mech. Min. Sci.*, 40, pp. 1257–70.
- Cornet FH, Berard Th, Bourouis, S, 2007.** How close to failure is a natural granite rock mass at 5 km depth? *Int. J. Rock Mech. Min. Sci.*, 44, pp. 47–66.
- Doe WT, Hustrulid WA, 1981.** Determination of the state of stress at the Stripa mine, Sweden. *Proc. Workshop on Hydraulic fracturing Stress Measurements*, Monterey, CA, pp. 119–29.
- Eloranta P, 2004a.** Drill hole KFM01A: Indirect tensile strength test (HUT). SKB P-04-171, Svensk Kärnbränslehantering AB.
- Eloranta P, 2004b.** Drill hole KFM01A: Uniaxial compression test (HUT). SKB P-04-176, Svensk Kärnbränslehantering AB.
- Eloranta P, 2004c.** Drill hole KFM01A: Triaxial compression test (HUT). SKB P-04-177, Svensk Kärnbränslehantering AB.
- Enever J, Chopra PN, 1989.** Experience with hydraulic fracturing stress measurements in granites. *Proc. Int. Conf. on Rock Stress and Rock Stress Measurements* (Stephansson Ed.), Stockholm. Centek Publisher, Luleå, pp. 411–20.
- Evans KF, Engelder T, Plumb RA, 1989.** Appalachian stress study. 1. A detailed description of *in situ* stress variations in Devonian shales of the Appalachian plateau. *J. Geophys. Res.*, 94, pp. 7129–54.
- Evans KFT, Kohl RJ, Rybach L, 1998.** Analysis of the hydraulic behaviour of the 3.5 km deep reservoir during the 1995–1997 test series, and other contributions to the European Hot Dry Rock project, Soultz-sous-forêts, France. Final report to the Swiss Department of Education and science, BBW 95.0673-2, Swiss Federal Institute of Technology, July 1998.
- Gallagher K, Sambridge M, Drijkoningen G, 1991.** Genetic algorithms: an evolution from Monte Carlo methods for strongly non-linear geophysical optimization problems. *J. Geophys. Res.*, 18, pp. 2177–80.
- Gronseth JM, Kry PR, 1983.** Instantaneous shut-in pressure and its relationship to the minimum *in-situ* stress. *Proc. from the Hydraulic fracturing Stress Measurements*, Monterey, National Academy Press, Washington DC, pp. 55–60.
- Guo F, Morgenstern NR, Scott JD, 1993.** Interpretation of hydraulic fracturing pressure: a comparison of eight methods used to identify shut-in pressure. *Int. J. Rock Mech. Min. Sci.*, 30, pp. 627–31.
- Gustafsson J, Gustafsson, C, 2004.** RAMAC and BIPS logging in borehole KFM01B and RAMAC directional re-logging in borehole KFM01A. SKB P-04-79, Svensk Kärnbränslehantering AB.
- Haimson BC, Lee CF, Huang JHS, 1986.** High horizontal stresses at Niagara falls, their measurement, and the design of a new hydroelectric plant. *Proc. Int. Symp. Rock Stress*, Centek, Luleå, pp. 615–24.
- Haimson BC, Cornet FH, 2003.** ISRM Suggested Methods for rock stress estimation – Part 3: hydraulic fracturing (HF) and/or hydraulic testing of pre-existing fractures (HTPF). *Int. J. Rock Mech. Min. Sci.*, 40, pp. 1011–20.
- Hardy MP, 1973.** Fracture mechanics applied to rock. Unpublished PhD Thesis, University of Minnesota, Minneapolis.
- Hayashi K, Sakurai I, 1989.** Interpretation of hydraulic fracturing shut-in curves for tectonic stress measurements. *Int. J. Rock Mech. Min. Sci. & Geomech. Abstr.*, 26, pp. 477–82.

- Hayashi K, Haimson BC, 1991.** Characteristics of shut-in curves in hydraulic fracturing stress measurements and the determination of the *in situ* compressive stress. *J. Geophys. Res.*, 96, pp. 18311–21.
- Hirashima K, Koga A, 1977.** Determination of stresses in anisotropic elastic medium unaffected by boreholes from measured strains or deformations. *Proc. Int. Symp. on Field Measurements in Rock Mechanics*, Zurich. A.A. Balkema Publ. Rotterdam, pp. 173–82.
- Hubbert MK, Willis DG, 1957.** Mechanics of hydraulic fracturing. *Pet. Trans.*, 210, pp. 153–68.
- Hudson JA, 1970.** A critical examination of indirect tensile strength tests for brittle rocks. Doctoral Thesis, University of Minnesota.
- Hudson JA, Cooling CM, 1988.** *In situ* rock stresses and their measurements in the UK – Part 1. The current state of knowledge. *Int. J. Rock Mech. & Geomech. Abstr.*, 25, pp. 363–70.
- Ingevald K, Strindell L, 1981.** Mätning av bergspänningar (bergtryck) i djupa vertikala borrhål. Statens Vattenfallsverk, Rapport L-543:2 (In Swedish).
- Ito T, Evans K, Kawai K, Hayashi K, 1999.** Hydraulic fracturing reopening pressure and the estimation of maximum horizontal stress. *Int. J. Rock Mech. & Geomech. Abstr.*, 36, pp. 811–26.
- Jacobsson L, 2004a.** Drill hole KFM01A. Indirect tensile strength test. SKB P-04-170, Svensk Kärnbränslehantering AB.
- Jacobsson L, 2004b.** Drill hole KFM02A. Indirect tensile strength test. SKB P-04-172, Svensk Kärnbränslehantering AB.
- Jacobsson L, 2004c.** Drill hole KFM04A. Indirect tensile strength test. SKB P-04-174, Svensk Kärnbränslehantering AB.
- Jacobsson L, 2004d.** Borehole KFM01A. Uniaxial compression tests of intact rock. SKB P-04-223, Svensk Kärnbränslehantering AB.
- Jacobsson L, 2004e.** Borehole KFM01A. Triaxial compression tests of intact rock. SKB P-04-227, Svensk Kärnbränslehantering AB.
- Jaeger JC, Cook NGW, 1969.** *Fundamentals of rock mechanics*. Chapman and Hall Ltd and Science Paperbacks, London.
- Kirsch G, 1898.** Die Theorie der Elastizität und die Bedürfnisse der Festigkeitslehre. *Zeit Ver. Dt. Ingenieure*, 42, pp. 797–807.
- Klee G, Rummel F, 2004.** Rock stress measurements with hydraulic fracturing and hydraulic testing of pre-existing fractures in borehole nos. KFM01A, KFM01B, KFM02A and KFM04A. Results of in-situ tests. SKB P-04-311, Svensk Kärnbränslehantering AB.
- Lee MY, Haimson BC, 1989.** Statistical evaluation of hydraulic fracturing stress measurement parameters. *Int. J. Rock Mech. Min. Sci. & Geomech. Abstr.*, 26, p. 447–56.
- Lindfors U, Perman F, Sjöberg J, 2005.** Evaluation of overcoring results from KFM01B. SKB P-05-66, Svensk Kärnbränslehantering AB.
- Lund B, 2001.** Crustal stress studies using microearthquakes and boreholes. Doctoral Thesis, Uppsala University, Uppsala.
- Martin CD, Simmons GR, 1993.** The Atomic Energy of Canada Limited Underground Research Laboratory: an overview of geomechanics characterization. In: *Comprehensive Rock Engineering*, 3, (J. Hudson, Ed.). Pergamon Press, Oxford, pp. 915–50.
- Martin CD, Christiansson R, 1991.** Overcoring in highly stressed granite – the influence of microfracturing. *Int. J. Rock Mech. Min. Sci. & Geomech. Abstr.*, 28, pp. 53–70.

- McGarr A, 1980.** Some constraints on level of shear stress in the crust from observations and theory. *J. Geophys. Res.*, 85, pp. 6231–38.
- McLennan JD, Rogieres J-C, 1981.** Do instantaneous shut-in pressures accurately represent the minimum principal stress? *Proc. Workshop on Hydraulic fracturing Stress Measurements*, Monterey, CA, pp. 68–78.
- Merril RH, 1964.** *In situ* determination of stress by relief techniques. *Proc. Int. Conf. State of Stress in the Earth's Crust*, Santa Monica, Elsevier, New York, pp. 343–69.
- Parker RL, McNutt MK, 1980.** Statistics for one-norm misfit measure. *J. Geophys. Res.*, 85, pp. 4429–30.
- Perman F, Sjöberg J, 2003.** Transient strain analysis of overcoring measurements in boreholes DBT-1 and DBT-3. SKB P-03-119, Svensk Kärnbränslehantering AB.
- Ratigan JL, 1992.** The use of the fracture reopening pressure in hydraulic fracturing stress measurements. *Rock Mech. Rock Eng.*, 25, pp. 125–36.
- Roegiers J-C, McLennan JC, Schultz LD, 1982.** *In situ* stress determinations in northeastern Ohio. *Proc. 23rd US Symp. on Rock Mech.*, Univ. of California, Berkeley.
- Rummel F, Weber U, 2004.** Rock stress measurements with hydraulic fracturing and hydraulic testing of pre-existing fractures in borehole nos. KFM01A, KFM01B, KFM02A and KFM04A. Laboratory core investigations. SKB P-04-312, Svensk Kärnbränslehantering AB.
- Rutqvist J, 1995.** Coupled stress-flow properties of rock joints from hydraulic field testing. Doctoral Thesis, Royal Institute of Technology, Stockholm.
- Rutqvist J, Stephansson O, 1996.** A cyclic hydraulic jacking test to determine the *in situ* stress normal to a fracture. *Int. J. Rock Mech. Min. Sci. & Geomech. Abstr.*, 33, pp. 695–711.
- Rutqvist J, Tsang C-F, Stephansson O, 2000.** Uncertainty in the principal stress estimated from hydraulic fracturing measurements due to the presence of the induced fracture. *Int. J. Rock Mech. & Geomech. Abstr.*, 37, pp. 107–20.
- Schmitt DR, Zoback MD, 1989.** Poroelastic effects in the determination of the maximum horizontal principal stress in hydraulic fracturing tests – A proposed breakdown equation employing a modified effective stress relation for tensile failure. *Int. J. Rock Mech. Min. Sci. & Geomech. Abstr.*, 26, pp. 499–506.
- Sjöberg J, 2004.** Overcoring rock stress measurements in borehole KFM01B. SKB P-04-83, Svensk Kärnbränslehantering AB.
- Sjöberg J, Lindfors U, Perman F, Ask D, 2005.** Evaluation of the state of stress at the Forsmark site. SKB R-05-35, Svensk Kärnbränslehantering AB.
- Sjöberg J, Klasson H, 2003.** Stress measurement in deep boreholes using the Borre (SSPB) probe. *Int. J. Rock Mech. Min. Sci.*, 40, pp. 1205–23.
- SKB, 2004.** Preliminary site description. Forsmark area – version 1.1. SKB R-04-15, Svensk Kärnbränslehantering AB.
- SKB, 2005.** Preliminary site description. Forsmark area – version 1.2. SKB R-05-18, Svensk Kärnbränslehantering AB .
- SSPB (The Swedish State Power Board), 1982.** Characterization of deep-seated rock masses by means of borehole investigations. *In-situ rock stress measurements, hydraulic testing and core logging. Final Report, April 1982, Research and Development Report 5:1*, Stockholm: The Swedish State Power Board.
- Stephens MB, Fox A, La Pointe P, Simeonov A, Isaksson H, Hermansson J, Öhman J, 2007.** Geology Forsmark. Site descriptive modelling Forsmark stage 2.2. SKB R-07-45, Svensk Kärnbränslehantering AB.

Tarantola A, Valette B, 1982. Generalized non-linear inverse problem solved using the least square criterion. *Rev. Geophys. Space. Phys.*, 20, pp. 219–32.

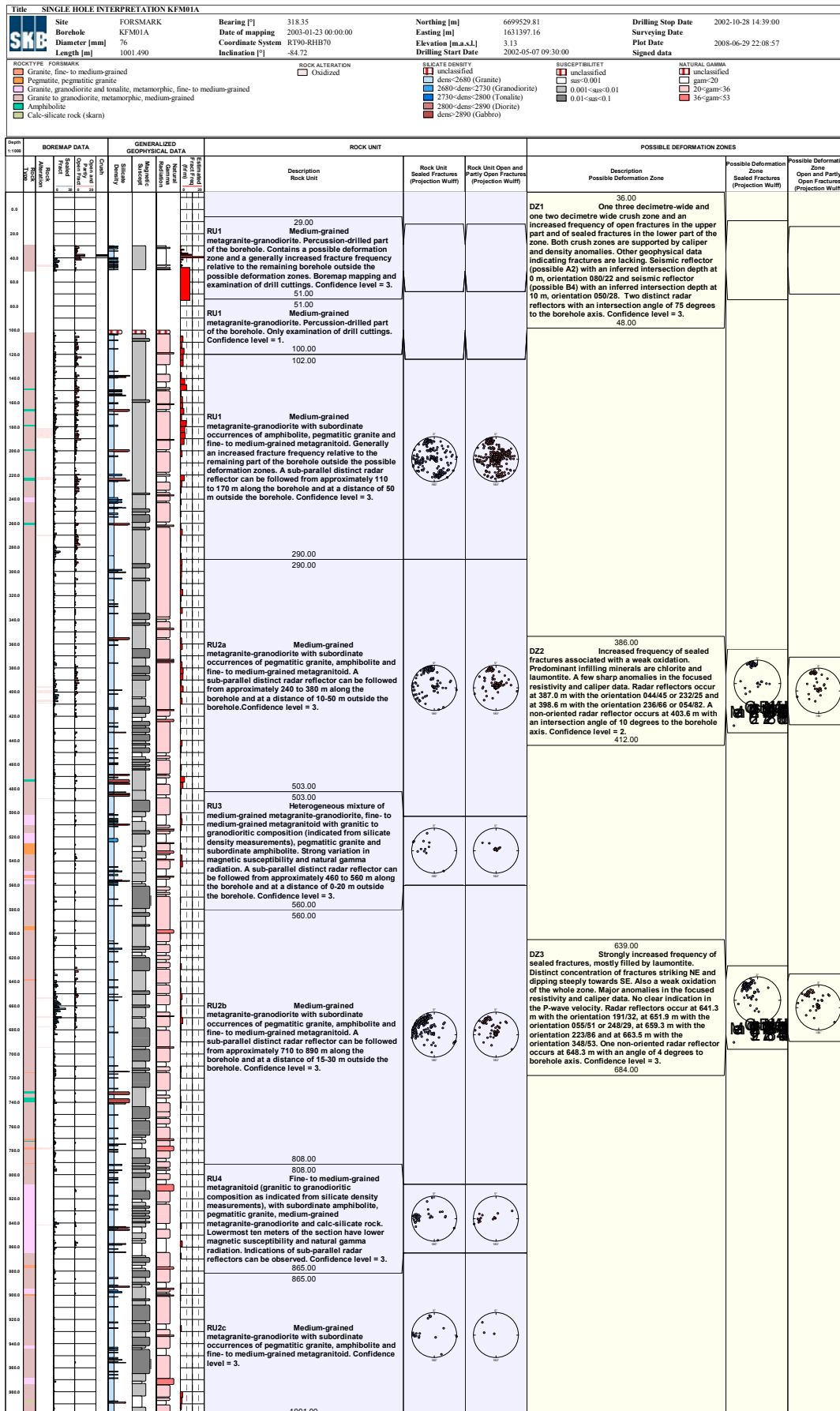
Worotnicki G, 1993. CSIRO triaxial stress measurement cell. In: *Comprehensive Rock Engineering*, 3, (J. Hudson, Ed.) Pergamon Press, Oxford, pp. 329–94.

Wileveau Y, Cornet FH, Desroches J, Blumling P, 2007. Complete *in situ* stress determination in an argillite sedimentary formation. *Physics and Chemistry of the Earth*, 32, pp. 866–878.

Yin JM, 1994. Détermination du champ de contrainte régional à partir de mesures hydrauliques et de mécanismes au foyer de microséismes induit. Doctoral Thesis, Institute de Physique du Globe de Paris, Paris.

Yin JM, Cornet FH, 1994. Integrated stress determination by joint inversion of hydraulic tests and focal mechanisms. *Geophys. Res. Lett.*, 21, pp. 2645–48.

Single hole interpretation KFM01A, KFM01B, KFM02A, KFM04A including measurement depth for overcoring and hydraulic data



Title SINGLE HOLE INTERPRETATION KFM02A																																																																																																																																																																																																																																																																																																																																																																																																																																																																																																																																																																				
Site		Bearing [°]		Northing [m]		Drilling Stop Date		2003-03-12 21:30:00																																																																																																																																																																																																																																																																																																																																																																																																																																																																																																																																																												
KFM02A		275.76		6698712.50		2003-03-12 21:30:00																																																																																																																																																																																																																																																																																																																																																																																																																																																																																																																																																														
Date of mapping		Date of mapping		Easting [m]		Surveying Date		2008-06-29 22:08:57																																																																																																																																																																																																																																																																																																																																																																																																																																																																																																																																																												
2003-04-22 00:00:00		RT90-KHB70		1633182.86		2008-06-29 22:08:57																																																																																																																																																																																																																																																																																																																																																																																																																																																																																																																																																														
Diameter [mm]		Coordinate System		Elevation [m.a.s.l.]		Plot Date																																																																																																																																																																																																																																																																																																																																																																																																																																																																																																																																																														
77		RT90-KHB70		7.35		2008-06-29 22:08:57																																																																																																																																																																																																																																																																																																																																																																																																																																																																																																																																																														
Length [m]		Inclination [°]		Drilling Start Date		Signed data																																																																																																																																																																																																																																																																																																																																																																																																																																																																																																																																																														
1002.440		-85.37		2002-11-20 14:03:00																																																																																																																																																																																																																																																																																																																																																																																																																																																																																																																																																																
<p>ROCKTYPE FORSMARK</p> <ul style="list-style-type: none"> Granite, fine- to medium-grained Pegmatite, pegmatitic granite Granite, granodiorite and tonalite, metamorphic, fine- to medium-grained Granite to granodiorite, metamorphic, medium-grained Amphibolite <p>ROCK ALTERATION</p> <ul style="list-style-type: none"> Oxidized Epidotized Quartz dissolution Argillization Albitization Sauserization <p>SILICATE DENSITY</p> <ul style="list-style-type: none"> dens<2800 (Granite) 2800<dens<2730 (Granodiorite) 2730<dens<2800 (Tonalite) 2800<dens<2890 (Diorite) dens<2890 (Gabbro) <p>SUSCEPTIBILITY</p> <ul style="list-style-type: none"> sus<0.001 0.001<sus<0.01 0.01<sus<0.1 <p>NATURAL GAMMA</p> <ul style="list-style-type: none"> gam<20 20<gam<36 36<gam<53 53<gam<70 70<gam<87 87<gam<104 104<gam<121 121<gam<138 138<gam<155 																																																																																																																																																																																																																																																																																																																																																																																																																																																																																																																																																																				
<table border="1"> <thead> <tr> <th rowspan="2">Depth [m]</th> <th colspan="4">BOREMAP DATA</th> <th colspan="4">GENERALIZED GEOPHYSICAL DATA</th> <th colspan="2">ROCK UNIT</th> <th colspan="4">POSSIBLE DEFORMATION ZONES</th> </tr> <tr> <th>Open Fractures</th> <th>Sealed Fractures</th> <th>Caliper</th> <th>Seismic</th> <th>Seismic</th> <th>Seismic</th> <th>Seismic</th> <th>Seismic</th> <th>Seismic</th> <th>Description</th> <th>Possible Deformation Zone</th> <th>Possible Deformation Zone</th> <th>Possible Deformation Zone</th> <th>Possible Deformation Zone</th> </tr> </thead> <tbody> <tr> <td>12.00</td> <td></td> </tr> <tr> <td>RU1a</td> <td></td> <td></td> <td></td> <td></td> <td></td> <td></td> <td></td> <td></td> <td></td> <td>Medium-grained metagranite to granodiorite with subordinate occurrences of amphibolite (mainly limited to the lower 50 m of the interval) and pegmatitic granite (primarily in the upper 40 m of the interval). Percussion-drilled part of the borehole. Boremap mapping and examination of drill cuttings. Confidence level = 3.</td> <td></td> <td></td> <td></td> <td></td> </tr> <tr> <td>96.00</td> <td></td> </tr> <tr> <td>100.00</td> <td></td> </tr> <tr> <td>RU1a</td> <td></td> <td></td> <td></td> <td></td> <td></td> <td></td> <td></td> <td></td> <td></td> <td>Medium-grained metagranite to granodiorite with subordinate occurrences of amphibolite and pegmatitic granite. Confidence level = 3</td> <td></td> <td></td> <td></td> <td></td> </tr> <tr> <td>155.00</td> <td></td> </tr> <tr> <td>RU2a</td> <td></td> <td></td> <td></td> <td></td> <td></td> <td></td> <td></td> <td></td> <td></td> <td>Heterogeneous interval, predominantly with a fine-grained metagranitoid. The second most important bedrock component is the metagranite-granodiorite, and then the amphibolite. The central part of the interval is strongly oxidised with three minor intervals of vuggy metagranitoid. Confidence level = 3.</td> <td></td> <td></td> <td></td> <td></td> </tr> <tr> <td>205.00</td> <td></td> </tr> <tr> <td>RU1b</td> <td></td> <td></td> <td></td> <td></td> <td></td> <td></td> <td></td> <td></td> <td></td> <td>Same dominant rock as between 100-155 m depth, with one about 5 m wide occurrence of fine-grained metagranitoid and several minor occurrences of pegmatitic granite. Confidence level = 3</td> <td></td> <td></td> <td></td> <td></td> </tr> <tr> <td>240.00</td> <td></td> </tr> <tr> <td>RU3</td> <td></td> <td></td> <td></td> <td></td> <td></td> <td></td> <td></td> <td></td> <td></td> <td>Vuggy metagranite (low density, resistivity, susceptibility and P-wave velocity) subjected to a strong albite-hematite-chlorite alteration. Also some minor occurrences of fine-grained metagranitoid, amphibolite and pegmatitic granite. All also altered. The radar measurements indicate a limited extension in at least one direction. Confidence level = 3</td> <td></td> <td></td> <td></td> <td></td> </tr> <tr> <td>310.00</td> <td></td> </tr> <tr> <td>RU1c</td> <td></td> <td></td> <td></td> <td></td> <td></td> <td></td> <td></td> <td></td> <td></td> <td>Same dominant rock as between 100-155 m depth, with one about 8 m wide occurrence of fine-grained metagranitoid, one about 3 m wide amphibolite and some minor occurrences of pegmatitic granite, fine-grained metagranite and amphibolite. Indications of sub-parallel radar reflectors outside the borehole are observed. Confidence level = 3</td> <td></td> <td></td> <td></td> <td></td> </tr> <tr> <td>485.00</td> <td></td> </tr> <tr> <td>RU2b</td> <td></td> <td></td> <td></td> <td></td> <td></td> <td></td> <td></td> <td></td> <td></td> <td>Heterogeneous interval, predominantly with the fine-grained metagranitoid. The second most important bedrock component is the metagranite-granodiorite, and then pegmatitic granite. Also some subordinate amphibolite. Most of the interval has been subjected to a variable degree of oxidation. Confidence level = 3.</td> <td></td> <td></td> <td></td> <td></td> </tr> <tr> <td>520.00</td> <td></td> </tr> <tr> <td>RU1d</td> <td></td> <td></td> <td></td> <td></td> <td></td> <td></td> <td></td> <td></td> <td></td> <td>Same dominant rock as between 100-155 m depth, with several minor occurrences of pegmatitic granite and amphibolite. To a variable extent oxidised. Confidence level = 3</td> <td></td> <td></td> <td></td> <td></td> </tr> <tr> <td>540.00</td> <td></td> </tr> <tr> <td>RU2c</td> <td></td> <td></td> <td></td> <td></td> <td></td> <td></td> <td></td> <td></td> <td></td> <td>The upper two thirds of the interval consists of fine-grained metagranite, whereas the lower third is more heterogeneous and composed of amphibolite, pegmatitic granite and the metagranite-granodiorite. Confidence level = 3.</td> <td></td> <td></td> <td></td> <td></td> </tr> <tr> <td>575.00</td> <td></td> </tr> <tr> <td>RU1e</td> <td></td> <td></td> <td></td> <td></td> <td></td> <td></td> <td></td> <td></td> <td></td> <td>Same dominant rock as between 100-155 m depth. Confidence level = 3</td> <td></td> <td></td> <td></td> <td></td> </tr> <tr> <td>600.00</td> <td></td> </tr> <tr> <td>RU2d</td> <td></td> <td></td> <td></td> <td></td> <td></td> <td></td> <td></td> <td></td> <td></td> <td>Fine-grained metagranite and the metagranite-granodiorite in approximately equal proportions. Also, several minor occurrences of pegmatitic granite. Confidence level = 3.</td> <td></td> <td></td> <td></td> <td></td> </tr> <tr> <td>635.00</td> <td></td> </tr> <tr> <td>RU1f</td> <td></td> <td></td> <td></td> <td></td> <td></td> <td></td> <td></td> <td></td> <td></td> <td>Same dominant rock as between 100-155 m depth, with some up to 8 m wide occurrences of fine-grained metagranitoid, amphibolite and pegmatitic granite. The uppermost part of the interval has been subjected to a variable extent of oxidation. Confidence level = 3</td> <td></td> <td></td> <td></td> <td></td> </tr> <tr> <td>835.00</td> <td></td> </tr> <tr> <td>RU2e</td> <td></td> <td></td> <td></td> <td></td> <td></td> <td></td> <td></td> <td></td> <td></td> <td>Heterogeneous interval, predominantly with the fine-grained metagranitoid, and then the metagranite-granodiorite and amphibolite. Also some subordinate occurrences of pegmatitic granite. Confidence level = 3</td> <td></td> <td></td> <td></td> <td></td> </tr> <tr> <td>867.00</td> <td></td> </tr> <tr> <td>RU1g</td> <td></td> <td></td> <td></td> <td></td> <td></td> <td></td> <td></td> <td></td> <td></td> <td>Same dominant rock as between 100-155 m depth, with several minor occurrences of pegmatitic granite, up to about 1.5 m in width. Confidence level = 3</td> <td></td> <td></td> <td></td> <td></td> </tr> <tr> <td>903.00</td> <td></td> </tr> <tr> <td>RU4</td> <td></td> <td></td> <td></td> <td></td> <td></td> <td></td> <td></td> <td></td> <td></td> <td>A homogeneous interval of a tonalitic (high density, low gamma) variety of the fine-grained metagranitoid. Also with some minor occurrences of amphibolite and pegmatitic granite. Confidence level = 3.</td> <td></td> <td></td> <td></td> <td></td> </tr> <tr> <td>938.00</td> <td></td> </tr> <tr> <td>RU1h</td> <td></td> <td></td> <td></td> <td></td> <td></td> <td></td> <td></td> <td></td> <td></td> <td>Same dominant rock as between 100-155 m depth, with several minor occurrences of pegmatitic granite and amphibolite. Confidence level = 3</td> <td></td> <td></td> <td></td> <td></td> </tr> <tr> <td>1001.00</td> <td></td> </tr> </tbody> </table>										Depth [m]	BOREMAP DATA				GENERALIZED GEOPHYSICAL DATA				ROCK UNIT		POSSIBLE DEFORMATION ZONES				Open Fractures	Sealed Fractures	Caliper	Seismic	Seismic	Seismic	Seismic	Seismic	Seismic	Description	Possible Deformation Zone	Possible Deformation Zone	Possible Deformation Zone	Possible Deformation Zone	12.00															RU1a										Medium-grained metagranite to granodiorite with subordinate occurrences of amphibolite (mainly limited to the lower 50 m of the interval) and pegmatitic granite (primarily in the upper 40 m of the interval). Percussion-drilled part of the borehole. Boremap mapping and examination of drill cuttings. Confidence level = 3.					96.00															100.00															RU1a										Medium-grained metagranite to granodiorite with subordinate occurrences of amphibolite and pegmatitic granite. Confidence level = 3					155.00															RU2a										Heterogeneous interval, predominantly with a fine-grained metagranitoid. The second most important bedrock component is the metagranite-granodiorite, and then the amphibolite. The central part of the interval is strongly oxidised with three minor intervals of vuggy metagranitoid. Confidence level = 3.					205.00															RU1b										Same dominant rock as between 100-155 m depth, with one about 5 m wide occurrence of fine-grained metagranitoid and several minor occurrences of pegmatitic granite. Confidence level = 3					240.00															RU3										Vuggy metagranite (low density, resistivity, susceptibility and P-wave velocity) subjected to a strong albite-hematite-chlorite alteration. Also some minor occurrences of fine-grained metagranitoid, amphibolite and pegmatitic granite. All also altered. The radar measurements indicate a limited extension in at least one direction. Confidence level = 3					310.00															RU1c										Same dominant rock as between 100-155 m depth, with one about 8 m wide occurrence of fine-grained metagranitoid, one about 3 m wide amphibolite and some minor occurrences of pegmatitic granite, fine-grained metagranite and amphibolite. Indications of sub-parallel radar reflectors outside the borehole are observed. Confidence level = 3					485.00															RU2b										Heterogeneous interval, predominantly with the fine-grained metagranitoid. The second most important bedrock component is the metagranite-granodiorite, and then pegmatitic granite. Also some subordinate amphibolite. Most of the interval has been subjected to a variable degree of oxidation. Confidence level = 3.					520.00															RU1d										Same dominant rock as between 100-155 m depth, with several minor occurrences of pegmatitic granite and amphibolite. To a variable extent oxidised. Confidence level = 3					540.00															RU2c										The upper two thirds of the interval consists of fine-grained metagranite, whereas the lower third is more heterogeneous and composed of amphibolite, pegmatitic granite and the metagranite-granodiorite. Confidence level = 3.					575.00															RU1e										Same dominant rock as between 100-155 m depth. Confidence level = 3					600.00															RU2d										Fine-grained metagranite and the metagranite-granodiorite in approximately equal proportions. Also, several minor occurrences of pegmatitic granite. Confidence level = 3.					635.00															RU1f										Same dominant rock as between 100-155 m depth, with some up to 8 m wide occurrences of fine-grained metagranitoid, amphibolite and pegmatitic granite. The uppermost part of the interval has been subjected to a variable extent of oxidation. Confidence level = 3					835.00															RU2e										Heterogeneous interval, predominantly with the fine-grained metagranitoid, and then the metagranite-granodiorite and amphibolite. Also some subordinate occurrences of pegmatitic granite. Confidence level = 3					867.00															RU1g										Same dominant rock as between 100-155 m depth, with several minor occurrences of pegmatitic granite, up to about 1.5 m in width. Confidence level = 3					903.00															RU4										A homogeneous interval of a tonalitic (high density, low gamma) variety of the fine-grained metagranitoid. Also with some minor occurrences of amphibolite and pegmatitic granite. Confidence level = 3.					938.00															RU1h										Same dominant rock as between 100-155 m depth, with several minor occurrences of pegmatitic granite and amphibolite. Confidence level = 3					1001.00														
Depth [m]	BOREMAP DATA				GENERALIZED GEOPHYSICAL DATA				ROCK UNIT		POSSIBLE DEFORMATION ZONES																																																																																																																																																																																																																																																																																																																																																																																																																																																																																																																																																									
	Open Fractures	Sealed Fractures	Caliper	Seismic	Seismic	Seismic	Seismic	Seismic	Seismic	Description	Possible Deformation Zone	Possible Deformation Zone	Possible Deformation Zone	Possible Deformation Zone																																																																																																																																																																																																																																																																																																																																																																																																																																																																																																																																																						
12.00																																																																																																																																																																																																																																																																																																																																																																																																																																																																																																																																																																				
RU1a										Medium-grained metagranite to granodiorite with subordinate occurrences of amphibolite (mainly limited to the lower 50 m of the interval) and pegmatitic granite (primarily in the upper 40 m of the interval). Percussion-drilled part of the borehole. Boremap mapping and examination of drill cuttings. Confidence level = 3.																																																																																																																																																																																																																																																																																																																																																																																																																																																																																																																																																										
96.00																																																																																																																																																																																																																																																																																																																																																																																																																																																																																																																																																																				
100.00																																																																																																																																																																																																																																																																																																																																																																																																																																																																																																																																																																				
RU1a										Medium-grained metagranite to granodiorite with subordinate occurrences of amphibolite and pegmatitic granite. Confidence level = 3																																																																																																																																																																																																																																																																																																																																																																																																																																																																																																																																																										
155.00																																																																																																																																																																																																																																																																																																																																																																																																																																																																																																																																																																				
RU2a										Heterogeneous interval, predominantly with a fine-grained metagranitoid. The second most important bedrock component is the metagranite-granodiorite, and then the amphibolite. The central part of the interval is strongly oxidised with three minor intervals of vuggy metagranitoid. Confidence level = 3.																																																																																																																																																																																																																																																																																																																																																																																																																																																																																																																																																										
205.00																																																																																																																																																																																																																																																																																																																																																																																																																																																																																																																																																																				
RU1b										Same dominant rock as between 100-155 m depth, with one about 5 m wide occurrence of fine-grained metagranitoid and several minor occurrences of pegmatitic granite. Confidence level = 3																																																																																																																																																																																																																																																																																																																																																																																																																																																																																																																																																										
240.00																																																																																																																																																																																																																																																																																																																																																																																																																																																																																																																																																																				
RU3										Vuggy metagranite (low density, resistivity, susceptibility and P-wave velocity) subjected to a strong albite-hematite-chlorite alteration. Also some minor occurrences of fine-grained metagranitoid, amphibolite and pegmatitic granite. All also altered. The radar measurements indicate a limited extension in at least one direction. Confidence level = 3																																																																																																																																																																																																																																																																																																																																																																																																																																																																																																																																																										
310.00																																																																																																																																																																																																																																																																																																																																																																																																																																																																																																																																																																				
RU1c										Same dominant rock as between 100-155 m depth, with one about 8 m wide occurrence of fine-grained metagranitoid, one about 3 m wide amphibolite and some minor occurrences of pegmatitic granite, fine-grained metagranite and amphibolite. Indications of sub-parallel radar reflectors outside the borehole are observed. Confidence level = 3																																																																																																																																																																																																																																																																																																																																																																																																																																																																																																																																																										
485.00																																																																																																																																																																																																																																																																																																																																																																																																																																																																																																																																																																				
RU2b										Heterogeneous interval, predominantly with the fine-grained metagranitoid. The second most important bedrock component is the metagranite-granodiorite, and then pegmatitic granite. Also some subordinate amphibolite. Most of the interval has been subjected to a variable degree of oxidation. Confidence level = 3.																																																																																																																																																																																																																																																																																																																																																																																																																																																																																																																																																										
520.00																																																																																																																																																																																																																																																																																																																																																																																																																																																																																																																																																																				
RU1d										Same dominant rock as between 100-155 m depth, with several minor occurrences of pegmatitic granite and amphibolite. To a variable extent oxidised. Confidence level = 3																																																																																																																																																																																																																																																																																																																																																																																																																																																																																																																																																										
540.00																																																																																																																																																																																																																																																																																																																																																																																																																																																																																																																																																																				
RU2c										The upper two thirds of the interval consists of fine-grained metagranite, whereas the lower third is more heterogeneous and composed of amphibolite, pegmatitic granite and the metagranite-granodiorite. Confidence level = 3.																																																																																																																																																																																																																																																																																																																																																																																																																																																																																																																																																										
575.00																																																																																																																																																																																																																																																																																																																																																																																																																																																																																																																																																																				
RU1e										Same dominant rock as between 100-155 m depth. Confidence level = 3																																																																																																																																																																																																																																																																																																																																																																																																																																																																																																																																																										
600.00																																																																																																																																																																																																																																																																																																																																																																																																																																																																																																																																																																				
RU2d										Fine-grained metagranite and the metagranite-granodiorite in approximately equal proportions. Also, several minor occurrences of pegmatitic granite. Confidence level = 3.																																																																																																																																																																																																																																																																																																																																																																																																																																																																																																																																																										
635.00																																																																																																																																																																																																																																																																																																																																																																																																																																																																																																																																																																				
RU1f										Same dominant rock as between 100-155 m depth, with some up to 8 m wide occurrences of fine-grained metagranitoid, amphibolite and pegmatitic granite. The uppermost part of the interval has been subjected to a variable extent of oxidation. Confidence level = 3																																																																																																																																																																																																																																																																																																																																																																																																																																																																																																																																																										
835.00																																																																																																																																																																																																																																																																																																																																																																																																																																																																																																																																																																				
RU2e										Heterogeneous interval, predominantly with the fine-grained metagranitoid, and then the metagranite-granodiorite and amphibolite. Also some subordinate occurrences of pegmatitic granite. Confidence level = 3																																																																																																																																																																																																																																																																																																																																																																																																																																																																																																																																																										
867.00																																																																																																																																																																																																																																																																																																																																																																																																																																																																																																																																																																				
RU1g										Same dominant rock as between 100-155 m depth, with several minor occurrences of pegmatitic granite, up to about 1.5 m in width. Confidence level = 3																																																																																																																																																																																																																																																																																																																																																																																																																																																																																																																																																										
903.00																																																																																																																																																																																																																																																																																																																																																																																																																																																																																																																																																																				
RU4										A homogeneous interval of a tonalitic (high density, low gamma) variety of the fine-grained metagranitoid. Also with some minor occurrences of amphibolite and pegmatitic granite. Confidence level = 3.																																																																																																																																																																																																																																																																																																																																																																																																																																																																																																																																																										
938.00																																																																																																																																																																																																																																																																																																																																																																																																																																																																																																																																																																				
RU1h										Same dominant rock as between 100-155 m depth, with several minor occurrences of pegmatitic granite and amphibolite. Confidence level = 3																																																																																																																																																																																																																																																																																																																																																																																																																																																																																																																																																										
1001.00																																																																																																																																																																																																																																																																																																																																																																																																																																																																																																																																																																				

Title SINGLE HOLE INTERPRETATION KFM04A											
Site FORSMARK Borehole KFM04A Diameter [mm] 77 Length [m] 1001.420		Bearing [°] 45.24 Date of mapping 2003-12-08 00:00:00 Coordinate System RT90-RHB70 Inclination [°] -60.07		Northing [m] 6698921.74 Easting [m] 1630978.96 Elevation [m.a.s.l.] 8.77 Drilling Start Date 2003-05-20 07:00:00		Drilling Stop Date 2003-11-19 15:15:00 Surveying Date Plot Date 2008-06-29 22:08:57 Signed data					
ROCK TYPE FELSIC <input type="checkbox"/> Granite, fine- to medium-grained <input type="checkbox"/> Pegmatitic, pegmatitic granite <input type="checkbox"/> Granite, granodiorite and tonalite, metamorphic, fine- to medium-grained <input type="checkbox"/> Granite to granodiorite, metamorphic, medium-grained <input type="checkbox"/> Granodiorite, metamorphic <input type="checkbox"/> Amphibolite <input type="checkbox"/> Felsic to intermediate volcanic rock, metamorphic		ALTERATION <input type="checkbox"/> Oxidized <input type="checkbox"/> Chloritized <input type="checkbox"/> Epidotized <input type="checkbox"/> Sericitized <input type="checkbox"/> Argillization		MAGNETIC SUSCEPTIBILITY <input type="checkbox"/> dens=2680 (Granite) <input type="checkbox"/> 2680-dens=2730 (Granodiorite) <input type="checkbox"/> 2730-dens=2800 (Tonalite) <input type="checkbox"/> 2800-dens=2890 (Diorite) <input type="checkbox"/> dens=2890 (Gabbro)		SUSCEPTIBILITY <input type="checkbox"/> sus=0.001 <input type="checkbox"/> 0.001<sus=0.01 <input type="checkbox"/> 0.01<sus=0.1 <input type="checkbox"/> sus=0.1		NATURAL GAMMA <input type="checkbox"/> gam=20 <input type="checkbox"/> 20-gam=36 <input type="checkbox"/> 36-gam=53			
BOREMAP DATA		GENERALIZED GEOPHYSICAL DATA		ROCK UNIT		POSSIBLE DEFORMATION ZONES					
Depth [m]	Gamma [cps]	Resistivity [ohm-m]	Gamma [cps]	Description	Rock Unit	Rock Unit Open and Partly Open Fractures (Projection Wulff)	Rock Unit Open and Partly Open Fractures (Projection Wulff)	Description	Possible Deformation Zone Sealed Fractures (Projection Wulff)	Possible Deformation Zone Open and Partly Open Fractures (Projection Wulff)	
12.00				RU1 Fine-grained, felsic to intermediate metavolcanic rock and fine- to medium-grained metagranodiorite and metagranite in approximately equal proportions. Subordinate occurrences of pegmatitic granite and at base of the section one c. 1 m wide amphibolite. Confidence level = 2							
88.00				RU2 Strongly foliated, fine- to medium-grained metagranodiorite with subordinate occurrences of pegmatitic granite, fine-grained, felsic to intermediate metavolcanic rock in the upper half of the interval and amphibolite in the lower half of the interval. Generally increased fracture frequency relative to the lower half of the borehole. Generally higher density and lower natural gamma radiation relative to the rock unit below. Confidence level = 3				DZ1 169.00 Slightly increased frequency of both sealed and open, steeply dipping fractures. Generally weak oxidation. Predominant fracture fillings are calcite, chlorite, hematite and prehnite. Clearly decreased electric resistivity and slightly decreased P-wave velocity. One oriented radar reflector occurs at 179.9 m with the orientation 326/32 and one non-oriented at 168.6 m with the angle 55 degrees to borehole axis. Confidence level = 2.			
177.00				RU3a Strongly foliated, fine- to medium-grained metagranite-granodiorite with subordinate occurrences of pegmatitic granite and amphibolite, and a few occurrences of fine-grained, felsic to intermediate metavolcanic rock and fine- to medium-grained metagranitoid. Generally increased fracture frequency relative to the lower half of the borehole. Confidence level = 3.				DZ2 176.00 202.00 Marked increased frequency of flat lying, open fractures and steeply dipping, sealed fractures. Fracture apertures range up to 7 mm in width. Generally faint to weak oxidation. Predominant fracture minerals are calcite, hematite and chlorite. Also a few fractures with epidote and laumontite. Clearly decreased electric resistivity and slightly decreased P-wave velocity. Two radar reflectors occur at 205.9 m (128/73) and at 210.9 m (316/11) and one non-oriented radar reflector at 208.6 m with an intersection angle to the borehole of 48 degrees. Confidence level = 3.			
275.00				RU4 More inhomogeneous mixture of strongly foliated, fine- to medium-grained metagranite-granodiorite and fine-grained, felsic to intermediate metavolcanic rock. Subordinate occurrences of pegmatitic granite, amphibolite and fine- to medium-grained metagranitoid. Two ductile, high strain zones in the lower part of the rock unit. Generally increased fracture frequency relative to the lower half of the borehole. Confidence level = 3.				DZ3 232.00 Marked increased frequency of flat lying, open fractures filled by laumontite and chlorite. Fracture apertures range up to more than 10 mm in width. One c. 15 cm wide crush zone and sealed network in the lower part of the possible zone. Faint to strong oxidation. Clearly decreased electric resistivity and P-wave velocity. Distinct caliper anomaly. One radar reflector at 234.7 m with the orientation 136/57 or 044/9. Confidence level = 3.			
342.00				RU5 Mixture of fine- to medium-grained metagranitoid and strongly foliated, fine- to medium-grained metagranite-granodiorite. Subordinate occurrences of pegmatitic granite and amphibolite. Several ductile, high strain zones, some of which are associated with muscovite alteration. Generally increased fracture frequency relative to the lower half of the borehole. Also minor oxidation and a c. 15 cm wide crush zone at a length of c. 369 m. In the interval 342-393 m there are several thin sections with high natural gamma radiation. The interval 393-443 m shows a dominantly low magnetic susceptibility. Confidence level = 3.				DZ4 242.00 412.00 Marked by a network of fractures mainly sealed by laumontite, calcite and chlorite. Also some open fractures with apertures greater or equal to 5 mm. Alterations in the interval include varying degrees of oxidation, epidotization and clay alteration. The possible zone includes parts affected by high ductile strain. Section 412-435 m indicated by a low electric resistivity. No other geophysical anomalies. Five oriented radar reflectors occur at 425.0 m (243/61), 434.5 m (338/7), 447.6 m (253/6 or 120/70), 455.2 m (350/8) and 459.3 m (206/57). Three non-oriented radar reflectors occur at 412.5 m, 444.0 m and 459.3 m with the angle 46, 11 and 49 degrees to borehole axis, respectively. Confidence level = 3.			
443.00				RU3b Strongly foliated, fine- to medium-grained metagranite-granodiorite with subordinate occurrences of pegmatitic granite and amphibolite, and a few occurrences of fine- to medium-grained metagranitoid. Generally increased fracture frequency relative to the lower half of the borehole. Several thin intervals of high natural gamma radiation. One distinct radar reflector intersects the borehole at c. 425 m and can be followed down to c. 600 m; strike 300 degrees and dip 60 degrees, which corresponds in orientation with a pegmatite contact at 443 m. Confidence level = 3.				DZ5 462.00 654.00 Marked by increased frequency of sealed fractures and weak oxidation. Corresponds also to a brittle-ductile high strain zone and a c. 1 m wide amphibolite. Predominant fracture sealing minerals are prehnite, calcite, epidote and chlorite. Clearly decreased electric resistivity and slightly decreased P-wave velocity. One distinct radar reflector at 658.0 m with the orientation 143/78 and one non-oriented at a length of 654.6 m with the angle 55 degrees to borehole axis. Confidence level = 2.			
500.00				RU6a Medium-grained metagranite-granodiorite with subordinate occurrences of pegmatitic granite, amphibolite and fine- to medium-grained metagranitoid. The upper 25 m interval of the rock unit has low magnetic susceptibility, whereas the interval 536-724 m has high magnetic susceptibility. Confidence level = 3.				DZ6 661.00			
724.00				RU7a Fine- to medium-grained, hornblende-rich quartz-feldspar rock (mapped as amphibolite), with sulphide dissemination. Subordinate occurrences of medium-grained metagranite-granodiorite and pegmatitic granite. High density, low magnetic susceptibility and low natural gamma radiation. Confidence level = 3.							
743.00				RU6b Medium-grained metagranite-granodiorite with subordinate occurrences of pegmatitic granite and amphibolite, as well as two minor occurrences of fine- to medium-grained metagranitoid and one, almost 2 m wide occurrence of fine-grained, felsic to intermediate metavolcanic rock. Confidence level = 3.							
938.00				RU8 Fine- to medium-grained metagranitoid with subordinate occurrences of pegmatitic granite and medium-grained metagranite-granodiorite. The whole rock unit has low magnetic susceptibility and partly increased density. Confidence level = 3.							
957.00				RU6c Medium-grained metagranite-granodiorite with subordinate occurrences of fine- to medium-grained metagranitoid and pegmatitic granite. Confidence level = 3.							
990.00				RU7b Fine- to medium-grained, hornblende-rich quartz-feldspar rock (mapped as amphibolite), with sulphide dissemination. Subordinate occurrences of medium-grained metagranite-granodiorite and pegmatitic granite. High density, low magnetic susceptibility and low natural gamma radiation. Confidence level = 3.							
999.00				RU6d Medium-grained metagranite-granodiorite with one, minor occurrence of pegmatitic granite. Confidence level = 3.							
1001.42											